FE-ANN BASED MODELING OF 3D SIMPLE REINFORCED CONCRETE GIRDERS FOR OBJECTIVE STRUCTURAL HEALTH EVALUATION

by

ERIC MATTHEW FLETCHER

B.S., Kansas State University, 2014

A THESIS

submitted in partial fulfillment of the requirements for the degree

MASTER OF SCIENCE

Department of Civil Engineering
College of Engineering

KANSAS STATE UNIVERSITY
Manhattan, Kansas

2016

Approved by:

Major Professor
Hayder A. Rasheed

Copyright

ERIC FLETCHER

2016

Abstract

The structural deterioration of aging infrastructure systems is becoming an increasingly important issue worldwide. To compound the issue, economic strains limit the resources available for repair or replacement of such systems. Over the past several decades, structural health monitoring (SHM) has proved to be a cost-effective method for detection and evaluation of damage in structures. Visual inspection and condition rating is one of the most commonly applied SHM techniques, but the effectiveness of this method suffers due to its reliance on the availability and experience of qualified personnel performing largely qualitative damage evaluations. The artificial neural network (ANN) approach presented in this study attempts to augment visual inspection methods by developing a crack-induced damage quantification model for reinforced concrete bridge girders that requires only the results of limited field measurements to operate. Simply-supported three-dimensional reinforced concrete T-beams with varying geometric, material, and cracking properties were modeled using Abaqus finite element (FE) analysis software. Up to five cracks were considered in each beam, and the ratios of stiffness between cracked and healthy beams with the same geometric and material parameters were measured at nine equidistant nodes along the beam. Two feedforward ANNs utilizing backpropagation learning algorithms were then trained on the FE model database with beam properties serving as inputs for both neural networks. The outputs for the first network consisted of the nodal stiffness ratios, and the sole output for the second ANN was a health index parameter, computed by normalizing the area under the stiffness ratio profile over the span length of the beam. The ANNs achieved excellent prediction accuracies with coefficients of determination (R^2) exceeding 0.99 for both networks. Additional FE models were created to further assess the networks' prediction capabilities on data not utilized in the training process.

The ANNs displayed good prediction accuracies ($R^2 > 0.8$) even when predicting damage levels in beams with geometric, material, and cracking parameters dissimilar from those found in the training database. A touch-enabled user interface was developed to allow the ANN models to be utilized for on-site damage evaluations. The results of this study indicate that application of ANNs with FE modeling shows great promise in SHM for damage evaluation.

Table of Contents

List of Figures

List of Tables

Acknowledgements

Chapter 1 - Introduction

Background

The deterioration of aging infrastructure is becoming an increasingly important issue both domestically and abroad, especially in the midst of an uncertain economic climate. Structures such as reinforced concrete bridges are subject to damage over time due to physical or chemical processes. Structural health monitoring (SHM) strategies are frequently applied to bridges and other infrastructure systems to detect, monitor, and evaluate damage, resulting in improved and economic repair or remediation solutions. Numerous SHM techniques utilizing various technologies have been proposed as alternatives to the subjective visual inspection and condition rating method. Artificial neural networks (ANNs) are robust and innovative tools that demonstrate promising potential for application in SHM.

Objectives

The primary goal of this research project was to utilize ANNs to produce a SHM model for objective damage evaluation of reinforced concrete bridge T-girders. Initially, a reinforced concrete beam finite element (FE) model database was generated using Abaqus FE analysis software. Beams in the database consisted of simply-supported reinforced concrete T-beams with varying geometric, material, and cracking parameters, and beams were modeled with zero to five cracks by dividing the girders into five equal segments with no more than one crack per segment. Damage was characterized by the ratios of stiffness between cracked and uncracked beams at nine equidistant nodes, and a health index parameter was used to resolve the nodal stiffness ratios into a single objective measure of structural health. Feedforward ANNs employing a backpropagation learning algorithm were trained on the database to predict nodal stiffness ratios and health indices of the beams given their geometric, material, and cracking parameters.

Ultimately, the optimum models from the ANN modeling process were utilized to create touch-enabled graphical user interfaces for on-site damage evaluation applications.

Scope

This thesis is divided into six chapters. Chapter 1 introduces the background for the research, details the objectives of the study, and summarizes the scope of the thesis. Chapter 2 provides justification for the research, discusses the practice of SHM, reviews several studies related to SHM for damage evaluation, and introduces ANNs. Chapter 3 describes the creation of the reinforced concrete beam FE model database and discusses the techniques used to apply ANNs in order to create structural health prediction models. Chapter 4 presents the statistical results from the ANN training process and optimal model selection procedure and details the additional tests performed to assist in the selection of the top-performing damage evaluation network architectures. Chapter 5 describes the development of the touch-enabled graphical user interface, which allows the optimal ANN structural health prediction models to be applied in real-world SHM investigations. Chapter 6 reviews the study, summarizes the research conclusions, and provides recommendations for continuation and expansion of the work performed.

Chapter 2 - Literature Review

Introduction to Structural Health Monitoring

Bridges are vital components of national infrastructures, and transportation systems throughout the world depend upon their safe and reliable operation. To ensure such operation, bridge structures require periodic maintenance and eventual rehabilitation or replacement. While all structures require upkeep, bridges often demand more attention due to hardships endured during their service lives. Harsh external environments, extreme loading events, and fatigue due to service loading all induce structural damage over time. Bridges that sustain significant damage are classified as structurally deficient, thereby indicating they require immediate attention. According to the Federal Highway Administration (FHWA), 61,365, or 10% of the nation's 610,749 bridges were classified as structurally deficient in 2014 (FHWA (a), 2014). Furthermore, 25% of the bridge decking area in the United States was classified as structurally deficient (FHWA (a), 2014). The American Society of Civil Engineers (ASCE) 2013 Report Card for America's Infrastructure reported that annual funding of $20.5 billion would be required to eliminate the bridge investment backlog by 2028, yet only $12.8 billion is currently spent on bridges annually (ASCE, 2013). This infrastructure problem is not limited to the United States, however, and as industrialization and population growth accelerate throughout the world, bridge structure maintenance and repair will increasingly present itself as a global issue.

Although all bridges are subject to damage, concrete bridges, which account for over 65% of the bridge structures in the United States (FHWA (b), 2014), are especially prone to crack-related damage, often stemming from the subsequently described mechanism. Loading of bridge structures can induce sufficient stress to initiate the formation of flexural and shear cracks on the tension faces of reinforced concrete members. Although crack propagation is inhibited by

3

tensile steel reinforcement, the reinforcement is left exposed to the environment, and moisture and chemicals, such as deicing salts, stimulate corrosion of the steel reinforcement over time. Corrosion and cracking reduce load-carrying capacities of reinforced concrete members, thereby reducing the durability and functionality of the bridge structure. Cracking necessitates frequent and costly repairs and limits the service lives of concrete bridges. In order to cost-effectively address cracking issues in concrete bridges, structural health monitoring (SHM) is frequently applied.

Structural health monitoring can be described as the process of implementing a damage detection and characterization strategy for infrastructure systems (Sohn et al., 2004). Although various texts define the steps in SHM differently, fundamentals of the process remain consistent. A Los Alamos National Laboratory report presents SHM as a four-part process: operational evaluation; data acquisition, fusion, and cleansing; feature extraction and information condensation; and statistical model development for feature discrimination (Sohn et al., 2004). In this process, operational evaluations attempt to provide justifications and generalized goals for the monitoring process. These goals identify desired information and dictate required equipment and techniques for data acquisition. During data fusion, the collected data is assimilated into a robust, central source, and data cleansing filters the relevant and irrelevant data. Properties of acquired data that influence damage are identified and classified in the feature extraction stage, and the vast amount of data often retrieved throughout the SHM process is compressed during information condensation. Lastly, statistical models are developed from the analysis of damage sensitive features. These models are often used for applications such as damage detection, localization, and quantification. An in-depth description of the SHM process and an extensive

literature review of SHM applications in the aerospace, civil, and mechanical engineering fields

is presented in the full report: LA-13976-MS (Sohn et al., 2004).

Visual inspection and condition rating is one of the most common forms of SHM

employed by bridge owners in the United States. In this method, trained and certified personnel

visually inspect the bridge and use simple tools, such as hammers or chains, to detect damage.

After inspection, the bridge condition is assessed in a largely qualitative manner and assigned a

rating of 0–9 to indicate the level to which repairs are required or replacement should be

considered (Ahlborn et al., 2010). Although the visual inspection and condition rating system is

standardized domestically by the National Bridge Inspection Standards (NBIS), it relies on the

experience and subjective judgement of bridge inspectors to characterize the structural health of

the bridge.

In lieu of visual inspection, a number of alternative damage detection techniques that rely

on the processing of features extracted by equipment in the SHM process have been utilized over

the past several decades. Features can consist of static properties such as flexural stiffness, but

dynamic characteristics including modal properties, wave responses, and digital images are more

commonly used because dynamic properties can be directly obtained using non-destructive test

methods. Methods such as modal analysis, wavelet analysis, digital image correlation, fractal

analysis, finite element (FE) model updating, and artificial neural networks (ANNs) are used to

process and analyze these features. Al-Rahmani (2012) completed a literature review concerning

damage detection and localization techniques and studies.

Damage Evaluation and Structural Health Prediction Techniques

Although a significant amount of SHM research has been conducted, the research appears

to focus more on damage detection and localization as opposed to structural health assessment

and damage quantification. Similar data extraction and feature processing techniques utilized in damage detection are applied to assess structural health, but metrics must also be established by which damage can be measured quantitatively. These damage metrics often rely on reference static or dynamic characteristics extracted from a healthy, or undamaged structure. A review of available literature regarding quantification of damage in the SHM process revealed that numerous feature extraction, processing, and analysis techniques have been utilized for structural health assessment.

Modal properties such as damping, eigenfrequencies, and mode shapes have been used by several researchers to characterize structural damage. Ndambi, Vantomme, and Harri (2002) investigated the potential for use of eigenfrequencies and mode shape-derived properties to detect the location and estimate the severity of damage in reinforced concrete beams. A symmetrically and an asymmetrically loaded experimental beam were monotonically loaded in stages to induce damage. An electromagnetic shaker prompted dynamic responses of each beam, and eigenfrequencies and mode shape properties were captured by accelerometers. Properties including modal assurance criterion factors, coordinate modal assurance criterion factors, strain energy evolutions, and changes in the flexibility matrices were derived from the mode shape data. These mode shape-derived properties were used to detect and localize cracking damage in the concrete beams to varying degrees of accuracy; the strain energy method produced optimal results. Additionally, decreasing eigenfrequencies were found to correlate to a decrease in the flexural rigidity, or stiffness, of the beams. The results of these tests suggest that eigenfrequencies of reinforced concrete members can be numerically correlated to changes in stiffness, allowing damage to be quantified with non-destructive test methods (Ndambi et al., 2002).

Ghods and Esfahani (2009) conducted static loading tests and dynamic modal analyses on eight reinforced concrete beams with varying compressive strengths and reinforcement ratios. Frequency response function (FRF) diagrams were plotted from dynamic responses of the beams under impact hammer excitation after each static loading step. Mode shapes derived from the diagrams were determined to be good indicators of the location of damage, and frequencies across all modes decreased as damage levels in the beams increased. Large reductions in frequencies were recorded after the first loading step, which corresponded to the cracking load. Frequencies then decreased at an increasingly slower rate until yielding of the tensile reinforcement, at which point they decreased more rapidly to member failure. This experiment highlighted the ability of modal analyses to characterize the specific damage level in reinforced concrete beams (Ghods & Esfahani, 2009).

Al-Ghalib, Mohammad, Rahman, and Chilton (2011) subjected a single reinforced concrete beam to static loading and dynamic tests. Dynamic responses were recorded on FRF diagrams, and properties were retrieved for the first four modes of vibration. Frequencies were found to decrease with increasing levels of damage, and significant drops in natural frequencies were observed even before crack formation. Damping ratios extracted from the FRF diagrams behaved inversely to natural frequencies; damping ratios increased as the damage level in the beam increased. In addition to detecting and localizing damage, mode shapes provided curvature data that was used with modal bending moment distributions to dynamically calculate the beam stiffness (EI). The researchers suggested a damage indicator parameter (D) to quantify damage in terms of loss of stiffness, where $D = 1 - (EI_{damaged})/(EI_{intact})$ (Al-Ghalib et al., 2011).

FE model updating is a data processing and analysis technique by which an analytical FE model of a damaged structure is adjusted to account for property variations from the initial,

healthy state. Teughels, Maeck, and De Roeck (2002) presented an approach to damage quantification using FE model updating. In their research, an analytical model was adjusted by experimentally obtained modal properties such as natural frequencies and mode shapes. Damage functions derived from shape functions were implemented in order to optimize the FE updating process and more effectively relate modal properties to damage levels. The researchers dynamically tested an experimental reinforced concrete beam under various levels of static loading. Properties of the healthy, or reference state of the beam were used to create the FE model, and the model was calibrated to the experimentally extracted modal analysis data. After static loading, the model was updated with the damaged beam's modal properties, and the stiffness distribution over the beam was obtained. A direct stiffness calculation was performed using modal frequencies and curvatures, and the stiffness distribution showed good agreement with results of the FE model updating procedure. Results of this research demonstrated that modal properties can be used with processing and analysis techniques, such as FE model updating, to reliably quantify damage in reinforced concrete structures (Teughels et al., 2002).

Reynders and De Roeck (2009) applied modal analysis parameters to develop a flexibility-based damage assessment method for beam members. The research established the process by which modal data gathered from vibration tests was applied to construct a quasi-static local flexibility matrix. Deviations of flexibility and stiffness from the healthy condition of a beam were then detected and quantified through application of the flexibility matrix. Analyses of an experimental reinforced concrete beam and a decommissioned, post-tensioned girder bridge in Switzerland verified this method. Modal data was retrieved from vibration tests conducted on both subjects before and after damage was introduced by static loading, and damage was quantified by variations in stiffness as calculated by the flexibility method. Direct stiffness

calculations were also performed for both subjects, and the results of both methods displayed good agreement. The conclusion was made that the modal data-based flexibility method shows promise as a nondestructive method for quantifying damage in concrete beams (Reynders & De Roeck, 2009).

Lenett, Griessmann, Helmicki, and Aktan (1999) investigated the variation between subjective and objective evaluations of a reinforced concrete bridge deck on a decommissioned steel stringer bridge in Ohio. The bridge, built in 1953, was closed due to consistently poor health inspection ratings and low usage. Instead of demolishing the bridge, the Ohio Department of Transportation and the FHWA conducted modal analyses and truckload testing on the bridge for a variety of induced damage scenarios. A FE model was then developed using design material properties, observed geometric properties, and natural frequencies, mode shapes, and modal flexibilities acquired during testing. This model was used to load rate and quantitatively assess the structural health of the bridge. Qualified personnel also visually inspected and evaluated the bridge according to the NBIS rating system. These evaluations characterized the bridge as being more severely damaged than the damage level indicated by results of the objective FE model. Additionally, subjective ratings of the bridge varied from 4–5, or poor to fair, between inspectors. This research detailed the usefulness of modal properties and FE model updating in quantifying damage and highlighted the potential inaccuracies of visual inspections and subjective evaluations of bridges (Lenett et al., 1999).

Researchers have also used wave response methods to localize and quantify damage in reinforced concrete structures. One such method, acoustic emission (AE), uses mechanical loading to cause damaged material sections to emit elastic waves that are read by surface sensors. Sagar, Prasad, and Sharma (2012) utilized the AE technique to assess damage in three

experimental reinforced concrete beams subjected to cyclic loading stages. Four AE sensors were attached to each beam in order to gather wave response data during each loading cycle, and calculated calm and load ratios were used to evaluate damage severity in the beams. The calm ratio is the ratio of the cumulative AE signal strengths recorded during unloading and loading of the beams, and the load ratio is the ratio of applied load at the onset of AE activity in the subsequent and previous loading cycles. It was observed that as the damage level in the beams increased, the calm ratio increased and the load ratio decreased. The calm and load ratios were also compared to beam displacement and concrete and steel strain data gathered throughout the experiment in order to correlate the ratios with conventional damage quantification properties. Although the experiment was limited to three experimental beams, the researchers proposed that AE techniques and the calm and load ratios display significant potential for structural damage assessment applications (Sagar et al., 2012).

Shiotani et al. (2012) utilized AE and elastic wave tomography techniques to assess the structural health of an experimental reinforced concrete bridge deck subjected to fatigue damage. Fatigue loading was simulated by load stages of 0, 10,000, and 20,000 passes of a 100 kN moving wheel load, and wave data was recorded for the bridge deck under incremental static load steps after each fatigue loading stage. Elastic wave tomography analyses revealed that P-wave velocities could be used to determine the health of the deck, and wave velocities less than 3,000 m/s indicated increasing levels of damage. Although the AE analysis utilized the calm ratio and a parameter referred to as the RTRI (similar to the load ratio described above), the researchers did not quantitatively assess the health of the deck according to these parameters. Instead, peak frequencies of AE activity were found to be good damage level indicators, and decreasing frequencies were noted as damage in the deck increased. Elastic wave tomography

and AE analyses of two in-situ bridge decks substantiated these findings, and wave velocities and natural frequencies again showed great promise as damage quantification parameters (Shiotani et al., 2012).

In the impact-echo method, another wave response technique, excitation of elastic waves is achieved when the surface of a structure is impacted with a rigid object. These waves propagate throughout the material and are redirected by material property changes that often indicate damage. Gassman and Tawhed (2004) employed the impact-echo method to assess the structural health of a precast reinforced concrete deck removed from a decommissioned maintenance bridge in South Carolina. The surface of the bridge deck was divided into a grid, and wave response properties were measured from the impact of a small steel ball in each section of the grid. After baseline measurements for the structure were recorded, the deck was loaded to flexural failure. Impact-echo tests were then performed on the damaged structure, and peak frequencies and P-wave velocities were correlated to four levels of damage in the deck: no damage, loss of stiffness, crack propagation, and localized failure. The results showed that reductions in wave velocity of over 900 m/s with respect to healthy sections indicated heavy damage, and reductions in velocity of 2%–6% suggested a loss of stiffness or crack propagation. Cores taken from the deck after testing verified the conclusions drawn from the wave response characteristic analyses and confirmed the usefulness of the impact-echo method in structural health assessment (Gassman & Tawhed, 2004).

Researchers have also utilized digital imaging techniques such as digital image correlation (DIC), light detection and ranging (LiDAR), and fractal analysis to evaluate damage in reinforced concrete structures. DIC relies on algorithms that process data from high resolution images to measure surface displacements and strains. Li, Ghrib, and Lee (2008) used DIC to

detect cracks and assess damage for several experimental reinforced concrete beams. Loland's model was selected to quantify damage and damage evolution, and data recorded through DIC was applied in FE model updating to define the initial damage and material parameters in the damage model. The damage parameter, D, was calculated according Loland's model where $D = D_0 + m\varepsilon^n$. The D_0 term represents the initial damage in the beam and its value was determined through FE modeling. The m and n terms in Loland's model are material parameters and their values were correlated to measured strains. The critical value of D was found to be 0.76 at which point the compressive strain in the concrete beams reached 0.003, corresponding to the limit state of concrete crushing. The results of this experiment suggested that DIC combined with techniques such as FE model updating can effectively quantify structural damage (Li et al., 2008).

LiDAR, another digital imaging technique, relies on laser scanners to collect a multitude of optical-photonic points and their coordinate locations. These points are then assembled to produce a three-dimensional (3D) image with a resolution dependent upon the scanning density. Applications of 3D LiDAR technology in damage detection and quantification were investigated in three case studies summarized by Chen, Liu, Bian, and Smith (2012). One case study of a bridge in Iowa highlighted the ability of LiDAR to not only detect cracks, but also to describe their precise location and dimensions. The other two case studies investigated the application of LiDAR to quantify mass, area, and volume loss for reinforced concrete bridges. Although such properties are not conventional measures of damage, they do quantify changes in structural properties and could be correlated to various damage metrics (Chen et al., 2012).

Fractal analyses of visual images have also been applied to assess structural damage. The basic unit of a fractal analysis is the fractal dimension, which indicates the complexity of a visual

image. Although a variety of methods can be used to calculate fractal dimensions, Farhidzadeh, Dehghan-Niri, Moustafa, Salamone, and Whittaker (2013) applied the widely used box-counting algorithm in their analysis of two experimental reinforced concrete shear walls. The walls were subjected to cyclic lateral loading in a structural laboratory. Photographs were taken after the peak load of each cycle in order to allow for calculation of fractal dimensions. The researchers then proposed an index to quantify damage based on the change in fractal dimension relative to the fractal dimension of the healthy wall. This damage index was correlated to the relative loss of stiffness of the shear walls. Based upon the experimental results, the researchers concluded that damage indices correlated to fractal analyses show promise as tools for quantitatively predicting the damage in reinforced concrete structures (Farhidzadeh et al., 2013).

Although ANNs have been utilized in a variety of damage detection and localization studies, seemingly fewer researchers have applied ANNs for damage quantification. ANNs are computational models that establish relationships between parameters by analyzing sample data. Jeyasehar and Sumangala (2006) investigated the ability of ANNs to quantitatively predict damage in an experiment involving five experimental post-tensioned prestressed concrete beams. Damage in the beams was introduced by snapping a variable percentage of the wires through inducing localized pitting corrosion at a crack former placed at the center of the beams, and the beams were subjected to static loading stages of increasing magnitude. Deflections, strains, and cracking data were recorded after each static loading stage, and impact tests were performed to obtain natural frequencies. Due to the fact a large amount of data is often required to train ANNs, the static and dynamic test results for the beams were plotted, and a more robust set of results were synthesized from the experimental beam results via interpolation. A feedforward ANN that utilized a backpropagation learning algorithm was trained on the datasets with input parameters

consisting of the applied load and static and dynamic test results. The sole output of the ANN was the damage level, which was defined as the number of reinforcing wires that had been snapped. The authors suggested that ANNs trained with only dynamic test data could assess the damage level in the prestressed concrete beams with less than 10% error. However, the results also showed that the damage level assessment error could be further reduced with the introduction of static test data to the ANN (Jeyasehar & Sumangala, 2006).

Researchers have also investigated fusion of ANNs and the FE model updating approach. Hasançebi and Dumlupinar (2013) discussed the potential of using ANNs to perform FE model updating operations for reinforced concrete T-beam bridges. The researchers developed analytical FE bridge models with various boundary stiffnesses, elastic moduli, and deck masses. Changes in these properties from an initial state were used to characterize damage and assess structural health. Natural frequencies associated with the first three modes of vibration and deflections at the quarter-span points of the bridge were then retrieved from the models. A feedforward ANN was trained using backpropagation learning with natural frequencies and deflections as the inputs, and stiffnesses, elastic moduli, and deck masses as outputs. To validate the effectiveness of the trained ANN, a single-span reinforced concrete T-beam bridge was subjected to in-situ static and dynamic tests to obtain all parameters utilized by the ANN. Good agreement was found between the measured stiffnesses, elastic moduli, and deck masses and the values of these properties predicted by the ANN. The researchers concluded that ANNs can be successfully used in conjunction with FE model updating to quantitatively evaluate damage, provided they utilize both static and dynamic test results (Hasançebi & Dumlupinar, 2013).

Al-Rahmani (2012) conducted research involving the application of a feedforward ANN utilizing a backpropagation learning algorithm to develop both structural health prediction and

damage detection models. Databases composed of material, geometric, and cracking properties of simply-supported two-dimensional concrete beams were constructed by modeling healthy and damaged beams with Abaqus FE analysis software. The ratios of stiffness between damaged and healthy beams with identical geometric and material properties were measured via application of a defined point load at equidistant nodes along the span of the beam. The study consisted of three phases corresponding to various Abaqus modeling techniques, varying numbers of stiffness nodes, presence of reinforcement, and existence of one or two cracks in the damaged beams. Two ANNs were trained in each phase. The first network utilized material, geometric, and cracking properties as inputs to determine the nodal stiffness ratios as well as a health index parameter based off these ratios. The second network solved the inverse problem of predicting the cracking parameters using the material and geometric properties and nodal stiffness ratios as inputs. In general, the damage evaluation ANNs achieved excellent prediction accuracies, whereas the damage detection ANNs provided less accurate predictions. Al-Rahmani's work (2012) demonstrated the effectiveness of ANNs as SHM tools for both damage prediction and evaluation. This work was summarized in two publications. The first paper focused on damage detection in simple beams with a single crack (Al-Rahmani, Rasheed, & Najjar, 2013). The second paper addressed damage quantification and damage detection in simple beams with dual cracks (Al-Rahmani, Rasheed, & Najjar, 2014).

Artificial Neural Networks

ANNs are highly capable computational models inspired by increasing insight into the structure of the human brain and the processes related to operation of the biological nervous system. At the basic level, ANNs are composed of layers of interconnected neurons that process information in parallel. Provided sample information, ANNs learn to generalize complex and

nonlinear relationships and synthesize data for scenarios they have not experienced (Basheer, 1998). Researchers in a wide variety of fields have recognized and utilized the processing potential of ANNs. Al-Rahmani (2012) discussed their applications in SHM as tools for damage detection and localization. His own research and examples within this literature review also highlight the effectiveness of ANNs in damage quantification applications.

Structure and Learning Techniques

ANNs are often classified by their structures and learning techniques. Most network structures consist of at least three layers of neurons, or nodes: an input layer, one or more hidden layers, and an output layer. The input and output layers provide information to and extract results from the ANN. Learning occurs through mathematical operations performed within the hidden layers and their connections to the input and output layers. The two primary types of network structures are feedforward (static) and recurrent (dynamic). In feedforward networks, signal flow is unidirectional from the input layer to the output layer, and nodes within layers are not interconnected. Nodes within layers can be interconnected for recurrent networks, and output signals are transmitted back into the ANN in a variety of loop configurations (Al-Rahmani, 2012). Figure 2-1 displays the general structure for a feedforward network with a single hidden layer.
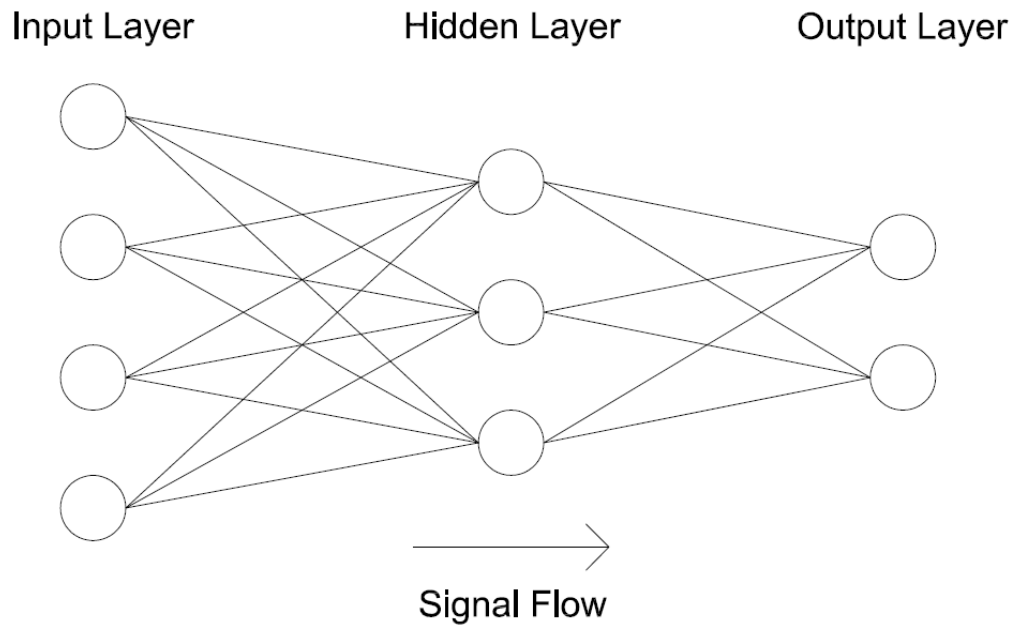
Figure 2-1: General feedforward ANN structure

Learning techniques govern how connection weights between layers are adjusted to minimize output errors. Three commonly applied learning techniques are supervised, reinforcement, and unsupervised learning. In supervised learning, outputs predicted by the ANN are judged against the actual, or provided outputs. Errors associated with these predictions are then used to adjust connection weights. Reinforcement learning is similar to supervised learning, however, only evaluations of the quality of the predicted outputs are used to adjust connection weights – actual outputs are not provided to the ANN. In the unsupervised method, learning occurs as the network explores patterns in the input data and makes inferences and correlations (Basheer, 1998). The research presented in this master's thesis relies on a feedforward ANN program that utilizes a backpropagation learning technique, which is a popular form of supervised learning. This program and the ANN modeling methodology used in this study stem from the work of Dr. Yacoub Najjar of the University of Mississippi. The procedure described in the following section, although general in many aspects, relates specifically to the ANN used in this study.

17

Data Preparation and Training Procedure

The process of training and verifying an ANN begins with the generation of analytically or experimentally created datasets. Because ANNs learn by example, larger datasets typically produce networks with enhanced prediction accuracies when compared to ANNs produced from limited data. After production, the datasets are divided into training, testing, and validation sets. The ANN learning process is accomplished by iterations of connection weight adjustment over the training datasets. Testing datasets help evaluate the prediction accuracy of the ANN on data not applied in the training process. Because multiple network configurations are often considered in an ANN analysis, validation datasets are used to reevaluate the top-performing network structures from the training and testing stage (Basheer, 1998). To ensure that the network is exposed to the full range of data in the training process, datasets containing the minimum and maximum values of input parameters are assigned to the training dataset, and the remaining datasets are divided so that the training, testing, and validation subsets receive 50%, 25%, and 25% of the data, respectively (Al-Rahmani, 2012).

Prior to initiation of the ANN, the range of minimum and maximum parameter values are expanded to enhance the sensitivity of the actual data to the activation functions within the hidden layer(s). The ranges are expanded so that the input parameters fit within 10%–90% of the expanded range and the output parameters fit within 20%–80% of the expanded range (Al-Rahmani, 2012). After the datasets are subdivided and the parameter ranges expanded, the ANN is initiated. Yaserer (2010) describes the calculations performed within the neural network. Normalization of the input parameters is initially performed to prevent any single input from dominating the learning process. Each node in the input layer is connected to every node in the hidden layer, and connection weights between the nodes are randomly assigned during the first

iteration. The hidden nodes receive an input signal equal to the summation of the input values

multiplied by their corresponding connection weights plus the bias, or threshold, associated with

the hidden node as represented by the following equation:

$$I_j = \sum_{i=1}^{n} w_{ij} O_i + b_j \qquad \text{2-1}$$

where:

I_j = input value for node j

w_{ij} = connection weight between nodes i and j

O_i = output value at node i

b_j = bias for node j

An activation function then processes the input signal to eliminate large or negative

values and expose the ANN to nonlinearity. The activation function utilized by the ANN in this

study was the sigmoidal function, which normalizes input values outside the range of

approximately -5–5 to 0 or 1, respectively. The sigmoidal function was applied using Equation 2-

2 and is displayed graphically in Figure 2-2.

$$O_j = f(I_j) = \frac{1}{1+e^{-I_j}} \qquad \text{2-2}$$

where:

O_j = output at node j

$f(I_j)$ = sigmoidal activation function

I_j = input value at for node j

19
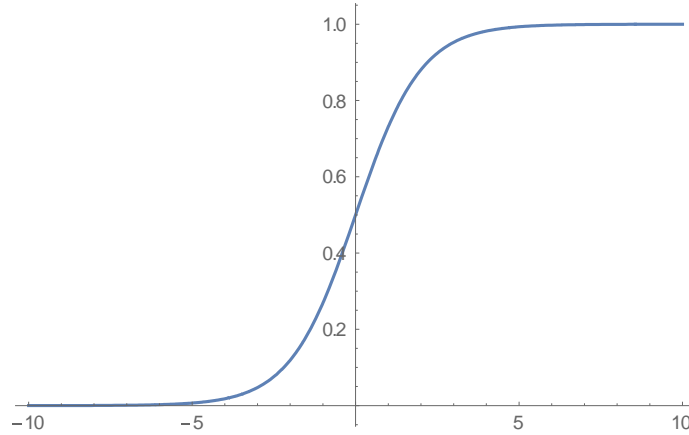
Figure 2-2: Sigmoidal function plot

Outputs from the hidden layer are then multiplied by their corresponding connection weights, summed, and added to the biases associated with the output nodes according to Equation 2-1 to obtain the input values for the output layer. These input values are then processed by the activation function and de-normalized to provide the predicted output values for the ANN. Error factors are calculated and used to compute the necessary incremental connection weight adjustments according to the following equation:

$$\Delta w_{ij} = \eta \delta_i O_j + \mu \Delta w_{ij}^{previous} \qquad \text{2-3}$$

where:

Δw_{ij} = incremental connection weight adjustment between nodes i and j

η = learning rate

δ_i = error factor of node i

μ = momentum rate

$\Delta w_{ij}^{previous}$ = incremental adjustment in connection weight from the previous iteration

Incremental changes in the biases are also calculated by the following equation:

$$\Delta b_i = \eta \delta_i + \mu \Delta b_i^{previous} \qquad \text{2-4}$$

where:

Δb_i = incremental bias adjustment for node i

20

$\Delta b_i{}^{previous}$ = incremental adjustment in bias from the previous iteration

Error factors are calculated for output nodes and hidden nodes using the following two equations, respectively:

$$\delta_i = (y_i - O_i)(1 - O_i)O_i \qquad \text{2-5}$$

$$\delta_i = \left(\sum_{k=1}^{n} \delta_k w_{ki}\right)(1 - O_i)O_i \qquad \text{2-6}$$

where:

δ_k = error factor of output node k calculated by Equation 2-6

w_{ki} = connection weight between hidden node and output nodes

y_i = actual value at output node i

O_i = predicted value at node i

Connection weights and biases are updated for all nodes in the network, and the entire process is repeated for every training dataset until a predetermined number of training iterations are reached or the output errors are reduced to an acceptable level. The ANN completes these iterations over a range of hidden nodes specified by the user. Utilizing too few hidden nodes can result in a network structure that is unable to solve the problem depending on its complexity, while using too many hidden nodes may result in overtraining, or memorization, of the data. The absolute maximum number of hidden nodes is calculated by the following equation:

$$MHN = \frac{TR - O}{I + O + 1} \qquad \text{2-7}$$

where:

MHN = maximum number of hidden nodes

TR = number of training datasets

O = number of output parameters

I = number of input parameters

Optimum Model Selection Criteria

The ANNs applied in this study were evaluated according to statistics calculated throughout the modeling process. Statistical measures including the coefficient of determination (R^2), the mean absolute relative error (MARE), and the average of squared error (ASE) were used to evaluate the models. These measures are calculated by the following equations:

$$R^2 = \sum{}^o \left(\frac{n \sum{}^n xy - \sum{}^n x \sum{}^n y}{\sqrt{n \sum{}^n x^2 - (\sum{}^n x)^2} \sqrt{n \sum{}^n y^2 - (\sum{}^n y)^2}} \right)^2 / o \qquad \text{2-8}$$

$$MARE(\%) = \frac{\sum{}^o \sum{}^n (\frac{|y-x|}{x} \times 100)}{o*n} \qquad \text{2-9}$$

$$ASE = \frac{\sum{}^o \sum{}^n (y-x)^2}{o*n} \qquad \text{2-10}$$

where:

x = actual value of a parameter

y = ANN predicted value

o = number of outputs

n = number of datasets

More effective ANNs are typically characterized by low MARE and ASE values and high R^2 values. The prediction capabilities of ANNs that display optimum statistical performance and utilize the fewest number of hidden nodes during the training and testing phase are reassessed with the validation datasets. Provided the optimum models perform well in the validation phase, the ANNs are then retrained on all datasets so that predictions can be made using the optimal network architecture trained with the entirety of the available data.

Chapter 3 - Methodology

The research project presented in this thesis is a continuation and expansion of the damage evaluation component of Al Rahmani's M.S. thesis (2012). The work in this study took place over two primary phases: establishment of a reinforced concrete beam database using the finite element (FE) method, and application of artificial neural networks (ANNs) to develop damage evaluation, or structural health prediction models.

Generation of Reinforced Concrete Beam Database

Consistent with Al-Rahmani's work (2012), reinforced concrete beams were modeled using the FE analysis software program Abaqus, version 6.13 (Dassault Systèmes Simulia Corp., 2013). However, Al-Rahmani's study (2012) was restricted to FE analysis of rectangular sections composed of two-dimensional (2D) plane stress elements with up to two cracks. It was desired that the FE models in this research represent concrete T-beams reinforced with mild steel bars in order to accurately emulate real-world bridge girders. Although all beams modeled in this study were simply-supported, future work can apply the processes described in this chapter to beams with any boundary condition configurations. Because construction and analysis of three-dimensional (3D) FE models requires a significant amount of time and computational processing power, the potential for using 2D reinforced concrete beams was first investigated. 2D planar shell parts with thicknesses equal to the beam widths were used to model both the concrete beam and steel reinforcement. Although rectangular beams were initially analyzed, T-beams were later modeled by partitioning the concrete beams so that the thicknesses and widths of the flanges could vary from those of the webs. The FE mesh applied to the beams and reinforcement consisted of 8-node quadratic (CPS8) and 6-node triangular (CPS6) plane stress elements. To provide a standard against which the performance of the 2D beam models could be measured, 3D

reinforced concrete T-beams were also modeled using Abaqus. These beam models were composed of 3D solid parts and were meshed with 10-node quadratic tetrahedral (C3D10) elements utilizing a free meshing technique. Reinforcement was modeled using 3D wire parts meshed with 3-node truss elements (T3D3), and three equally spaced reinforcing bars were embedded in all concrete beam models. Figures 3-1 and 3-2 display 3D Abaqus views of a sample reinforced concrete T-beam. Reinforcement was present in the sample beam, but is not depicted.
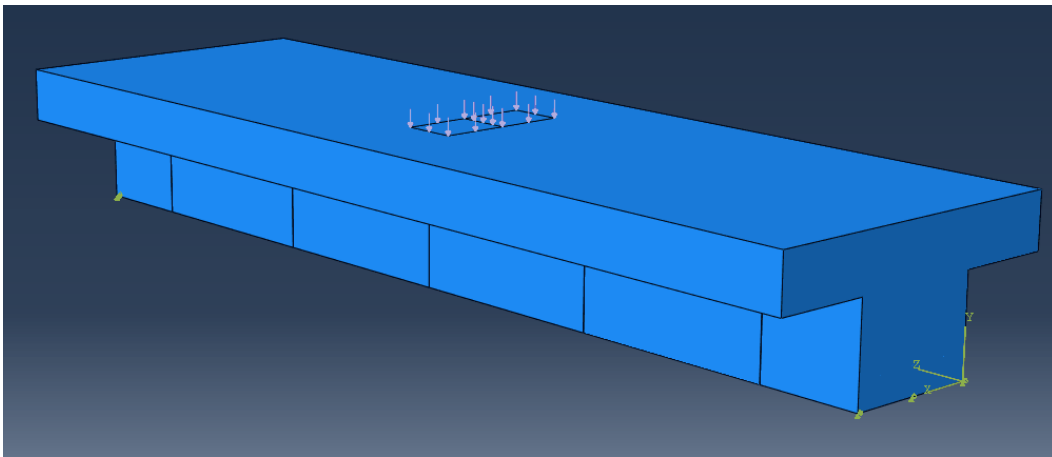
Figure 3-1: Abaqus view of 3D reinforced concrete T-beam model displaying cracks, boundary conditions, and applied load
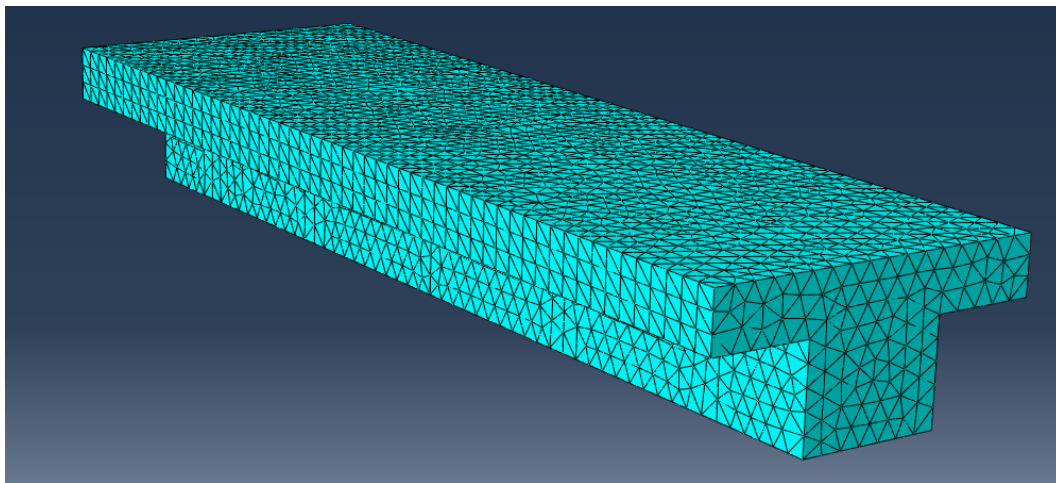
Figure 3-2: Abaqus view of 3D reinforced concrete T-beam model displaying concrete FE mesh

Material models were held constant throughout the study, and both concrete and steel were modeled as linear elastic. Poisson's ratios (*v*) for concrete and steel were set at 0.2 and 0.3, respectively, and the modulus of elasticity of steel (E_s) was taken to be 200,000 MPa. The modulus of elasticity of concrete was set according to the following equation:

$$E_C = 4{,}700\sqrt{f'_c} \hspace{4cm} \text{3-1}$$

where:

E_c = modulus of elasticity of concrete (MPa)

f'_c = 28-day compressive strength of concrete (MPa)

Other properties standardized between all models in this study included the concrete cover dimensions and the FE mesh size. The concrete cover was set at 50mm to the center of steel for both vertical and horizontal cover dimensions. The mesh size refers to the size of each element used in construction of the FE model and is entered in linear units for the applied measurement system (mm, in, etc.). The mesh size was initially established by attempting to achieve a balance between the precision of results afforded by a reduced mesh size, and the significantly increased Abaqus analysis time resulting from the use of small mesh sizes. The midspan deflection results for an uncracked sample 3D T-beam under a constant load with mesh sizes ranging from 50 mm – 25 mm are plotted in Figure 3-3. Sample Abaqus analysis times for the beam with mesh sizes of 48 mm, 35 mm, and 26 mm were 0:40, 1:00, and 2:13 minutes, respectively. From Figure 3-3, it can be seen that the variation in the deflection results is insignificant with respect to the variation in Abaqus analysis time. However, mesh attachment errors were noted for beams with small cracks having mesh sizes of 50 mm. Testing revealed that the frequency of mesh attachment errors reduced with decreasing mesh size. Therefore, the mesh size was set at 35 mm for both the concrete and steel elements in the beam models.
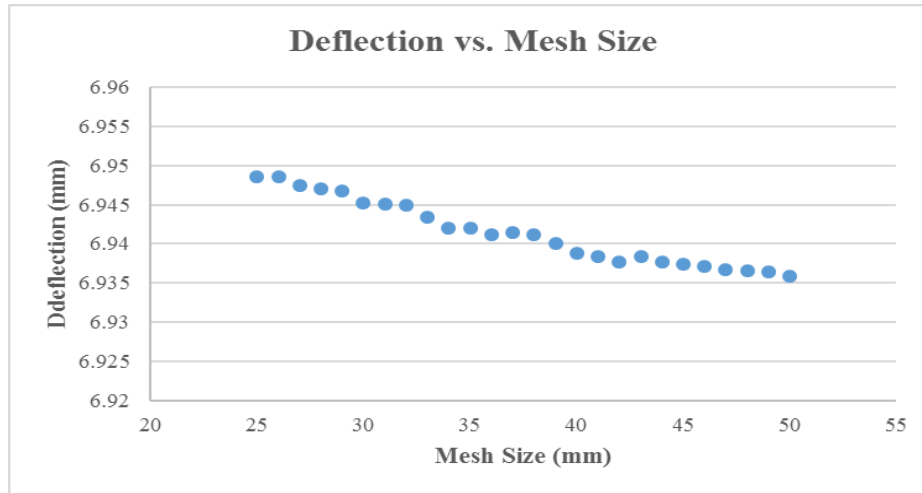
Figure 3-3: Variation in beam deflection with reduction of mesh size

For all FE models, nine stiffness nodes were inserted along the top face of the beam at equidistant spacing. The number of stiffness nodes was set according to Al-Rahmani's work (2012), in which beams with nine stiffness nodes provided optimal results. Each stiffness node was subjected to a static load of 100 kN in turn, and deflection results at the stiffness nodes were extracted from the Abaqus analysis. The load was applied as a point load for the 2D Abaqus analyses, but it was applied as an area load over a small section of the top face of the beam, centered on the stiffness node, for the 3D analyses. This variation in loading configurations was necessary because application of a point load for 3D beam models resulted in very high relative deflections at the stiffness node, suggesting that localized deformation was significant. For both 2D and 3D models, the stiffness at a given node was found by dividing the total applied force by the deflection at that node according to the following formula:

$$k_n = \frac{P_n}{\Delta_n}$$
<div align="right">3-2</div>

where:

k_n = stiffness at node n

P_n = applied load at node n

Δ_n = deflection at node n

Nodal stiffnesses were obtained for uncracked, or healthy, and cracked beams. Cracked

beams were modeled with discontinuities corresponding to the crack depth and width for 2D

beam models, and as extruded cuts in the beam web for 3D models. Only vertical flexural cracks

were considered in this study. The damage level in cracked beams was determined quantitatively

by calculating the stiffness ratio at each node, which was defined as the cracked stiffness divided

by the healthy stiffness of beams with identical geometries and material properties. Nodal

stiffness ratios were computed according to the following equation:

$$k\%_n = \frac{k_{n,cr}}{k_{n,h}}$$ 3-3

where:

$k\%_n$ = stiffness ratio at node n

$k_{n,cr}$ = stiffness at node n of a cracked beam

$k_{n,h}$ = stiffness at node n of a healthy beam

Nodal stiffness ratios were used to quantitatively describe the damage level, or residual

structural health, of the reinforced concrete beams. In general, beams with low nodal stiffness

ratios have deep, wide, or an extensive number of cracks. Nodal stiffness ratios were also found

to indicate damage locations within a beam; stiffness ratios of nodes near existing cracks are

typically lower than stiffness ratios of nodes far from damage locations. It was observed that

cracks placed very close to the beam supports resulted in unreasonably low nodal stiffness ratios.

This was thought to be due in part to a failure to meet Saint-Venant's principle, which suggests

that the stress distribution in a material may be assumed to be independent of the manner of load

application, except in the immediate vicinity of the applied loads (Beer, Johnston, Dewolf, &

Mazurek, 2012). The presence of both an applied load and a discontinuity (crack) in the beam

close to the supports likely introduced stress and strain concentrations that contributed to the

deflection of the beam. Therefore, crack placement was limited to 0.06–0.94 of the beam span

length; a range in which the nodal stiffness ratios were generally observed to stabilize to reasonable values.

Several healthy and cracked test beams were created with consistent geometric and material properties between the 2D rectangular beam, 2D T-beam, and 3D T-beam models. Stiffness ratios of these test beams were compared between the three Abaqus model types. Establishment of an equivalency between stiffness ratio results of the 2D rectangular beams and the 3D T-beams was not feasible due to the nonlinear nature of the stiffness relationship. Additionally, variations of nearly 25% were noted when comparing the stiffness ratios of the 2D and 3D T-beams; the stiffness ratios and percent variation between 2D and 3D models for a sample reinforced concrete beam with five cracks are displayed in Table 3-1. Therefore, the study proceeded using 3D reinforced concrete T-beam FE models in order to achieve the desired similarity to actual structural members.

Table 3-1: Stiffness ratio comparison of sample T-beam 2D and 3D models

	k_1	k_2	k_3	k_4	k_5	k_6	k_7	k_8	k_9
2D k%$_n$	0.78503	0.66801	0.64298	0.60362	0.59096	0.60470	0.64411	0.66866	0.78576
3D k%$_n$	0.69911	0.56362	0.53499	0.49667	0.47724	0.49490	0.54033	0.56585	0.69916
Variation (%)	12.29	18.52	20.18	21.53	23.83	22.19	19.21	18.17	12.39

It was anticipated that stiffness ratios at node pairs on opposite ends of the beam (k%$_1$ and k%$_9$, k%$_2$ and k%$_8$, etc.) would be equal for beams with symmetric cracks. Observation of Table 3-1 reveals that the mirrored stiffness ratios are very similar, but not identical, even though the cracks were modeled as perfectly symmetric. The variation was determined to be due to the automated meshing technique applied by Abaqus to develop the FE model. To fit the cracks and mesh the beam, the automated meshing technique produced a mesh that is not perfectly symmetric across the span of the beam. Therefore, the FE analysis produced slightly different deflections at mirrored stiffness nodes, even though theory indicates they should be identical.

The 3D reinforced concrete T-beam database was established by variation of the geometric and material parameters for all beams as well as cracking parameters for cracked beams. Geometric parameters included the width of the beam web cross-section (b_w), the depth of the entire beam cross-section (h), the height of the beam flange, or slab (h_s), and the beam span length (L). The beam flange was modeled according to the provisions of American Concrete Institute (ACI) 318-14 Section 8.4.1.8 for two-way slabs, which indicates that the total width of the T-beam flange should be equal to the sum of the web width and twice the depth of the beam extending below the flange as shown in Figure 3-4 (ACI Committee 318, 2014).
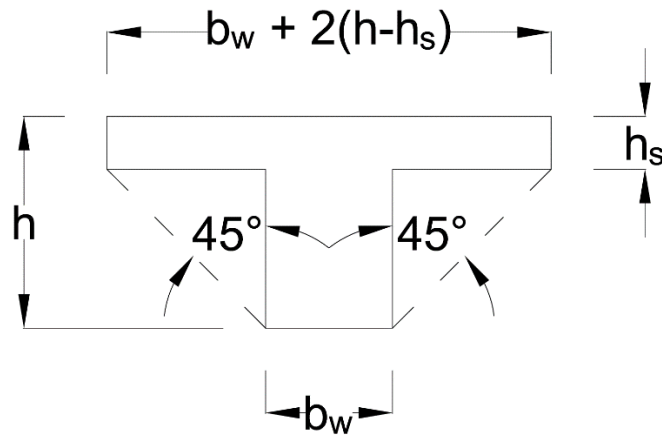
Figure 3-4: T-beam flange dimensions

The size of the reinforcing bars in each beam depended upon the steel ratio (ρ) and the beam's cross-sectional area according to the relationship $A_s = \rho b_w d$, where A_s is the total cross-sectional area of steel reinforcement and d is the effective depth of the beam section, taken as the beam depth minus the cover. The 28-day concrete compressive strength (f'_c) was the only variable material parameter. Cracking parameters included the location (b_{cr}), depth (d_{cr}), and width (w_{cr}) of each crack, and all crack locations were measured from a constant (left) edge of the beam. With the exception of f'_c, ρ, and w_{cr}, all parameters were directly normalized with respect to a beam web width of $b_w = 250$ mm, resulting in the normalized parameters b_w/h, h_s/h,

L/h, b_{cr}/L, and d_{cr}/h. This normalization was performed so that the results of this study could be applied to beams of various sizes. The slab height was also set to remain constant at $h_s = 100$ mm in order to limit the number of beams created through parametric variation, although the normalized parameter h_s/h fluctuated due to variability in the beam depth. Figure 3-5 displays an elevation view of a beam with two cracks and highlights several geometric property dimensions and all stiffness node locations.
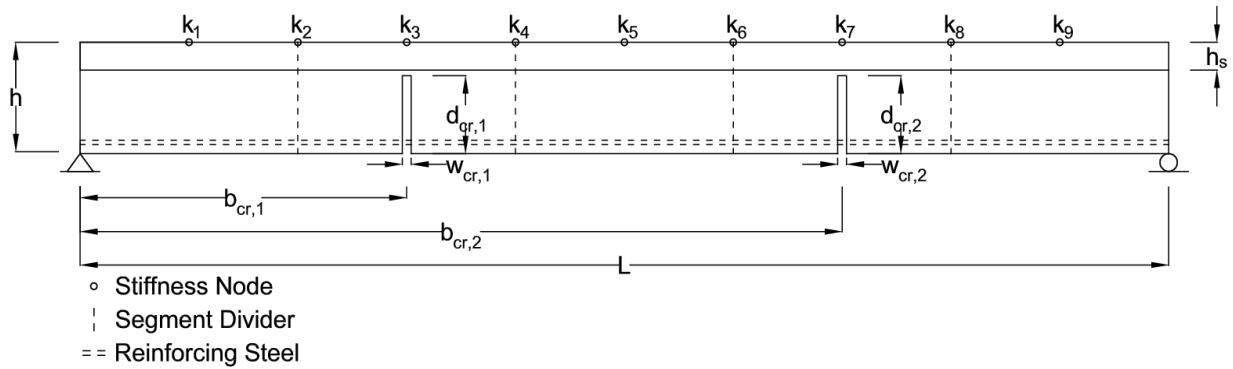
Figure 3-5: Reinforced concrete T-beam elevation view

All beams were initially divided into nine equal segments that could each contain up to one crack. Seventy-two healthy beams were first created to provide reference results for computation of the nodal stiffness ratios for cracked beams. A majority of the beam database was composed of beams with a single crack; a total of 6,624 singly-cracked beams were modeled. These beams were allowed to have a crack in any segment, and crack locations were varied between the beginning, middle, and end of each segment. Significantly fewer beams (1,296) with five cracks were generated. Two crack location configurations were allowed for these beams, and crack locations were set at the center of each segment. Crack location configurations are defined as a unique combination of cracked segments and b_{cr}/L values. Only 864 beams with nine cracks were created; three crack location configurations were considered and a crack existed in each segment. By exposing the ANNs to a large amount of data for singly-cracked beams with

30

sample data for beams with five and nine cracks, the neural networks were anticipated to provide reasonably accurate damage predictions for beams with 0–9 cracks in any configuration.

Although this methodology appeared to be sound according to statistical results provided by the ANN analysis, extended testing with various numbers of cracks and crack location configurations revealed that the trained ANN models produced unreasonable damage predictions in many scenarios. The hypothesis was made that more asymmetrical data, crack location variability within the segments, and crack location configurations were required to train the networks and achieve reasonable damage prediction results. Additional datasets were created for beams with five cracks (2,304), and a limited number of beams with two (384), three (448), and four (320) cracks were produced. Because an impractical number of datasets would need to be generated to provide enough training data for the ANNs to accurately predict damage in beams with 0–9 cracks, the datasets for beams with nine cracks were discarded and up to a single crack was allowed in five segments only. These segments are indicated by the dashed lines in Figure 3-3. The modeling process resulted in the generation of 11,448 unique datasets, and the parameter variability used to construct the beam database is displayed in Tables 3-2 to 3-7. For geometric and material parameters, the values in each column vary with respect to all other parameters. Similarly, values within each row vary with respect to all other parameters for the cracking parameters. The product of the number of variable terms for all parameters provides the total number of datasets (permutations) for beams with the specified number of cracks.

Table 3-2: Parameter variability for singly-cracked beams

Parameters	Values					Variable Terms
b_w/h	0.5	0.7	0.9			3
L/h	7	10	13			3
ρ	0.005	0.01				2
f'_c (MPa)	20	30	40	50		4
	Segment 1	Segment 2	Segment 3	Segment 4	Segment 5	
b_{cr}/L	0.06 0.1 0.15 0.2	0.2 0.25 0.3 0.35 0.4	0.4 0.45 0.5 0.55 0.6	0.6 0.65 0.7 0.75 0.8	0.8 0.85 0.9 0.94	23
	Crack 1					
d_{cr}/h	0.25 0.64					2
w_{cr} (mm)	1 5					2
			Number of Beam Datasets =			6624

* $b_w = 250$ mm and $h_s = 100$ mm

Table 3-3: Parameter variability for beams with five cracks

Parameters	Values					Variable Terms
b_w/h	0.5	0.7	0.9			3
L/h	7	10	13			3
ρ	0.005	0.01				2
f'_c (MPa)	20	30	40	50		4
	Segment 1	Segment 2	Segment 3	Segment 4	Segment 5	
b_{cr}/L	0.1	0.3	0.5	0.7	0.9	2
	0.2	0.4	0.5	0.6	0.8	
	Crack 1	Crack 2	Crack 3	Crack 4	Crack 5	
d_{cr}/h	0.25	0.25	0.25	0.25	0.25	3
	0.5	0.5	0.5	0.5	0.5	
	0.64	0.64	0.64	0.64	0.64	
w_{cr} (mm)	1	1	1	1	1	3
	2.5	2.5	2.5	2.5	2.5	
	5	5	5	5	5	
	Number of Beam Datasets =					1296

* $b_w = 250$ mm and $h_s = 100$ mm

Table 3-4: Parameter variability for additional beams with five cracks

Parameters	Values					Variable Terms
b_w/h	0.5	0.9				2
L/h	7	13				2
ρ	0.005	0.01				2
f'_c (MPa)	20	50				2
	Segment 1	Segment 2	Segment 3	Segment 4	Segment 5	
b_{cr}/L	0.06	0.21	0.41	0.61	0.81	4
	0.19	0.39	0.59	0.79	0.94	
	0.19	0.21	0.59	0.61	0.94	
	0.06	0.39	0.41	0.79	0.81	
	Crack 1	Crack 2	Crack 3	Crack 4	Crack 5	
d_{cr}/h	0.64	0.1	0.64	0.1	0.64	6
	0.1	0.64	0.64	0.64	0.1	
	0.1	0.64	0.1	0.64	0.1	
	0.64	0.1	0.1	0.1	0.64	
	0.1	0.1	0.64	0.64	0.64	
	0.64	0.64	0.64	0.1	0.1	
w_{cr} (mm)	2.5	0.05	2.5	0.05	2.5	6
	0.05	2.5	2.5	2.5	0.05	
	0.05	2.5	0.05	2.5	0.05	
	2.5	0.05	0.05	0.05	2.5	
	0.05	0.05	2.5	2.5	2.5	
	2.5	2.5	2.5	0.05	0.05	
	Number of Beam Datasets =					2304

* $b_w = 250$ mm and $h_s = 100$ mm

Table 3-5: Parameter variability for beams with two cracks

Parameters	Values					Variable Terms
b_w/h	0.5	0.9				2
L/h	7	13				2
ρ	0.005	0.01				2
f'_c (MPa)	20	50				2
	Segment 1	Segment 2	Segment 3	Segment 4	Segment 5	
b_{cr}/L	0.1	0.3				6
	0.1				0.9	
		0.3	0.5			
		0.3		0.7		
			0.5	0.7		
				0.7	0.9	
	Crack 1	Crack 2				
d_{cr}/h	0.64	0.1				2
	0.1	0.64				
w_{cr} (mm)	5	0.05				2
	0.05	5				
		Number of Beam Datasets =				384

* $b_w = 250$ mm and $h_s = 100$ mm

Table 3-6: Parameter variability for beams with three cracks

Parameters	Values					Variable Terms
b_w/h	0.5	0.9				2
L/h	7	13				2
ρ	0.005	0.01				2
f'_c (MPa)	20	50				2
	Segment 1	Segment 2	Segment 3	Segment 4	Segment 5	
	0.1		0.5		0.9	
	0.1			0.7	0.9	
	0.1	0.3	0.5			
b_{cr}/L	0.1	0.3		0.7		7
	0.1	0.3			0.9	
		0.3		0.7	0.9	
			0.5	0.7	0.9	
	Crack 1	Crack 2	Crack 3			
d_{cr}/h	0.64	0.25	0.1			2
	0.1	0.25	0.64			
w_{cr} (mm)	5	2.5	0.05			2
	0.05	2.5	5			
		Number of Beam Datasets =				448

* $b_w = 250$ mm and $h_s = 100$ mm

36

Table 3-7: Parameter variability for beams with four cracks

Parameters	Values					Variable Terms
b_w/h	0.5	0.9				2
L/h	7	13				2
ρ	0.005	0.01				2
f'_c (MPa)	20	50				2
	Segment 1	Segment 2	Segment 3	Segment 4	Segment 5	
	0.1	0.3	0.5	0.7		
	0.1	0.3	0.5		0.9	
b_{cr}/L	0.1	0.3		0.7	0.9	5
	0.1		0.5	0.7	0.9	
		0.3	0.5	0.7	0.9	
	Crack 1	Crack 2	Crack 3	Crack 4		
d_{cr}/h	0.64	0.25	0.64	0.1		2
	0.1	0.64	0.25	0.64		
w_{cr} (mm)	5	2.5	5	0.05		2
	0.05	5	2.5	5		
	Number of Beam Datasets =					320

* b_w = 250 mm and h_s = 100 mm

Segments absent of cracks were initially assigned b_{cr}/L, d_{cr}/h, and w_{cr} values of zero.

However, Dr. Najjar advised that the ANNs would require the crack locations to be nonzero in

order to establish adequate prediction logic (Y. Najjar, personal communication, December 11,

2015). Therefore, b_{cr}/L values were set at the center of each segment for all segments with no

crack present, while d_{cr}/h and w_{cr} values were maintained at zero. The possibility of expanding

the database without generating additional FE models was noted, and datasets for the healthy

beams and beams with one, two, three, and four cracks were duplicated according to the four

crack location configurations shown in Table 3-4. Segments without cracks for these beams were

assigned b_{cr}/L values corresponding to these four crack location configurations. For example, a

beam with a single crack at midspan would first be assigned b_{cr}/L values of 0.1, 0.3, 0.5, 0.7, and

0.9 in segments 1, 2, 3, 4, and 5, respectively. This beam would then be duplicated by copying

all parameters and changing the b_{cr}/L values for all segments without cracks, or segments 1, 2, 4,

and 5, to 0.06, 0.21, 0.61, and 0.81, respectively. These values correspond to the b_{cr}/L values for the first crack location configuration in Table 3-4. The beam could be duplicated three more times according to the three remaining crack location configurations. This duplication procedure would result in five beams with identical geometric, material, and cracking parameters (with the exception of crack locations in segments devoid of cracks), as well as identical nodal stiffness ratios and health indices. Using this methodology, the beam database was expanded from 11,448 datasets to 42,840 datasets. As advised by Dr. Najjar, all duplicated datasets were applied as training sets in ANN analyses.

Abaqus macros were recorded as Python scripts for the creation of healthy beams and beams with one, two, three, four, and five cracks. These scripts were adapted according to Al-Rahmani's work (2012) and were used to automate the generation of input files (.inp files) for 3D models through the Abaqus user interface. A Python script provided by Al-Rahmani allowed automated analysis of input files by directly interfacing with Abaqus, and a final script extracted the resultant nodal deflections from the Abaqus binary output databases (.odb files). These deflections were used to determine the nodal stiffness ratios, as previously described. Example generation, analysis, and extraction scripts are contained in Appendix A.

To verify that the results of this approach would be applicable to a range of typical girder sizes, 50 cracked beams were selected at random from the 11,448 unique datasets. All geometric, material, and cracking parameters for these beams were held constant with the exception of the web width, and additional healthy and cracked beams were modeled with these parameters for web widths of 200 mm and 300 mm. The h_s/h normalized parameter remained constant for these additional models, causing the height of the slab to be 80 mm and 120 mm for all beams with web widths of 200 mm and 300 mm, respectively. After the FE models were analyzed and nodal

deflections were extracted, the health indices, defined by Equation 3-5 and the corresponding text, of the additional cracked beams were calculated and compared to the health indices of the 50 reference cracked beams from the original dataset. Geometric, material, and cracking parameters for these beams and the health indices for the three web widths are included in Appendix B. The mean average relative errors (MARE), coefficients of determination (R^2), and average squared errors (ASE) were calculated for the variation between the health indices of the additional and reference beams, as shown in Table 3-8. These statistical measures were calculated according to Equations 2-8 to 2-10, where the health indices of the reference and additional beams functioned as the actual and predicted results, respectively. Health indices for beams with web widths of 250 mm are plotted against health indices of beams with web widths of 200 mm and 300 mm in Figures 3-6a and 3-6b, respectively.

Table 3-8: Statistical comparisons between health indices of beams with different widths

	Beam Widths 250mm and 200mm	Beam Widths 250mm and 300mm
MARE	1.4525	0.5198
R^2	0.99103	0.99771
ASE	0.000295	0.000034
ρ_c	0.97667	0.99687
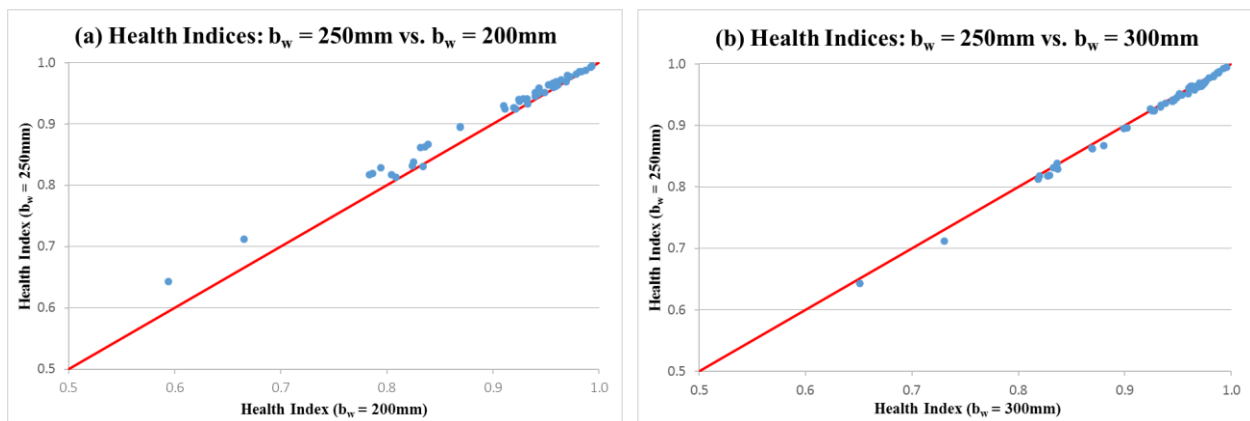
Figure 3-6: Graphical comparison between health indices of beams with web widths of (a) 250 mm and 200mm and (b) 250 mm and 300 mm

The low errors and high coefficients of determination evident in Table 3-8 indicate good agreement between the health index results of beams with different web widths. As shown in Figure 3-6, the health indices of large beams (b_w = 300 mm) are more similar to the health indices of the reference beams than are the health indices of small beams (b_w = 200 mm). A brief sensitivity analysis, performed by reducing the mesh size from 35 mm to 25 mm for the small beams, resulted in similar health indices and revealed that mesh coarseness did not substantially affect the results. It was therefore hypothesized that the relationship between the beam size and the stiffness provided by the FE model mesh is nonlinear and cracking damage affects the structural health of small beams significantly more than large beams. In addition to the MARE, R^2, and ASE results, Lin's concordance correlation coefficient values (ρ_c) are displayed in Table 3-8. Lin's concordance correlation coefficient, defined by Equation 3-4, serves as a reproducibility index by which the quality of new measurements can be judged, and ranges between 0 for poor correlation and 1 for perfect correlation (Lin, 1989). This coefficient assesses how well the damage results for beams with web widths of 250 mm can be applied to beams with web widths ranging from 200 mm to 300 mm. Lin's concordance correlation coefficients exceeded 0.975 for both comparisons. The high value of this coefficient, in addition to the favorable results of the other three statistical measures, indicated that the results of this study can be applied to a variety of typical girder sizes.

$$\rho_c = \frac{2\rho\,\sigma_r\sigma_t}{\sigma_r^2+\sigma_t^2+(\mu_r-\mu_t)^2} \hspace{4cm} 3\text{-}4$$

where:
ρ = square root of R^2, or Pearson correlation coefficient between the reference and test data
σ_r = square root of the variance, or standard deviation, of the reference data
σ_t = square root of the variance, or standard deviations of the test data
μ_r = mean of the reference data
μ_r = mean of the test data

ANN Modeling for Structural Health Prediction

Two ANNs were trained in order to develop structural health prediction models for reinforced concrete T-beams. The first network was trained with the geometric, material, and cracking parameters (b_w/h, h_s/h, L/h, ρ, f'_c, $b_{cr,m}/L$, $d_{cr,m}/h$, and $w_{cr,m}$, where m denotes the mth crack) as inputs and the stiffness ratios ($k\%_n$, where n is the nth stiffness node) at the nine equidistant stiffness nodes as outputs. Because solving for nine different outputs given 20 input parameters presents a highly complex problem, the second ANN was trained with the same input parameters, but only one output parameter: the health index ($ki\%$). Referencing Al-Rahmani's work (2012), the health index was calculated by integrating the area under the stiffness ratio profile over the beam span length. This relationship is displayed in Figure 3-7 where the health index is taken approximately as the hatched area under the stiffness ratio profile for a sample beam with five cracks. A quantifiable measure of damage was maintained by resolving the nodal stiffness ratios into a single term, thereby simplifying the problem that the ANN was required to solve. The health index is described by the following equation:

$$Health\ Index\ (ki\%) = \left(\frac{l_n}{L}\right)\left(1 + \sum_{n=1}^{n=9} k\%_n\right) \qquad \text{3-5}$$

where:

l_n = distance between two consecutive stiffness nodes

L = beam span length

$k\%_n$ = stiffness ratio at node n
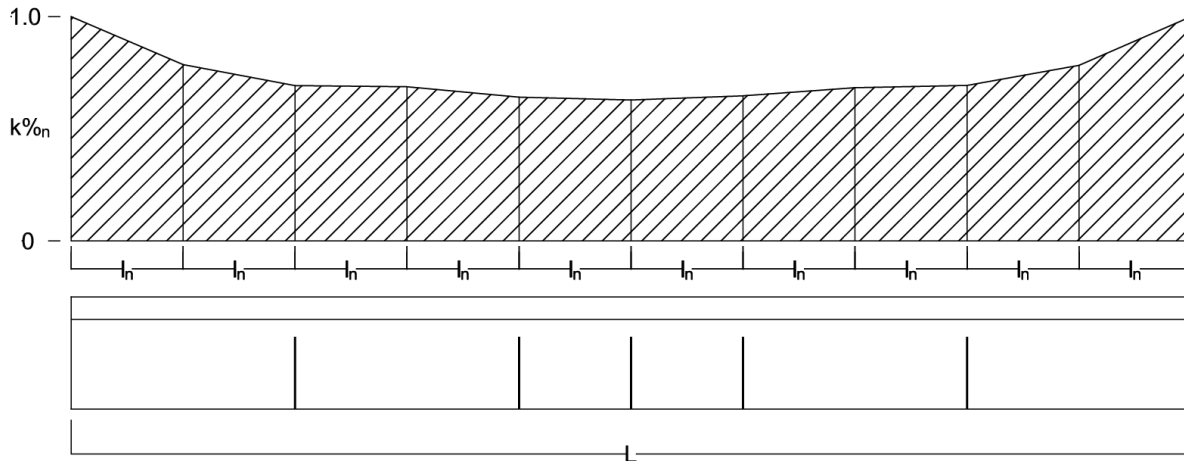
Figure 3-7: Graphical description of health index

Microsoft Excel spreadsheets were used to maintain the beam database and format the datasets for ANN analyses. In addition to the 20 geometric, material, and cracking input parameters and the nine nodal stiffness ratios or the health index, the spreadsheets also contained an identification number (*ID*) and a set identifier (*Set*). The identification number served as a term by which beams were referenced between the spreadsheets and ANNs. The set identifiers had values of one, two, or three, and indicated whether the beam data was used for training, testing, or validation of the ANN, respectively. These identifiers were assigned manually in a semi-random fashion, but some beams with parameters having extreme values were assigned to the training dataset according to the ANN modeling procedure described in Chapter 2. Also according to this procedure, 50%, 25%, and 25% of the original unique beam datasets were assigned to the training, testing, and validation sets, respectively. Table 3-9 displays a sample header for the Microsoft Excel spreadsheets where "I" indicates an input parameter, "O" indicates an output parameter, "m" indicates the mth crack, and "n" indicates the nth stiffness node. For the health index ANN analyses, the nine stiffness ratios were replaced with the health index. Although the parameters were reordered for formatting, the input and output parameters

for a sample of approximately 500 datasets from the unique beam database can are presented in

Appendix C.

Table 3-9: Sample Microsoft Excel database header

ID	b_w/h	h_s/h	L/h	ρ	f'_c (MPa)	$b_{cr,m}/L$	$d_{cr,m}/h$	$w_{cr,m}$ (mm)	$k\%_n$	Set
#	I	I	I	I	I	I	I	I	O	1, 2, or 3

Both the nodal stiffness ratio and health index prediction models were developed

according to the ANN modeling procedure described in Chapter 2. The final reinforced concrete

beam database contained data for 42,480 beams, and 37,116 (5,724 original and 31,392

duplicated), 2,862, and 2,862 beams were employed in training, testing, and validating the

ANNs, respectively. Minimum and maximum parameter value ranges supplied to the ANNs

were expanded to keep the actual parameter values in the sensitive region of the sigmoidal

activation function of the network. The input parameter range was expanded to allow the input

parameters to fit within 10%−90% of the expanded range. Nodal stiffness ratios and health

indices were limited to those of a healthy beam ($<=1.0$), so the output parameter range was

expanded so that only the minimum values were modified and the output parameters fit within

20%−100% of the expanded range. The expanded parameter ranges are displayed in Table 3-10.

Table 3-10: ANN expanded parameter ranges

Inputs			Outputs		
Parameter	Minimum	Maximum	Parameter	Minimum	Maximum
b_w/h	0.45	0.95	$k\%_1$	0.56788	1
h_s/h	0.18	0.38	$k\%_2$	0.41816	1
L/h	6.25	13.75	$k\%_3$	0.37999	1
ρ	0.00438	0.01063	$k\%_4$	0.3289	1
f'_c	16.25	53.75	$k\%_5$	0.30298	1
b_{cr1}/L	0.0425	0.2175	$k\%_6$	0.32653	1
d_{cr1}/h	-0.0799	0.71887	$k\%_7$	0.38711	1
w_{cr1}	-0.625	5.62506	$k\%_8$	0.42113	1
b_{cr2}/L	0.175	0.425	$k\%_9$	0.57258	1
d_{cr2}/h	-0.0799	0.71887	$ki\%$	0.47625	1
w_{cr2}	-0.625	5.62504			
b_{cr3}/L	0.375	0.625			
d_{cr3}/h	-0.0799	0.71887			
w_{cr3}	-0.625	5.62506			
b_{cr4}/L	0.575	0.825			
d_{cr4}/h	-0.0799	0.71887			
w_{cr4}	-0.625	5.62506			
b_{cr5}/L	0.7825	0.9575			
d_{cr5}/h	-0.0799	0.71887			
w_{cr5}	-0.625	5.62506			

An ANN program with a single hidden layer was utilized in this study, and the initial

number of hidden nodes was set to vary between 2 and 10. Although the maximum number of

hidden nodes calculated by Equation 2-7 exceeded 270, the use of 20 hidden nodes as a

maximum was found to sufficiently facilitate learning within the neural network. In addition to

reducing program run time, using fewer than the calculated maximum number of hidden nodes

helped the ANNs avoid memorization. The training and testing datasets were used to train nine

network architectures, each corresponding to a different number of initial hidden nodes. The

ANNs were first evaluated by their ASE, and then by their MARE and R^2. The optimal initial

and final numbers of hidden nodes and the number of iterations at the final hidden node were

recorded for the most effective three networks in terms of their statistical measure performance.

These optimal networks were then tested using the validation datasets and trained on the entire

reinforced concrete T-beam database in order to expose them to all available data and establish

robust structural health prediction models. Chapter 4 discusses the statistical results for these

optimum models and describes the other considerations made during the selection of the final

network structures for nodal stiffness ratio and health index prediction applications.

Chapter 4 - Results and Discussion

As described in Chapter 3, the artificial neural network (ANN) training process and optimal model selection procedure was applied to the finite element (FE) reinforced concrete beam model database to establish nodal stiffness ratio and health index prediction models. Model identification was based on the following nomenclature: (initial number of hidden nodes-final number of hidden nodes-iterations at the final number of hidden nodes). Statistical results from the initial training and testing phase revealed the best-performing network architectures to be models 4-18-20000, 5-19-20000, and 6-19-20000 for nodal stiffness ratio predictions and models 2-19-20000, 4-19-20000, and 6-19-20000 for health index predictions. These ANNs were then tested on the validation sets and trained on the entire database (All Data). Detailed statistical results for these optimal networks are displayed in Tables 4-1 and 4-2.

Table 4-1: Statistical results for optimal nodal stiffness ratio prediction ANNs

		Model 1 (4-18-20000)	Model 2 (5-19-20000)	Model 3 (6-19-20000)
Training	MARE	0.575	0.532	0.512
	R^2	0.9832	0.98515	0.98572
	ASE	0.000188	0.000158	0.000157
Testing	MARE	0.884	0.808	0.894
	R^2	0.9817	0.98617	0.98358
	ASE	0.000414	0.000334	0.000422
Validation	MARE	0.965	0.837	0.938
	R^2	0.97637	0.98492	0.98098
	ASE	0.000496	0.00034	0.000451
All Data	MARE	0.611	0.619	0.594
	R^2	0.986	0.98411	0.98499
	ASE	0.00019	0.000221	0.000195

Table 4-2: Statistical results for optimal health index prediction ANNs

		Model 1 (2-19-20000)	Model 2 (4-19-20000)	Model 3 (6-19-20000)
Training	MARE	0.17	0.144	0.162
	R^2	0.99762	0.99818	0.99778
	ASE	0.000018	0.000013	0.000017
Testing	MARE	0.262	0.204	0.233
	R^2	0.99808	0.9985	0.99808
	ASE	0.000041	0.000027	0.000035
Validation	MARE	0.259	0.25	0.282
	R^2	0.99761	0.99761	0.99683
	ASE	0.000038	0.00004	0.000052
All Data	MARE	0.171	0.258	0.179
	R^2	0.998	0.99578	0.99778
	ASE	0.000018	0.000041	0.00002

Several general observations and trends are evident in Tables 4-1 and 4-2. First and foremost, the networks displayed excellent prediction accuracies with low mean average relative errors (MARE) and average squared errors (ASE) in all phases and coefficients of determination (R^2) in excess of 0.975 and 0.995 for the nodal stiffness ratio and health index ANNs, respectively. As expected, the health index networks, which predicted one term, performed better according to all statistical measures when compared to the nodal stiffness ratio networks that had to predict nine terms. For both prediction networks, Model 2 displayed better performance in the testing and validation phases as compared to the other models. When trained with the entire database, however, the statistical performance of the Model 2 networks was lower than the Model 1 and 3 networks. Because no model displayed optimal prediction capabilities in all three phases, additional investigations were performed to determine which models were best suited for nodal stiffness ratio and health index prediction applications.

To further test the prediction accuracies of the optimum ANN models, a small database of beams with two, three, and four cracks was established. Input parameter values were selected to be within the range, but dissimilar from the input parameter values found within the main database for beams with two, three, and four cracks. Beam geometric and material parameters were set at $b_w/h = 0.7$, $h_s/h = 0.28$ $L/h = 10$, $\rho = 0.0075$, and $f'_c = 35$ MPa to limit the number of additional FE models required to be generated. Use of these parameters also ensured that only one healthy beam need be created. Cracking parameters were varied by inspection, and segments without cracks were assigned b_{cr}/L values at the center of the segment and crack depth and width values of zero. A summary of the variability in the cracking parameters is displayed in Tables 4-3 to 4-5. Each row represents a variable crack description term, and the product of the variable terms gives the number of additional testing datasets for beams with two, three, and four cracks. In total, 199 beams (1 healthy and 198 cracked) were used to populate the testing database.

Table 4-3: Parameter variability for additional test beams with two cracks

	Segment 1	Segment 2	Segment 3	Segment 4	Segment 5	Variable Terms
b_{cr}/L	0.06		0.4			8
	0.2	0.4				
		0.2	0.4			
		0.2		0.8		
		0.4		0.6		
			0.6	0.8		
			0.6		0.94	
				0.6	0.8	
	Crack 1	Crack 2				
d_{cr}/h	0.2	0.5				3
	0.4	0.4				
	0.5	0.2				
w_{cr} (mm)	2	4				3
	3	3				
	4	2				
				Number of Beam Datasets =		72

* $b_w = 250$ mm, $h_s = 100$ mm, $h_s/h = 0.28$, $b_w/h = 0.7$, $L/h = 10$, $\rho = 0.0075$, and $f'_c = 35$ MPa

Table 4-4: Parameter variability for additional test beams with three cracks

	Segment 1	Segment 2	Segment 3	Segment 4	Segment 5	Variable Terms
b_{cr}/L	0.06	0.2	0.4			8
	0.06	0.2		0.8		
	0.2	0.4	0.5			
	0.2	0.4		0.6		
		0.2		0.8	0.94	
		0.4		0.6	0.8	
			0.4	0.8	0.94	
			0.5	0.6	0.8	
	Crack 1	Crack 2	Crack 3			
d_{cr}/h	0.2	0.5	0.2			3
	0.4	0.4	0.4			
	0.5	0.2	0.5			
w_{cr} (mm)	2	4	2			3
	3	3	3			
	4	2	4			
				Number of Beam Datasets =		72

* $b_w = 250$ mm, $h_s = 100$ mm, $h_s/h = 0.28$, $b_w/h = 0.7$, $L/h = 10$, $\rho = 0.0075$, and $f'_c = 35$ MPa

Table 4-5: Parameter variability for additional test beams with four cracks

	Segment 1	Segment 2	Segment 3	Segment 4	Segment 5	Variable Terms
b_{cr}/L	0.06	0.2	0.4	0.8		6
	0.06	0.2		0.8	0.94	
	0.2	0.4	0.5	0.6		
	0.2	0.4		0.6	0.8	
		0.4	0.5	0.6	0.8	
		0.2	0.6	0.8	0.94	
	Crack 1	Crack 2	Crack 3	Crack 4		
d_{cr}/h	0.2	0.5	0.5	0.5		3
	0.4	0.4	0.4	0.4		
	0.5	0.2	0.2	0.5		
w_{cr} (mm)	2	4	4	2		3
	3	3	3	3		
	4	2	2	4		
				Number of Beam Datasets =		54

* $b_w = 250$ mm, $h_s = 100$ mm, $h_s/h = 0.28$, $b_w/h = 0.7$, $L/h = 10$, $\rho = 0.0075$, and $f'_c = 35$ MPa

The beam models were generated and analyzed, and deflection results were extracted using the Abaqus-Python interface scripts. Nodal stiffness ratios and health indices for the beams

were calculated, and the three optimum models for each ANN prediction network were reformatted to be trained on the entire main database and tested on the 199 additional datasets. Statistical results from the ANN analyses of the additional testing sets for nodal stiffness ratio and health index prediction models are displayed in Tables 4-6 and 4-7.

Table 4-6: Statistical results for optimal nodal stiffness ratio prediction ANNs tested on additional data for beams with two, three, and four cracks

	Model 1 (4-18-20000)	Model 2 (5-19-20000)	Model 3 (6-19-20000)
MARE	2.069	2.797	2.487
R^2	0.85052	0.79006	0.83598
ASE	0.002142	0.00326	0.002429

Table 4-7: Statistical results for optimal health index prediction ANNs tested on additional data for beams with two, three, and four cracks

	Model 1 (2-19-20000)	Model 2 (4-19-20000)	Model 3 (6-19-20000)
MARE	1.646	1.94	0.984
R^2	0.74262	0.80498	0.86761
ASE	0.00118	0.001599	0.000542

Although R^2 values for the nodal stiffness ratio and health index prediction models were similar, MARE and ASE values were lower for the health index prediction models, as expected. The statistical results revealed a drop in prediction accuracy for the additional testing sets with respect to the results of the main database, shown in Tables 4-1 and 4-2. Because parameter values used to generate the additional testing sets were intentionally selected to be dissimilar from parameter values found in the main database, some loss of prediction accuracy was expected. However, networks achieving R^2 values in excess of 0.85 were still established. Enhanced prediction accuracies would be attained by training the ANNs with additional data for beams with two, three, and four cracks.

Dr. Najjar recommended that the additional testing sets of beams with two, three, and four cracks be exchanged with random beams from the training sets of the main database in order to verify the ANNs (Y. Najjar, personal communication, December 11, 2015). The ANN training process and optimal model selection procedure was applied to the adjusted data to establish health index prediction networks, and the three optimum models were trained on the altered database and tested on the 199 exchanged beams. The statistical results were excellent with low errors and R^2 values exceeding 0.99 for all health index prediction models. Testing results for the exchanged beams are displayed in Table 4-8.

Table 4-8: Statistical results for optimal health index ANNs trained on altered database and tested on exchanged beam sets

	Model 1 (4-19-5400)	Model 2 (6-17-9100)	Model 3 (10-19-6000)
MARE	0.297	0.245	0.227
R^2	0.99823	0.99818	0.99869
ASE	0.000052	0.000032	0.000028

As previously described, the datasets for beams with two, three, and four cracks were successfully used to test the optimum ANN models' prediction accuracies on dissimilar data. However, it was desired that the networks be tested on entirely random data in order to obtain an unbiased assessment of the models' prediction capabilities. Therefore, 75 cracked beam datasets, corresponding to equal numbers of beams with 1–5 cracks, were generated using Microsoft Excel's RAND() function to establish the value of each input parameter. Seventy-five healthy beam datasets with geometric and material parameters identical to those of the cracked beams were also generated to serve as references for the calculation of nodal stiffness ratios and health indices. Input and output parameter values for these random testing sets are included in Appendix D. FE models were created and analyzed, deflection results were extracted, and nodal

51

stiffness ratios and health indices were computed. The three optimum models for both prediction networks were trained on the entirety of the main database and tested on the 75 randomly generated cracked beam datasets. Statistical testing results for these networks are displayed in Tables 4-9 and 4-10.

Table 4-9: Statistical results for optimal nodal stiffness ratio prediction ANNs tested on randomly generated beams with 1–5 cracks

	Model 1 (4-18-20000)	Model 2 (5-19-20000)	Model 3 (6-19-20000)
MARE	1.9571	2.4870	2.3765
R^2	0.86855	0.80863	0.84659
ASE	0.000885	0.001316	0.001222

Table 4-10: Statistical results for optimal health index prediction ANNs tested on randomly generated beams with 1–5 cracks

	Model 1 (2-19-20000)	Model 2 (4-19-20000)	Model 3 (6-19-20000)
MARE	1.8234	1.7318	1.7237
R^2	0.80351	0.80246	0.81527
ASE	0.000845	0.000869	0.000932

A loss in prediction accuracy with respect to the statistical results of the main database was evident for the datasets with randomly generated parameters. However, both the nodal stiffness ratio and health index prediction ANNs performed well with R^2 values exceeding 0.8 for all models.

The top-performing networks were selected by analyzing the statistical results of the main database, the additional datasets of beams with two, three, and four cracks, and the datasets with randomly generated parameters. For nodal stiffness ratio prediction applications, model 4-18-20000 generally produced the lowest MARE and ASE and highest R^2 values. Similarly, model 6-19-20000 displayed the best statistical performance for health index prediction applications. Visual representations of the prediction accuracies of these two optimal network

models are displayed in Figures 4-1 to 4-3, in which the ANN predicted nodal stiffness ratios and health indices are plotted against their actual values for the main database and the two additional testing sets.

(a) Predicted vs. Actual k%$_1$

(b) Predicted vs. Actual k%$_2$

(c) Predicted vs. Actual k%$_3$

(d) Predicted vs. Actual k%$_4$

(e) Predicted vs. Actual k%$_5$

(f) Predicted vs. Actual k%$_6$
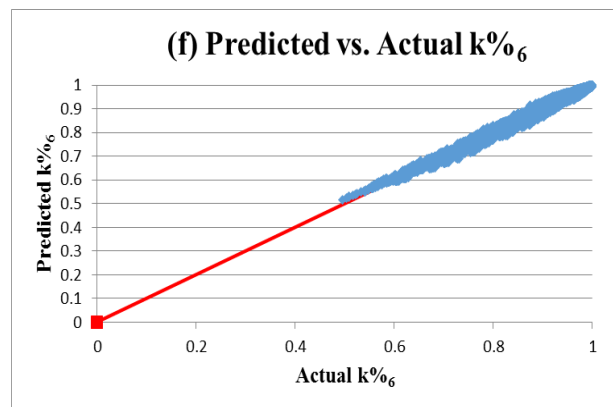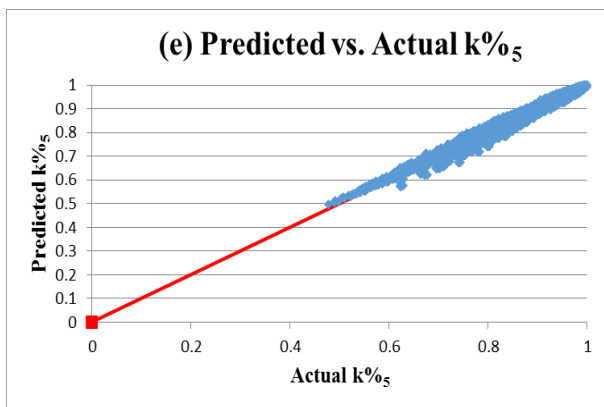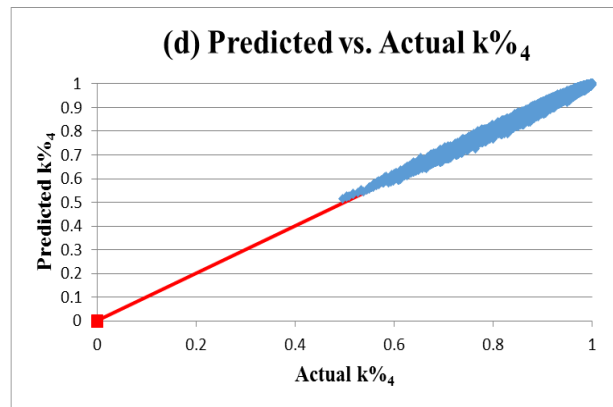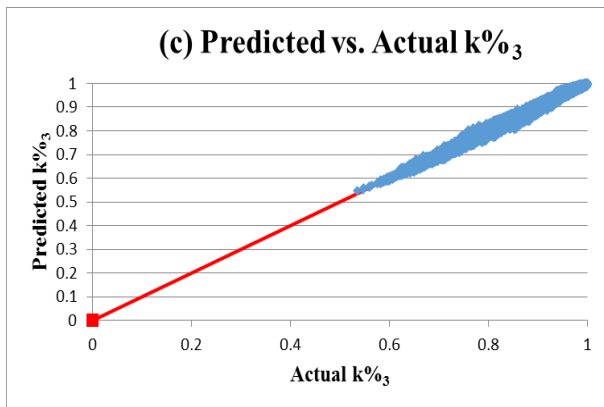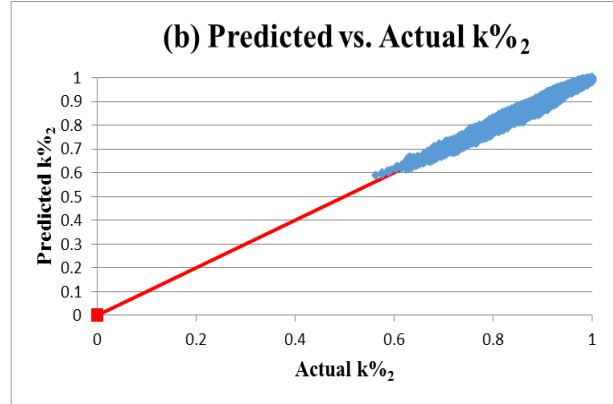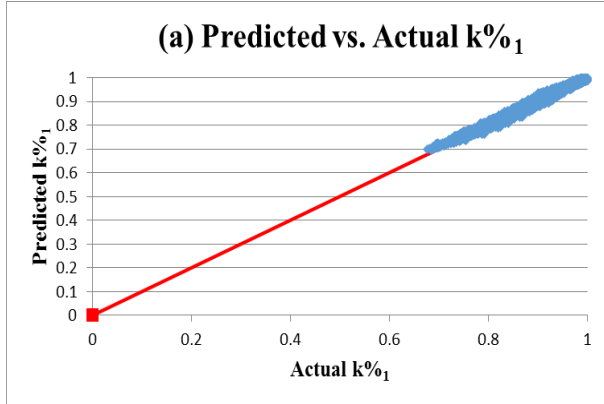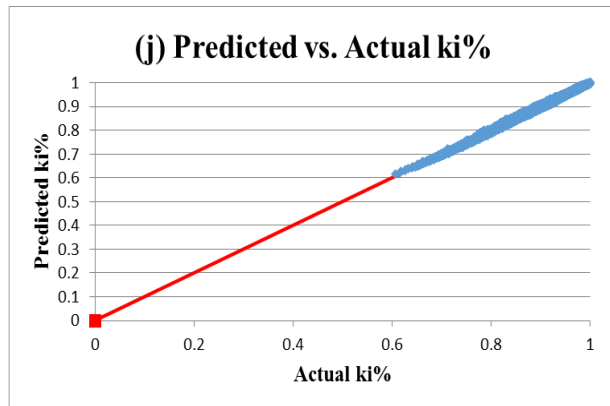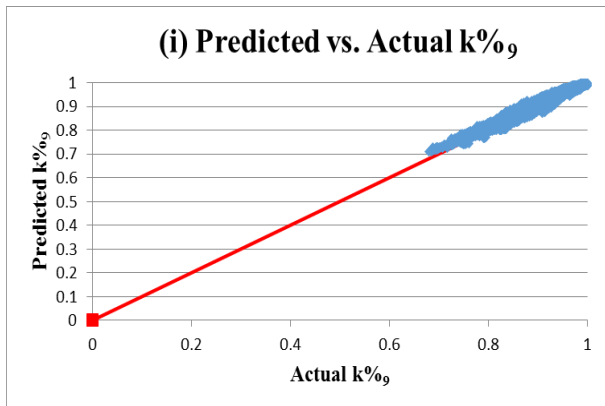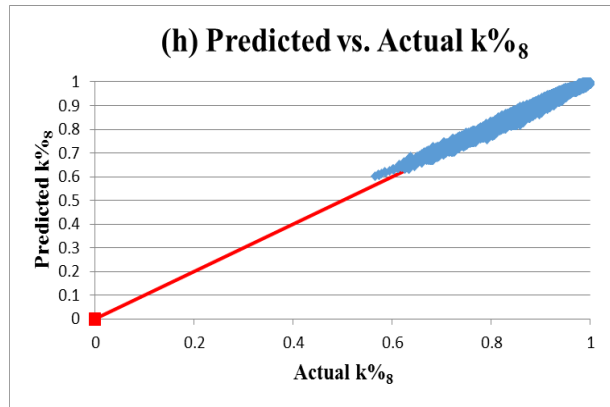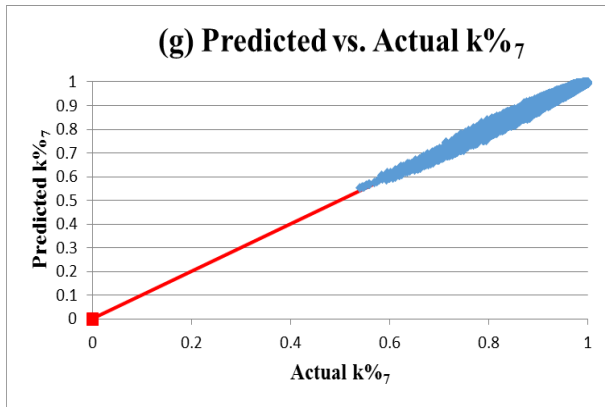
Figure 4-1: Main database – predicted versus actual values for (a) $k\%_1$, (b) $k\%_2$, (c) $k\%_3$, (d) $k\%_4$, (e) $k\%_5$, (f) $k\%_6$, (g) $k\%_7$, (h) $k\%_8$, (i) $k\%_9$, and (j) $ki\%$

(c) Predicted vs. Actual k%₃

(d) Predicted vs. Actual k%₄

(e) Predicted vs. Actual k%₅

(f) Predicted vs. Actual k%₆

(g) Predicted vs. Actual k%₇

(h) Predicted vs. Actual k%₈

(i) Predicted vs. Actual k%$_9$

(j) Predicted vs. Actual ki%
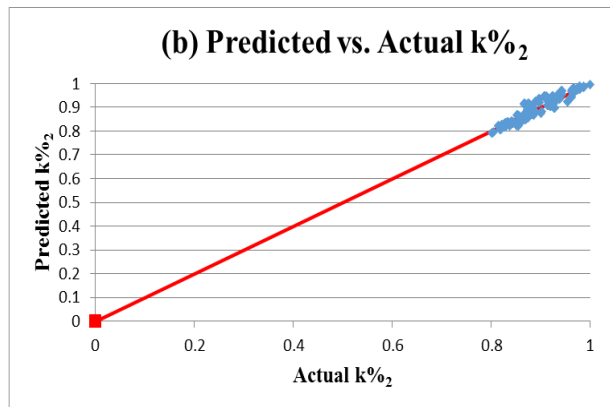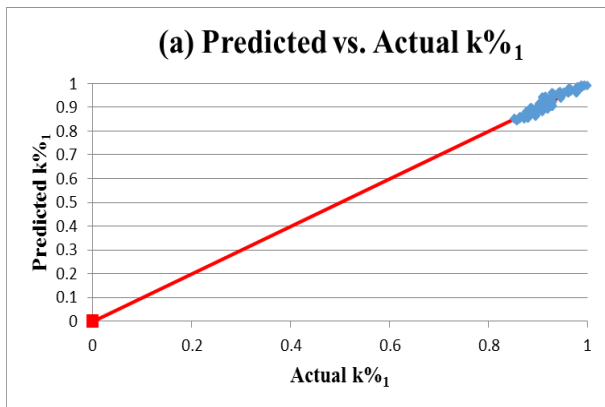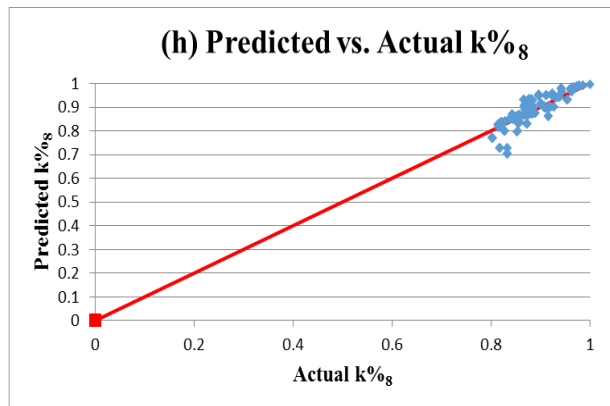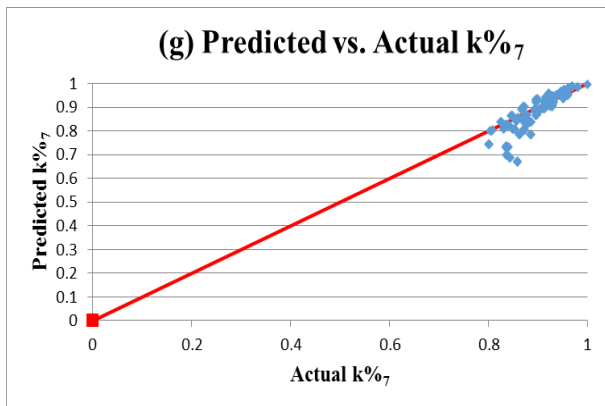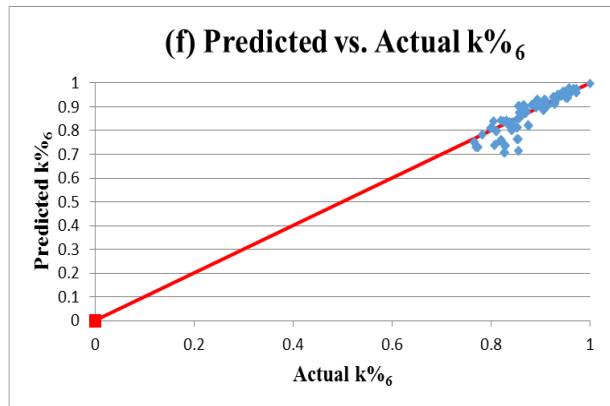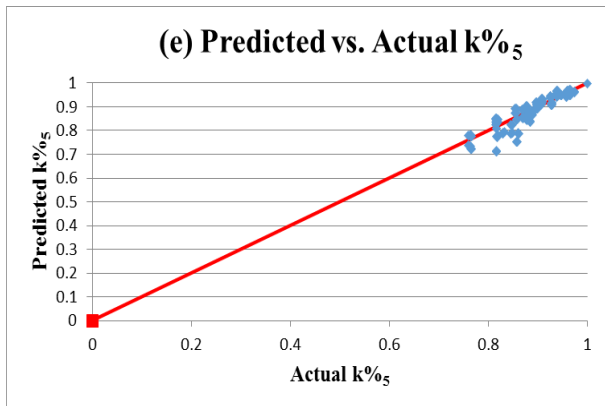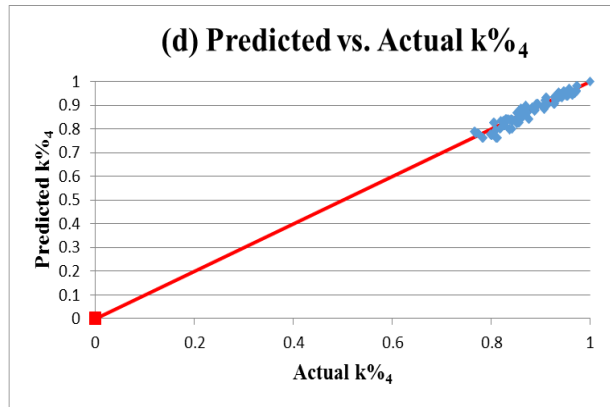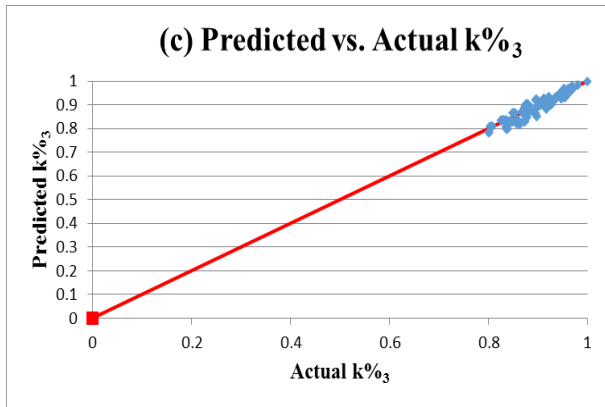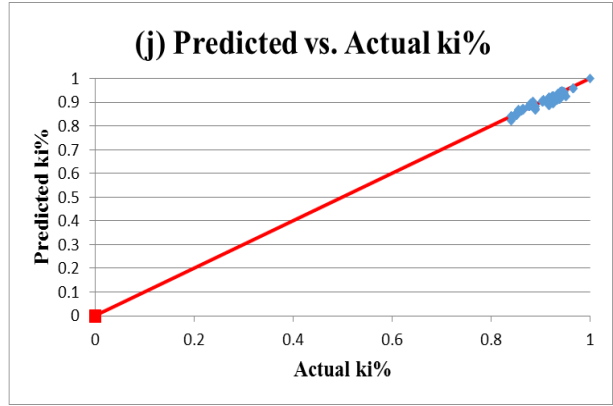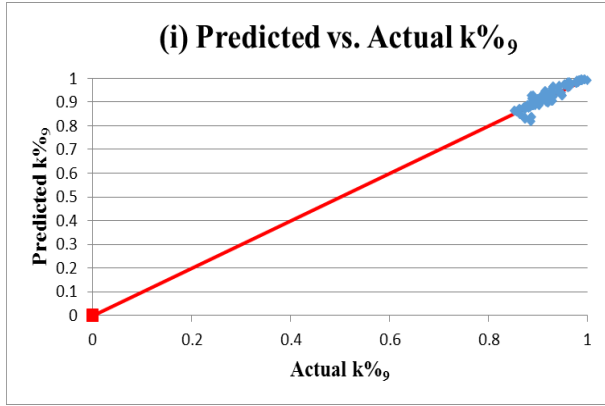
Figure 4-2: Testing sets of beams with two, three, and four cracks – predicted versus actual values for (a) k%$_1$, (b) k%$_2$, (c) k%$_3$, (d) k%$_4$, (e) k%$_5$, (f) k%$_6$, (g) k%$_7$, (h) k%$_8$, (i) k%$_9$, and (j) ki%

(a) Predicted vs. Actual k%$_1$

(b) Predicted vs. Actual k%$_2$

(c) Predicted vs. Actual k%$_3$

(d) Predicted vs. Actual k%$_4$

(e) Predicted vs. Actual k%₅

(f) Predicted vs. Actual k%₆

(g) Predicted vs. Actual k%₇

(h) Predicted vs. Actual k%₈

(i) Predicted vs. Actual k%₉

(j) Predicted vs. Actual ki%
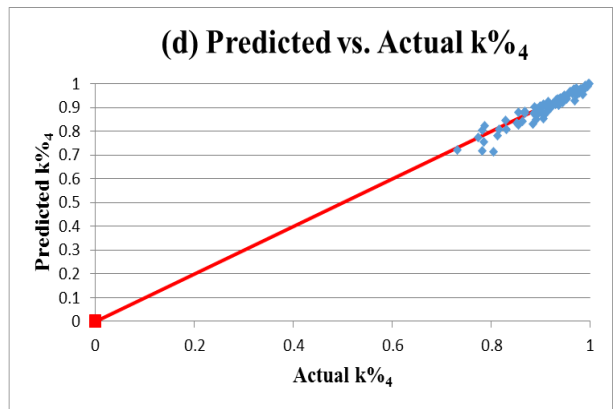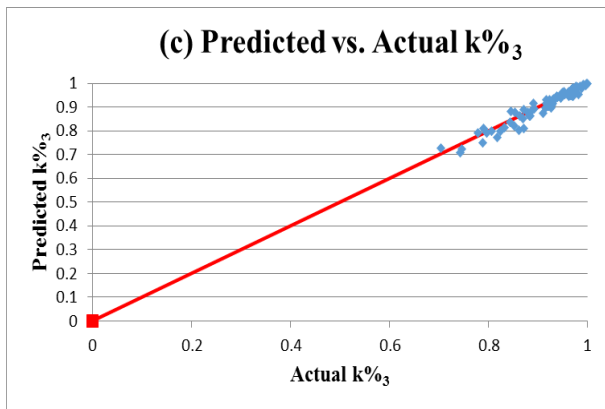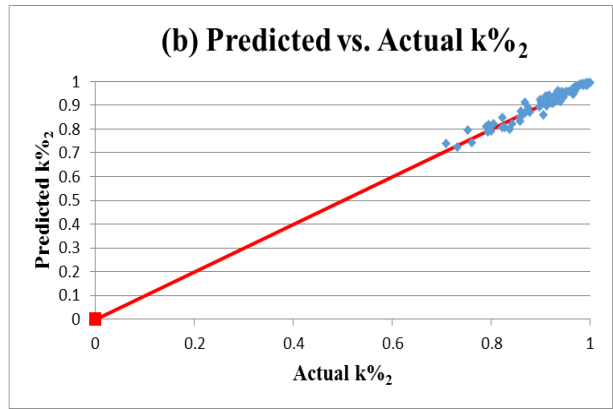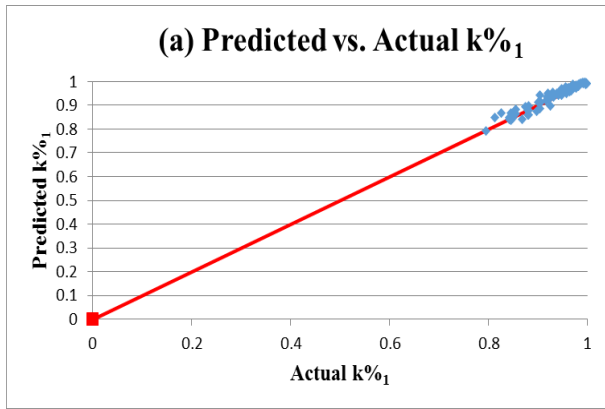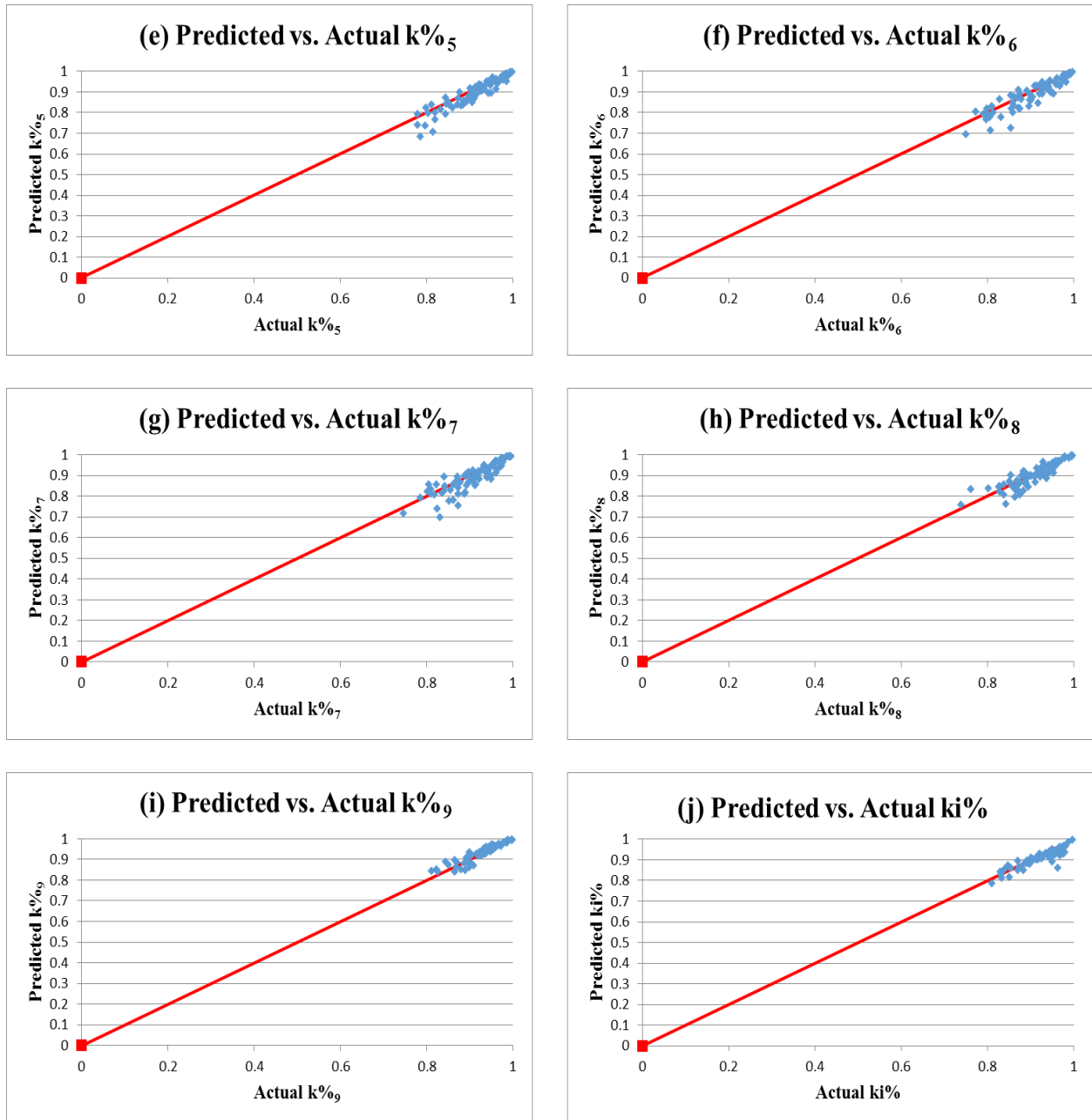
Figure 4-3: Randomly generated testing sets – predicted versus actual values for (a) k%₁, (b) k%₂, (c) k%₃, (d) k%₄, (e) k%₅, (f) k%₆, (g) k%₇, (h) k%₈, (i) k%₉, and (j) ki%

The ANN predictions are more accurate for points near the 45° fit line in Figures 4-1 to 4-3. Figure 4-1 highlights the excellent prediction performance of the optimal networks trained on all the data, and Figures 4-2 and 4-3 reveal the slightly less effective prediction performance of the optimal networks when tested on the additional datasets. For all three figures, data points

for the health index prediction model were very close to the 45° fit line, suggesting that ANNs provide excellent prediction capabilities when predicting a single measure of damage for the beams. The figures also show that accuracy of the nodal stiffness ratio prediction model decreased for nodes close to the center of the beam. Because these nodes typically have low nodal stiffness ratios, this loss of accuracy may correlate to reduced ANN prediction accuracies for heavily damaged sections. Although these results indicate that special considerations need be taken when using the optimum ANN models to evaluate the structural health of significantly damaged beams, the networks generally provide conservative predictions, somewhat reducing the impact of potential inaccuracies. This is evident in Figures 4-2 and 4-3 where the lower magnitude nodal stiffness ratios often fall below the 45° line, indicating that the predicted stiffness ratios are lower than the actual values. The generally tight spread of the data points about the 45° lines in Figures 4-1 to 4-3 affirms the effectiveness of the optimal ANN models for nodal stiffness ratio and health index prediction applications.

Chapter 5 - ANN User Interface Application

After applying the artificial neural network (ANN) training process and optimum model selection procedure and evaluating the top-performing models' prediction accuracies on additional testing datasets, the optimal ANN architectures for nodal stiffness ratio and health index prediction applications were established. Biases and connection weights for the input layer-hidden layer and hidden layer-output layer were retrieved after these network structures were trained on all the data in the main database. Application of these biases and connection weights to the summation and activation functions described in Equations 2-1 and 2-2 allowed for calculation of the ANN-predicted nodal stiffness ratios and health index for any simply-supported reinforced concrete T-beam having parameters within the range of those used to create the finite element (FE) model database. In order to automate these calculations and facilitate on-site damage evaluation using the optimal ANN models, a touch user-interface driven electronic application was developed.

Several development platform options were considered for the ANN touch user-interface, including a computer application written in Python, a Visual Studio Windows Presentation Foundation (WPF) computer application, a web-based application written in JavaScript, and Android and/or Apple mobile application(s). Many Python graphical user interface application frameworks are cross-platform, but the interface construction tools are limited for some frameworks. Although WPF applications are limited to Microsoft Windows computers, Visual Studio offers vast library of interface construction tools. Web-based JavaScript applications are touted as relatively easy to develop, but the fact they generally require internet connectivity to function restricts their field use. Although mobile platforms provide clean and simple user

interfaces, limiting the use of the ANN models to Android or Apple tablets and mobile devices is

not a robust enough sole option for an engineering application.

Due to the ease of graphical user interface constructability and integrated touch support,

the decision was made to develop a Visual Studio WPF application. The drawback of this option,

limitation of the ANN application to Microsoft Windows computers, is diminished due to the

fact that Microsoft Windows systems comprise a majority of the market share of desktops and

laptops. Additionally, general observations revealed that engineering companies typically utilize

Windows operating systems. The application was developed with Visual Studio 2015 using .net

framework version 4.5 on a desktop running the Windows 7 operating system. Figure 5-1

displays the final version of the graphical user interface.
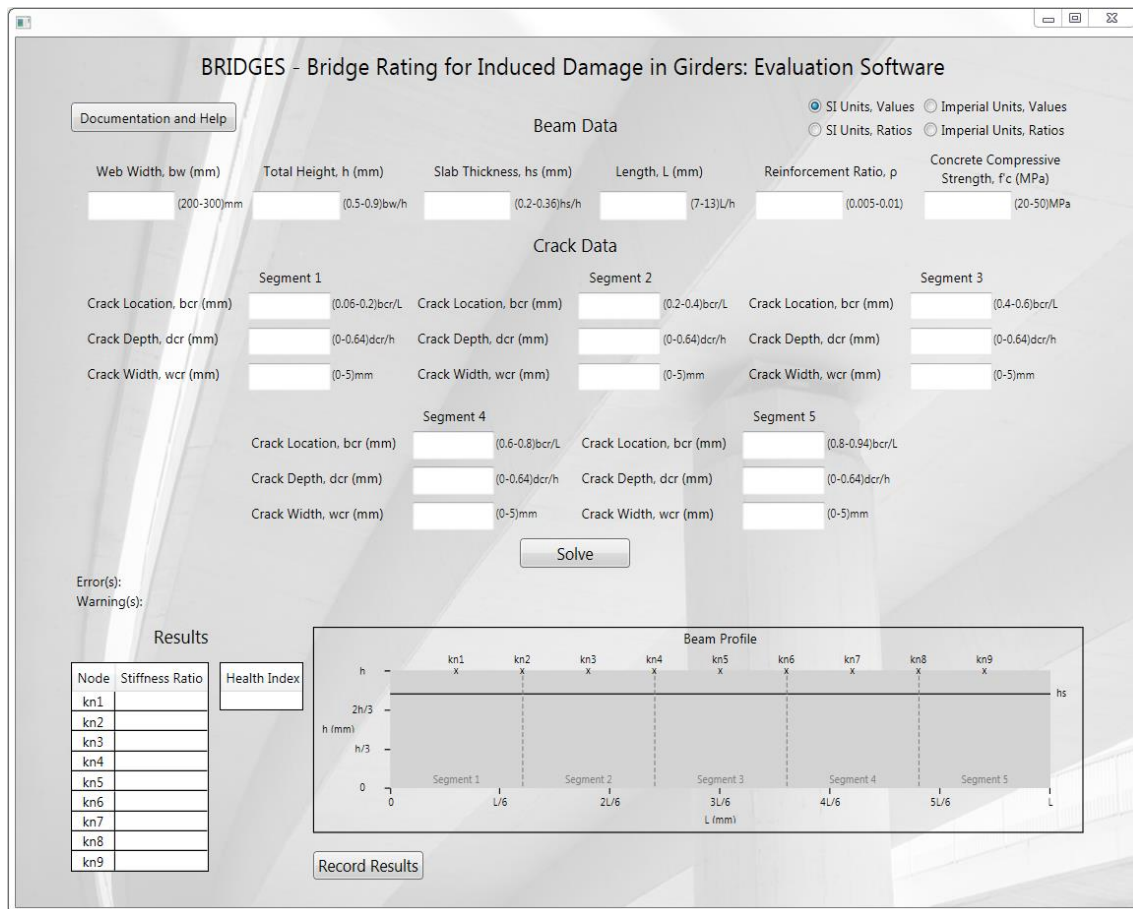
Figure 5-1: Nodal stiffness ratio and health index prediction graphical user interface

As shown in Figure 5-1, the user interface accepts geometric and material parameters (b_w, h, h_s, L, ρ, and f'_c) in the "Beam Data" section and cracking parameters (b_{crn}, d_{crn}, and w_{crn}) in the "Crack Data" section as inputs. Upon activation of the "Solve" button, the input parameters are normalized to function as input nodes for the ANN calculations. The biases and connection weights from the optimum nodal stiffness ratio and health index ANN models are applied to pass the input parameters to the hidden nodes and ultimately to the output nodes. The output parameters are then de-normalized, and the predicted nodal stiffness ratios and health index are displayed in the tables in the "Results" section at the lower left corner of the user interface. Also after pressing the "Solve" button, the "Beam Profile" is updated to display the location of the flange of the T-beam and the location and depth of each crack. The height and length labels are also changed to reflect the user-input height and length of the beam. Because the stiffness nodes are equidistant fractions of the span length of the beam, the "x" and "kn" labels for the stiffness nodes are static and serve as a visual reference for the location of the tabulated stiffness ratios. Similarly, the "Segment" labels and dashed lines are static and graphically display the five equal segments into which the beam is divided. Selection of the "SI Units" and "Imperial Units" radio buttons in the upper right corner of the interface change the parameter unit and range labels and automatically alter the ANN calculations for the selected measurement system. The "SI Units, Ratios" and "Imperial Units, Ratios" radio buttons allow the program to accept crack locations and depths as ratios of the length and height of the beam, respectively, instead of absolute values.

Once calculations have been run and results are displayed in the tables, selection of the "Record Results" button writes the beam's input properties and health results to a text file and opens the file with the computer's default text editor. The space to the right of the "Record Results" button displays the name of the results file and the directory in which the file is stored;

61

the directory from which the application's executable file is being run. Similarly, selection of the "Documentation and Help" button opens a read-only text file and stores the file in the application's working directory. This text file contains information about the development of the damage evaluation application and instructions on how to use the program, including a description of the range of parameter values on which the ANN models were trained. If the user enters data outside the applicable parameter value training ranges, selection of the "Solve" button causes text to fill the "Warning(s):" label indicating which parameters produced warnings. Although the program will run if warnings are present, use of parameter values outside the range of the training data may produce unreliable results. In addition to being described in the "Documentation and Help" file, the parameter value ranges are displayed next to the input text box for each parameter. If errors are present, the program will not run and new results will not be recorded. Errors can occur by failing to enter values in all text boxes of the "Beam Data" section. Setting crack locations to values outside their applicable segment will also produce an error. In an effort to minimize errors, if the user fails to enter data, or enters zero for any of the crack locations, depths, or widths in the "Crack Data" section, the crack location value defaults to the center of the segment and the depth and width values for the crack in that segment are set to zero.

This application was created to serve as an in-situ bridge member damage evaluation tool. Because the application was developed using the Visual Studio WPF framework, the program is intended to be compatible with Windows 7 or newer touch-enabled devices and works with both touch or conventional mouse and keyboard input. To illustrate the functionality of the program, the following figures display the interface window after solving for the nodal stiffness ratios and health indices of two damaged reinforced concrete T-beams. The beam solutions in Figures 5-2 and 5-3 correspond to cracked beams from the main training database

and randomly generated testing datasets, respectively. Table 5-1 displays the ANN models'

nodal stiffness ratio and health index predictions for these two beams. The effectiveness of the

developed application was validated as the ANN predictions match the application's outputs.
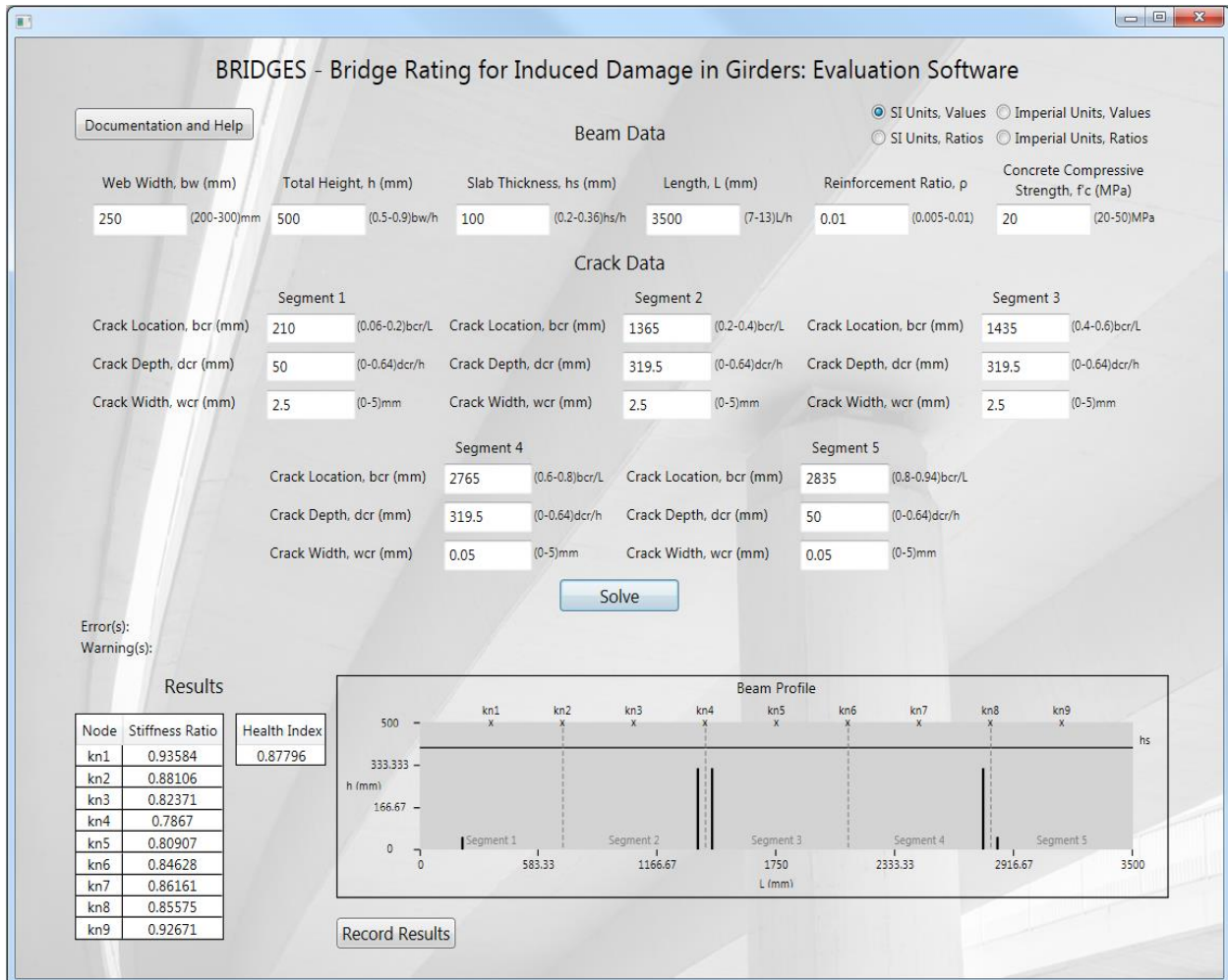
Figure 5-2: ANN user interface application results for test beam 1 (ANN ID 8400)
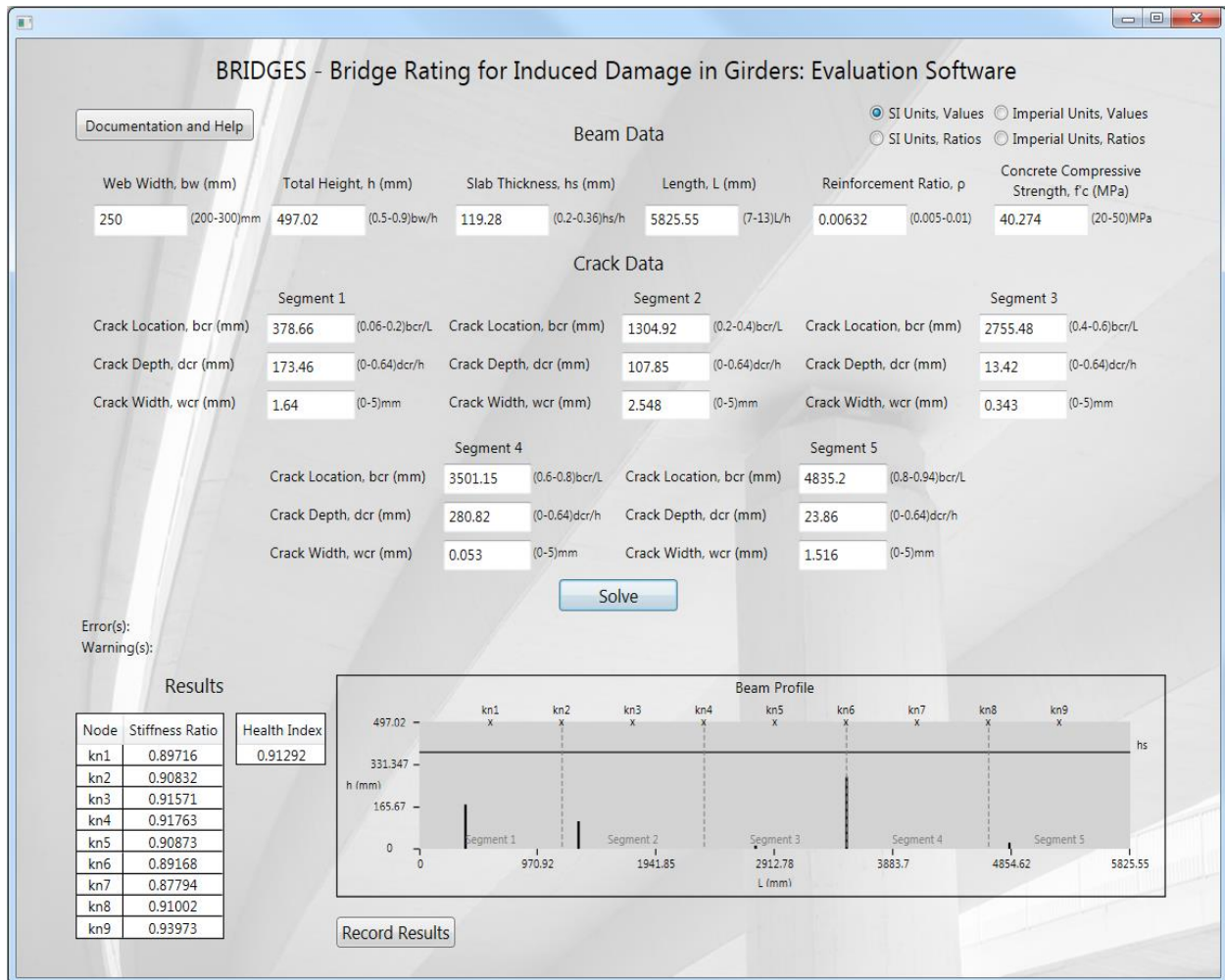
Figure 5-3: ANN user interface application results for test beam 2 (ANN ID 43180)

Table 5-1: ANN prediction results for test beams

ID	k%$_1$	k%$_2$	k%$_3$	k%$_4$	k%$_5$	k%$_6$	k%$_7$	k%$_8$	k%$_9$	ki%
8400	0.93585	0.88107	0.82371	0.78670	0.80906	0.8463	0.86160	0.85574	0.92670	0.87795
43180	0.89717	0.90832	0.91571	0.91763	0.90874	0.8917	0.87794	0.91002	0.93973	0.91292

The relative impacts of cracking parameters on the structural health of beams were investigated using the developed application. Figure 5-4 displays the application's solution for a beam with a single crack in the middle of the span. The health index of this reference beam was predicted to be 0.97832. Three different beams were then tested by changing one cracking parameter while holding all other parameters of the reference beam constant. Increasing the depth of the crack from 125 mm to 250 mm reduced the predicted health index to 0.94658.

Increasing the width of the crack of the reference beam from 0.5 mm to 5 mm only reduced the predicted health index to 0.97682. Adding a 125 mm deep and 0.5 mm wide crack in the middle of the second segment (b_{cr} = 1500 mm) of the reference beams reduced the health index to 0.95875. These results, as well as several observations made while testing the functionality of the program, indicate that the extension or addition of cracks significantly reduces beam structural health while increasing the width of cracks only marginally affects the beam stiffness.
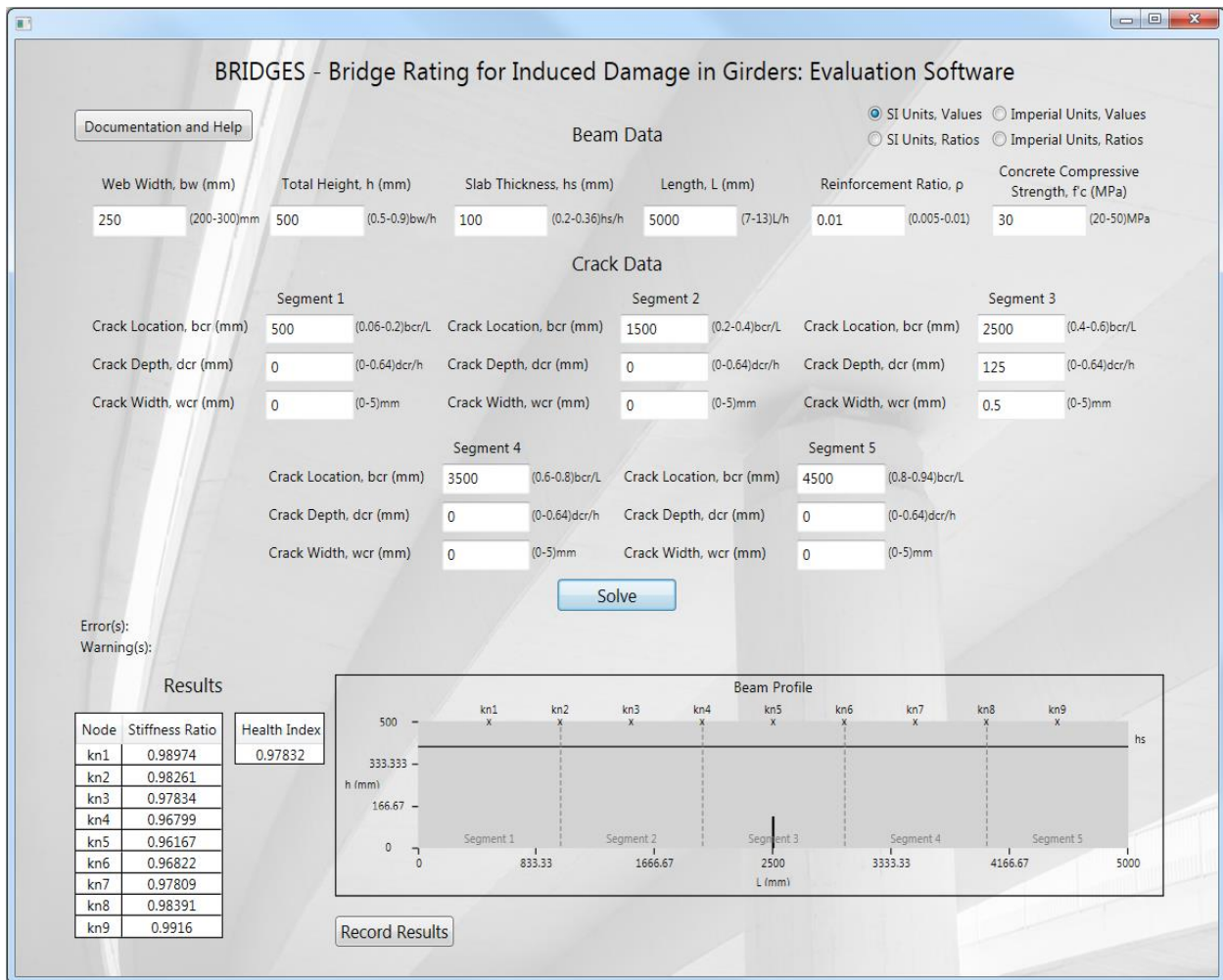
Figure 5-4: Visual Studio WPF application results for reference beam used in parameter impact testing

Chapter 6 - Conclusions and Recommendations

Conclusions

This research project investigated the potential for application of the finite element (FE) method and artificial neural networks (ANNs) to create an objective damage evaluation model for reinforced concrete T-girders that could be utilized with visual inspection crack inputs. A review of the literature identified the need for accurate damage evaluation of deteriorating infrastructure, discussed the drawbacks in the commonly applied visual inspection and condition rating method, and reviewed various structural health monitoring (SHM) techniques for damage evaluation and structural health prediction. A three-dimensional (3D) reinforced concrete T-beam FE model database was constructed using Abaqus FE analysis software. Geometric (b_w/h, h_s/h, L/h, and ρ), material (f'_c), and cracking ($b_{cr,m}/L$, $d_{cr,m}/h$, and $w_{cr,m}$) parameters varied between the models, and up to five cracks were allowed per beam. Damage evaluation measures were then computed, including the stiffness ratios of cracked to healthy beams with identical geometric and material properties at nine equidistant nodes along the beams ($k\%_n$) and the health index parameter ($ki\%$), which is an integration of the nodal stiffness ratio profile across the beam span length. Since most parameters were normalized with respect to a beam web width of 250 mm, a random sample of the database, holding constant the normalized geometric, material, and cracking parameters, was generated for beams with web widths of 200 mm and 300 mm. Health indices for these beams displayed good agreement with the results for the reference beams. Coefficients of determination (R^2) and Lin's concordance correlation coefficients exceeding 0.99 and 0.975, respectively, indicated that the results of this study are reproducible for a variety of beam sizes.

A feedforward ANN program utilizing a backpropagation learning algorithm was employed to establish structural health prediction models based on the data in the reinforced concrete T-beam database. The ANNs accepted the geometric, material, and cracking parameters as inputs and predicted the nodal stiffness ratios or health indices as outputs. A distinct ANN training process and optimal model selection procedure was followed to determine the optimum models for nodal stiffness ratio and health index prediction applications. Statistical results for these optimum models were excellent with R^2 values exceeding 0.99 in the training, testing, and validation phases. Additional FE model datasets with dissimilar and randomly generated input parameters were constructed, and the prediction capabilities of the fully-trained optimum models were assessed on the new datasets. The top-performing nodal stiffness ratio and health index prediction models displayed good statistical performance with R^2 values of 0.851 and 0.868 for the dissimilar parameter datasets, and R^2 values of 0.869 and 0.815 for the randomly generated parameter datasets, respectively. Utilizing these two top-performing network architectures, a touch-enabled application was developed to serve as an on-site damage evaluation tool. This application has been given the acronym BRIDGES, which stands for Bridge Rating for Induced Damage in Girders: Evaluation Software. This research demonstrated the effective application of FE modeling and ANNs in SHM for objective damage evaluation. Statistical results of this study indicate that ANN models can provide accurate predictions for the structural health of damaged reinforced concrete T-beams. The theory and techniques utilized in this study can be applied to any number of structural elements and SHM processes.

Recommendations

The following recommendations address the potential for refinement or expansion of this research:

- Further investigate the effects of different beam web widths: Analysis of the sample of beams with different web widths revealed that the results of this study are reasonably applicable to a variety of typical girder sizes. Further analysis could expand the applicable size range or develop correction factors to adjust the results for beams with different web widths.

- Increase the size of the beam database: Because ANNs are data-driven tools, increasing the amount of training data would enhance the model's prediction accuracies. As stated in Chapter 3, a large number of datasets were generated for beams with one crack. Additional datasets could be generated for beams with two, three, four, and five cracks with added crack configurations and more input parameter variation.

- Expand the number of cracks per beam: This study considered beams with up to five cracks. Although consideration of additional cracks would increase the complexity of the problem and potentially decrease prediction accuracies of the networks unless the size of the training database is increased exponentially, it would provide a more robust damage evaluation tool for more severely damaged girders.

- Add crack angle (θ_n) parameters: Only flexural cracks were analyzed as a result of this research. Addition of angled cracks to the database would allow for more accurate damage evaluations of beams with shear or flexural-shear cracks.

- Consider additional beam configurations: The beams in this research were limited to simply-supported concrete T-beams reinforced with steel rebar. The processes described

68

in the methodology could be applied to beams with different support types, such as multi-span continuous beams, and various reinforcement types, such as pretressing strands or fiber reinforced polymers. Other structural units, such as slabs, could also be investigated.

- Compare with experimental data: Comparing the ANN models' structural health predictions with experimental test data could further validate the effectiveness of this research technique. Such comparisons would also provide the opportunity to establish damage metrics for the health index term. With further research, the health index could be utilized as a standalone measure of structural health and dictate whether members are structurally sound, should be more closely monitored, or require immediate repair or replacement.

References

Ahlborn, T. M., Shuchman, R., Sutter, L. L., Brooks, C. N., Harris, D. H., Burns, J. W., Endsley, K. A., Evans, D. C., Vaghefi, K., & Oats, R. C. (2010). *The state-of-the-practice of modern structural health monitoring for bridges: A comprehensive review.* Retrieved from the TRID database.

Al-Ghalib, A., Mohammad, F., Rahman, M., & Chilton, J. (2011, September 26–28). *Damage and repair quantification in reinforced concrete beams using vibration data.* Paper presented at the 4th International Conference on Concrete Repair: Concrete Solutions. Dresden, Germany. Retrieved from Compendex database. (T20:47:24Z).

Al-Rahmani, A. (2012). *A combined soft computing-mechanics approach to damage evaluation and detection in reinforced concrete beams* (Master's thesis). Kansas State University, Manhattan, Kansas.

Al-Rahmani, A., Rasheed, H., & Najjar, Y. (2013). Intelligent damage detection in bridge girders: Hybrid approach. *Journal of Engineering Mechanics*, 139(3), 296-304. doi: 10.1061/(ASCE)EM.1943-7889.0000536

Al-Rahmani, A., Rasheed, H., & Najjar, Y. (2014). An artificial intelligence approach to objective health monitoring and damage detection in concrete bridge girders. *American Concrete Institute Special Publication*, 298(6), 73-89.

American Concrete Institute Committee 318. (2014). *Building code requirements for structural concrete and commentary.* (ACI No. 318R-14). Farmington Hills, MI: American Concrete Institute.

American Society of Civil Engineers. (2013). *2013 report card for America's infrastructure*.

Reston, VA, United States: American Society of Civil Engineers. Retrieved from

http://www.infrastructurereportcard.org/bridges/

Basheer, I., A. (1998). *Neuromechanistic-based modeling and simulation of constitutive*

behavior of fine-grained soils (Doctoral Dissertation). Kansas State University, Manhattan,

Kansas.

Beer, F. P., Johnston, E. R., Dewolf, J. T., & Mazurek, D. F. (2012). *Mechanics of Materials* (6th

ed.). New York, NY: McGraw-Hill Companies, Inc.

Chen, S., Liu, W., Bian, H., & Smith, B. (2012, October 31–November 3). *3D LiDAR scans for*

bridge damage evaluation. Paper presented at the 6th Congress on Forensic Engineering:

Gateway to a Better Tomorrow. San Francisco, CA, United States.

doi:10.1061/9780784412640.052

Dassault Systèmes Simulia Corp. (2013). Abaqus 6.13 [computer software]. Providence, RI:

Dassault Systèmes.

Farhidzadeh, A., Dehghan-Niri, E., Moustafa, A., Salamone, S., & Whittaker, A. (2013).

Damage assessment of reinforced concrete structures using fractal analysis of residual crack

patterns. *Experimental Mechanics, 53*(9), 1607–1619. doi:10.1007/s11340-013-9769-7

Federal Highway Administration (a). (2014). *Deficient bridges by state and highway system*

[Microsoft Excel spreadsheet]. Retrieved from https://www.fhwa.dot.gov/bridge/britab.cfm

Federal Highway Administration (b). (2014). *Structure type by state* [Microsoft Excel

spreadsheet]. Retrieved from https://www.fhwa.dot.gov/bridge/britab.cfm

Gassman, S. L., & Tawhed, W. F. (2004). Nondestructive assessment of damage in concrete

    bridge decks. *Journal of Performance of Constructed Facilities,* 18(4), 220–231.

    doi:10.1061/(ASCE)0887-3828(2004)18:4(220)

Ghods, A. S., & Esfahani, M. R. (2009, July 22–24). *Damage assessment of reinforced concrete*

    beams by modal test. Paper presented at the 4th International Conference on Structural

    Health Monitoring of Intelligent Infrastructure. Zurich, Switzerland. Retrieved from

    Compendex database.

Hasançebi, O., & Dumlupinar, T. (2013). Linear and nonlinear model updating of reinforced

    concrete T-beam bridges using artificial neural networks. *Computers & Structures, 119*, 1–

    11. doi:10.1016/j.compstruc.2012.12.017

Jeyasehar, C. A., & Sumangala, K. (2006). Damage assessment of prestressed concrete beams

    using artificial neural network (ANN) approach. *Computers & Structures, 84*(26), 1709–

    1718. doi:10.1016/j.compstruc.2006.03.005

Lenett, M. S., Griessmann, A., Helmicki, A. J., & Aktan, A. E. (1999). Subjective and objective

    evaluations of bridge damage. *Transportation Research Record, 1688*, 76–86.

    doi:10.3141/1688-10

Li, L., Ghrib, S., & Lee, S. (2008, Jun 10-13). *Damage identification of reinforced concrete*

    beams by digital image correlation and FE-updating. Paper presented at the Canadian

    Society for Civil Engineering Annual Conference: Partnership for Innovation. Quebec City,

    QC, Canada. Retrieved from Compendex database.

Lin, L., I. (1989). A concordance correlation coefficient to evaluate reproducibility. *Biometrics*,

    45. Retrieved from http://www.jstor.org/stable/2532051

Ndambi, J., Vantomme, J., & Harri, K. (2002). Damage assessment in reinforced concrete beams using eigenfrequencies and mode shape derivatives. *Engineering Structures, 24*(4), 501–515. doi:10.1016/S0141-0296(01)00117-1

Reynders, E., & De Roeck, G. (2009). A local flexibility method for vibration-based damage localization and quantification. *Journal of Sound and Vibration, 329*(12), 2367–2383. doi:10.1016/j.jsv.2009.04.026

Sagar, R. V., Prasad, B. K. R., & Sharma, R. (2012). Evaluation of damage in reinforced concrete bridge beams using acoustic emission technique. *Nondestructive Testing and Evaluation, 27*(2), 95–108. doi:10.1080/10589759.2011.610452

Shiotani, T., Ohtsu, H., Momoki, S., Chai, H. K., Onishi, H., & Kamada, T. (2012). Damage evaluation for concrete bridge deck by means of stress wave techniques. *Journal of Bridge Engineering, 17*(6), 847–856. doi:10.1061/(ASCE)BE.1943-5592.0000373

Sohn, H., Farrar, C. R., Hemez, F. M., Shunk, D. D., Stinemates, D. W., Nadler, B. R., & Czarnecki, J. J. (2004). *A review of structural health monitoring literature: 1996-2001.* Los Alamos National Laboratory report LA-13976-MS. Retrieved from https://institute.lanl.gov/ei/publications/structural-health-monitoring/

Teughels, A., Maeck, J., & De Roeck, G. (2002). Damage assessment by FE model updating using damage functions. *Computers & Structures, 80*(25), 1869–1879. doi:10.1016/S0045-7949(02)00217-1

Yaserer, H., I. (2010). *Characterizing the permeability of concrete mixes used in transportation applications: A neuronet approach* (Master's thesis). Kansas State University, Manhattan, Kansas.

Appendix A - Abaqus-Python Scripts

Example script for generation of a singly-cracked reinforced concrete T-beam:

```python
from abaqus import *
from abaqusConstants import *
import __main__
import section
import regionToolset
import displayGroupMdbToolset as dgm
import part
import material
import assembly
import step
import interaction
import load
import mesh
import optimization
import job
import sketch
import visualization
import xyPlot
import displayGroupOdbToolset as dgo
import connectorBehavior

beamdb = open('beamdb1c.txt')
lines = beamdb.readlines()
dbp = []
for line in lines:
    spline = line.split()
    spline[0] = spline[0] + spline[1]
    del spline[1]
    dbp.append(spline)
knodes = 9
kns = [x/(knodes+1.0) for x in range(knodes+1.0)[1:]]
Lns = ['L'+str(x) for x in range (knodes+1)[1:]]
knsdict = dict(zip(kns,Lns))

for beam in dbp:
    for kn in kns:
        Mdb()
        job = beam[0] + '-' + knsdict[kn]
        bwbeam = 250.0
        bwhratio = float(beam[1])
        Lhratio = float(beam[3])
        fconc = float(beam[5])
        hbeam = bwbeam / bwhratio
        Lbeam = hbeam * Lhratio
        tfbeam = float(beam[2])*hbeam
        hwbeam = hbeam - tfbeam
```

```
bfbeampos = hwbeam+bwbeam
bfbeamneg = -hwbeam
Econc = 4700.0 * fconc**0.5
vconc = 0.2

bcrLratio = float(beam[7])
dcrhratio = float(beam[8])
wcr = float(beam[9])
bcr = bcrLratio * Lbeam
dcr = dcrhratio * hbeam
xcr = -Lbeam/2+bcr-wcr/2

rho = float(beam[4])
cover = 50.0
d = hbeam - cover
As = rho*bwbeam*d
Ab = As/3
dbar = (Ab*4/pi)**0.5
'dbar = round(db)'
Abar = pi/4*dbar**2
Esteel = 200000.0
vsteel = 0.3

knode = kn
concmesh = 35.0
steelmesh = 35.0
load = 100000.0

s = mdb.models['Model-1'].ConstrainedSketch(name='__profile__',
    sheetSize=200.0)
g, v, d, c = s.geometry, s.vertices, s.dimensions, s.constraints
s.setPrimaryObject(option=STANDALONE)
s.Line(point1=(0.0, 0.0), point2=(bwbeam, 0.0))
s.HorizontalConstraint(entity=g[2], addUndoState=False)
s.Line(point1=(bwbeam, 0.0), point2=(bwbeam, hwbeam))
s.VerticalConstraint(entity=g[3], addUndoState=False)
s.PerpendicularConstraint(entity1=g[2], entity2=g[3], addUndoState=False)
s.Line(point1=(bwbeam, hwbeam), point2=(bfbeampos, hwbeam))
s.HorizontalConstraint(entity=g[4], addUndoState=False)
s.PerpendicularConstraint(entity1=g[3], entity2=g[4], addUndoState=False)
s.Line(point1=(bfbeampos, hwbeam), point2=(bfbeampos, hbeam))
s.VerticalConstraint(entity=g[5], addUndoState=False)
s.PerpendicularConstraint(entity1=g[4], entity2=g[5], addUndoState=False)
s.Line(point1=(bfbeampos, hbeam), point2=(bfbeamneg, hbeam))
s.HorizontalConstraint(entity=g[6], addUndoState=False)
s.PerpendicularConstraint(entity1=g[5], entity2=g[6], addUndoState=False)
s.Line(point1=(bfbeamneg, hbeam), point2=(bfbeamneg, hwbeam))
s.VerticalConstraint(entity=g[7], addUndoState=False)
s.PerpendicularConstraint(entity1=g[6], entity2=g[7], addUndoState=False)
s.Line(point1=(bfbeamneg, hwbeam), point2=(0.0, hwbeam))
s.HorizontalConstraint(entity=g[8], addUndoState=False)
```

```
s.PerpendicularConstraint(entity1=g[7], entity2=g[8], addUndoState=False)
s.Line(point1=(0.0, hwbeam), point2=(0.0, 0.0))
s.VerticalConstraint(entity=g[9], addUndoState=False)
s.PerpendicularConstraint(entity1=g[8], entity2=g[9], addUndoState=False)
p = mdb.models['Model-1'].Part(name='Concrete Beam',   dimensionality=THREE_D,
    type=DEFORMABLE_BODY)
p = mdb.models['Model-1'].parts['Concrete Beam']
p.BaseSolidExtrude(sketch=s, depth=Lbeam)
s.unsetPrimaryObject()
p = mdb.models['Model-1'].parts['Concrete Beam']
session.viewports['Viewport: 1'].setValues(displayedObject=p)
del mdb.models['Model-1'].sketches['__profile__']
p = mdb.models['Model-1'].parts['Concrete Beam']
f, e, d1 = p.faces, p.edges, p.datums
t = p.MakeSketchTransform(sketchPlane=f[2], sketchUpEdge=e[7],
    sketchPlaneSide=SIDE1, origin=(bwbeam/2, hbeam, Lbeam/2))
s1 = mdb.models['Model-1'].ConstrainedSketch(name='__profile__',
    sheetSize=20134.79, gridSpacing=503.36, transform=t)
g, v, d, c = s1.geometry, s1.vertices, s1.dimensions, s1.constraints
s1.setPrimaryObject(option=SUPERIMPOSE)
p = mdb.models['Model-1'].parts['Concrete Beam']
p.projectReferencesOntoSketch(sketch=s1, filter=COPLANAR_EDGES)
s1.Line(point1=(((knode*Lbeam)-Lbeam/2)-50, bwbeam/2), point2=(((knode*Lbeam)-
  Lbeam/2)+50, bwbeam/2))
s1.HorizontalConstraint(entity=g[6], addUndoState=False)
s1.Line(point1=(((knode*Lbeam)-Lbeam/2)+50, bwbeam/2), point2=(((knode*Lbeam)-
  Lbeam/2)+50, -bwbeam/2))
s1.VerticalConstraint(entity=g[7], addUndoState=False)
s1.PerpendicularConstraint(entity1=g[6], entity2=g[7], addUndoState=False)
s1.Line(point1=(((knode*Lbeam)-Lbeam/2)+50, -bwbeam/2), point2=(((knode*Lbeam)-
  Lbeam/2)-50, -bwbeam/2))
s1.HorizontalConstraint(entity=g[8], addUndoState=False)
s1.PerpendicularConstraint(entity1=g[7], entity2=g[8], addUndoState=False)
s1.Line(point1=(((knode*Lbeam)-Lbeam/2)-50, -bwbeam/2), point2=(((knode*Lbeam)-
  Lbeam/2)-50, bwbeam/2))
s1.VerticalConstraint(entity=g[9], addUndoState=False)
s1.PerpendicularConstraint(entity1=g[8], entity2=g[9], addUndoState=False)
    s1.Line(point1=(((knode*Lbeam)-Lbeam/2)-50, 0.0), point2=(((knode*Lbeam)-
    Lbeam/2)+50, 0.0))
s1.HorizontalConstraint(entity=g[10], addUndoState=False)
p = mdb.models['Model-1'].parts['Concrete Beam']
f = p.faces
pickedFaces = f.getSequenceFromMask(mask=('[#4 ]', ), )
e1, d2 = p.edges, p.datums
p.PartitionFaceBySketch(sketchUpEdge=e1[7], faces=pickedFaces, sketch=s1)
s1.unsetPrimaryObject()
del mdb.models['Model-1'].sketches['__profile__']
p = mdb.models['Model-1'].parts['Concrete Beam']
e = p.edges
pickedEdges = e.getSequenceFromMask(mask=('[#8 ]', ), )
p.PartitionEdgeByParam(edges=pickedEdges, parameter=0.5)
```

```
p = mdb.models['Model-1'].parts['Concrete Beam']
v = p.vertices
verts = v.getSequenceFromMask(mask=('[#10 ]', ), )
p.Set(vertices=verts, name='Load Node')
session.viewports['Viewport: 1'].view.setValues(nearPlane=17463.4,
    farPlane=27076.1, width=6557.32, height=5548.89, cameraPosition=(
    14351.3, -4687.54, 21413.3), cameraUpVector=(-0.544694, 0.795769,
    0.26469), cameraTarget=(-50.4581, -9.40674, 5434.86))
p = mdb.models['Model-1'].parts['Concrete Beam']
f1, e = p.faces, p.edges
t = p.MakeSketchTransform(sketchPlane=f1[8], sketchUpEdge=e[27],
    sketchPlaneSide=SIDE1, sketchOrientation=RIGHT, origin=(bwbeam/2, 0.0,
    Lbeam/2))
s = mdb.models['Model-1'].ConstrainedSketch(name='__profile__',
    sheetSize=20134.79, gridSpacing=503.36, transform=t)
g, v, d, c = s.geometry, s.vertices, s.dimensions, s.constraints
s.setPrimaryObject(option=SUPERIMPOSE)
p = mdb.models['Model-1'].parts['Concrete Beam']
p.projectReferencesOntoSketch(sketch=s, filter=COPLANAR_EDGES)
s.Line(point1=(xcr, bwbeam/2), point2=(xcr+wcr, bwbeam/2))
s.HorizontalConstraint(entity=g[6], addUndoState=False)
s.Line(point1=(xcr+wcr, bwbeam/2), point2=(xcr+wcr, -bwbeam/2))
s.VerticalConstraint(entity=g[7], addUndoState=False)
s.PerpendicularConstraint(entity1=g[6], entity2=g[7], addUndoState=False)
s.Line(point1=(xcr+wcr, -bwbeam/2), point2=(xcr, -bwbeam/2))
s.HorizontalConstraint(entity=g[8], addUndoState=False)
s.PerpendicularConstraint(entity1=g[7], entity2=g[8], addUndoState=False)
s.Line(point1=(xcr, -bwbeam/2), point2=(xcr, bwbeam/2))
s.VerticalConstraint(entity=g[9], addUndoState=False)
s.PerpendicularConstraint(entity1=g[8], entity2=g[9], addUndoState=False)
p = mdb.models['Model-1'].parts['Concrete Beam']
f, e1 = p.faces, p.edges
p.CutExtrude(sketchPlane=f[8], sketchUpEdge=e1[27], sketchPlaneSide=SIDE1,
    sketchOrientation=RIGHT, sketch=s, depth=dcr,
    flipExtrudeDirection=OFF)
s.unsetPrimaryObject()
del mdb.models['Model-1'].sketches['__profile__']
session.viewports['Viewport: 1'].partDisplay.setValues(sectionAssignments=ON,
    engineeringFeatures=ON)
session.viewports['Viewport: 1'].partDisplay.geometryOptions.setValues(
    referenceRepresentation=OFF)
mdb.models['Model-1'].Material(name='Concrete')
mdb.models['Model-1'].materials['Concrete'].Elastic(table=((Econc, vconc), ))
mdb.models['Model-1'].HomogeneousSolidSection(name='Concrete Beam',
    material='Concrete', thickness=None)
p = mdb.models['Model-1'].parts['Concrete Beam']
c = p.cells
cells = c.getSequenceFromMask(mask=('[#1 ]', ), )
region = p.Set(cells=cells, name='Concrete Beam')
p = mdb.models['Model-1'].parts['Concrete Beam']
p.SectionAssignment(region=region, sectionName='Concrete Beam', offset=0.0,
```

```
        offsetType=MIDDLE_SURFACE, offsetField='',
    thicknessAssignment=FROM_SECTION)
session.viewports['Viewport: 1'].partDisplay.setValues(sectionAssignments=OFF,
    engineeringFeatures=OFF, mesh=ON)
session.viewports['Viewport: 1'].partDisplay.meshOptions.setValues(
    meshTechnique=ON)
p = mdb.models['Model-1'].parts['Concrete Beam']
p.seedPart(size=concmesh, deviationFactor=0.1, minSizeFactor=0.1)
p = mdb.models['Model-1'].parts['Concrete Beam']
c = p.cells
pickedRegions = c.getSequenceFromMask(mask=('[#1 ]', ), )
p.setMeshControls(regions=pickedRegions, elemShape=TET, technique=FREE)
elemType1 = mesh.ElemType(elemCode=C3D20R)
elemType2 = mesh.ElemType(elemCode=C3D15)
elemType3 = mesh.ElemType(elemCode=C3D10)
p = mdb.models['Model-1'].parts['Concrete Beam']
c = p.cells
cells = c.getSequenceFromMask(mask=('[#1 ]', ), )
pickedRegions =(cells, )
p.setElementType(regions=pickedRegions, elemTypes=(elemType1, elemType2,
    elemType3))
p = mdb.models['Model-1'].parts['Concrete Beam']
p.generateMesh()
elemType1 = mesh.ElemType(elemCode=C3D20, elemLibrary=STANDARD)
elemType2 = mesh.ElemType(elemCode=C3D15, elemLibrary=STANDARD)
elemType3 = mesh.ElemType(elemCode=C3D10, elemLibrary=STANDARD)
p = mdb.models['Model-1'].parts['Concrete Beam']
c = p.cells
cells = c.getSequenceFromMask(mask=('[#1 ]', ), )
pickedRegions =(cells, )
p.setElementType(regions=pickedRegions, elemTypes=(elemType1, elemType2,
    elemType3))
session.viewports['Viewport: 1'].partDisplay.setValues(mesh=OFF)
session.viewports['Viewport: 1'].partDisplay.meshOptions.setValues(
    meshTechnique=OFF)
session.viewports['Viewport: 1'].partDisplay.geometryOptions.setValues(
    referenceRepresentation=ON)
s1 = mdb.models['Model-1'].ConstrainedSketch(name='__profile__',
    sheetSize=200.0)
g, v, d, c = s1.geometry, s1.vertices, s1.dimensions, s1.constraints
s1.setPrimaryObject(option=STANDALONE)
s1.Line(point1=(0.0, 0.0), point2=(Lbeam, 0.0))
s1.HorizontalConstraint(entity=g[2], addUndoState=False)
p = mdb.models['Model-1'].Part(name='Rebar', dimensionality=THREE_D,
    type=DEFORMABLE_BODY)
p = mdb.models['Model-1'].parts['Rebar']
p.BaseWire(sketch=s1)
s1.unsetPrimaryObject()
p = mdb.models['Model-1'].parts['Rebar']
session.viewports['Viewport: 1'].setValues(displayedObject=p)
del mdb.models['Model-1'].sketches['__profile__']
```

```
session.viewports['Viewport: 1'].partDisplay.setValues(sectionAssignments=ON,
    engineeringFeatures=ON)
session.viewports['Viewport: 1'].partDisplay.geometryOptions.setValues(
    referenceRepresentation=OFF)
mdb.models['Model-1'].Material(name='Steel')
mdb.models['Model-1'].materials['Steel'].Elastic(table=((Esteel, vsteel), ))
mdb.models['Model-1'].TrussSection(name='Rebar', material='Steel', area=Abar)
p = mdb.models['Model-1'].parts['Rebar']
e = p.edges
edges = e.getSequenceFromMask(mask=('[#1 ]', ), )
region = p.Set(edges=edges, name='Rebar')
p = mdb.models['Model-1'].parts['Rebar']
p.SectionAssignment(region=region, sectionName='Rebar', offset=0.0,
    offsetType=MIDDLE_SURFACE, offsetField='',
    thicknessAssignment=FROM_SECTION)
session.viewports['Viewport: 1'].partDisplay.setValues(sectionAssignments=OFF,
    engineeringFeatures=OFF, mesh=ON)
session.viewports['Viewport: 1'].partDisplay.meshOptions.setValues(
    meshTechnique=ON)
p = mdb.models['Model-1'].parts['Rebar']
p.seedPart(size=steelmesh, deviationFactor=0.1, minSizeFactor=0.1)
p = mdb.models['Model-1'].parts['Rebar']
p.generateMesh()
elemType1 = mesh.ElemType(elemCode=T3D3, elemLibrary=STANDARD)
p = mdb.models['Model-1'].parts['Rebar']
e = p.edges
edges = e.getSequenceFromMask(mask=('[#1 ]', ), )
pickedRegions =(edges, )
p.setElementType(regions=pickedRegions, elemTypes=(elemType1, ))
a = mdb.models['Model-1'].rootAssembly
session.viewports['Viewport: 1'].setValues(displayedObject=a)
session.viewports['Viewport: 1'].assemblyDisplay.setValues(
    optimizationTasks=OFF, geometricRestrictions=OFF, stopConditions=OFF)
a = mdb.models['Model-1'].rootAssembly
a.DatumCsysByDefault(CARTESIAN)
p = mdb.models['Model-1'].parts['Concrete Beam']
a.Instance(name='Concrete Beam-1', part=p, dependent=ON)
a = mdb.models['Model-1'].rootAssembly
p = mdb.models['Model-1'].parts['Rebar']
a.Instance(name='Rebar-1', part=p, dependent=ON)
p1 = a.instances['Rebar-1']
p1.translate(vector=(bfbeampos+1000.0, 0.0, 0.0))
session.viewports['Viewport: 1'].view.fitView()
a = mdb.models['Model-1'].rootAssembly
a.rotate(instanceList=('Rebar-1', ), axisPoint=(bfbeampos, hwbeam, 0.0),
    axisDirection=(0.0, tfbeam, 0.0), angle=90.0)
a = mdb.models['Model-1'].rootAssembly
a.translate(instanceList=('Rebar-1', ), vector=(-bfbeampos, 0.0, Lbeam+1000.0))
session.viewports['Viewport: 1'].assemblyDisplay.hideInstances(instances=(
    'Concrete Beam-1', ))
a = mdb.models['Model-1'].rootAssembly
```

a.translate(instanceList=('Rebar-1',), vector=(cover, cover, 0.0))
a = mdb.models['Model-1'].rootAssembly
a.LinearInstancePattern(instanceList=('Rebar-1',), direction1=(1.0, 0.0, 0.0),
    direction2=(0.0, 1.0, 0.0), number1=3, number2=1, spacing1=(bwbeam-2*cover)/2,
    spacing2=1.0)
session.viewports['Viewport: 1'].assemblyDisplay.setValues(interactions=ON,
    constraints=ON, connectors=ON, engineeringFeatures=ON)
a = mdb.models['Model-1'].rootAssembly
e1 = a.instances['Rebar-1'].edges
edges1 = e1.getSequenceFromMask(mask=('[#1]',),)
e2 = a.instances['Rebar-1-lin-2-1'].edges
edges2 = e2.getSequenceFromMask(mask=('[#1]',),)
e3 = a.instances['Rebar-1-lin-3-1'].edges
edges3 = e3.getSequenceFromMask(mask=('[#1]',),)
region1=a.Set(edges=edges1+edges2+edges3, name='Reinforcement')
mdb.models['Model-1'].EmbeddedRegion(name='Reinforcement',
    embeddedRegion=region1, hostRegion=None, weightFactorTolerance=1e-06,
    absoluteTolerance=0.0, fractionalTolerance=0.5, toleranceMethod=BOTH)
session.viewports['Viewport: 1'].assemblyDisplay.showInstances(instances=(
    'Concrete Beam-1',))
session.viewports['Viewport: 1'].assemblyDisplay.setValues(interactions=OFF,
    constraints=OFF, connectors=OFF, engineeringFeatures=OFF,
    adaptiveMeshConstraints=ON)
mdb.models['Model-1'].StaticStep(name='Step-1', previous='Initial')
session.viewports['Viewport: 1'].assemblyDisplay.setValues(step='Step-1')
del mdb.models['Model-1'].historyOutputRequests['H-Output-1']
mdb.models['Model-1'].fieldOutputRequests['F-Output-1'].setValues(variables=(
    'U',))
session.viewports['Viewport: 1'].assemblyDisplay.setValues(loads=ON, bcs=ON,
    predefinedFields=ON, connectors=ON, adaptiveMeshConstraints=OFF)
a = mdb.models['Model-1'].rootAssembly
s1 = a.instances['Concrete Beam-1'].faces
side1Faces1 = s1.getSequenceFromMask(mask=('[#200]',),)
region = a.Surface(side1Faces=side1Faces1, name='Surf-1')
mdb.models['Model-1'].Pressure(name='Load-1', createStepName='Step-1',
    region=region, distributionType=TOTAL_FORCE, field='',
    magnitude=load/2, amplitude=UNSET)
a = mdb.models['Model-1'].rootAssembly
s1 = a.instances['Concrete Beam-1'].faces
side1Faces1 = s1.getSequenceFromMask(mask=('[#20]',),)
region = a.Surface(side1Faces=side1Faces1, name='Surf-2')
mdb.models['Model-1'].Pressure(name='Load-2', createStepName='Step-1',
    region=region, distributionType=TOTAL_FORCE, field='',
    magnitude=load/2, amplitude=UNSET)
a = mdb.models['Model-1'].rootAssembly
e1 = a.instances['Concrete Beam-1'].edges
edges1 = e1.getSequenceFromMask(mask=('[#10000]',),)
region = a.Set(edges=edges1, name='Pin')
mdb.models['Model-1'].DisplacementBC(name='Pin', createStepName='Step-1',
    region=region, u1=0.0, u2=0.0, u3=0.0, ur1=UNSET, ur2=UNSET, ur3=UNSET,
    amplitude=UNSET, fixed=OFF, distributionType=UNIFORM, fieldName='',

```
        localCsys=None)
    session.viewports['Viewport: 1'].view.setValues(nearPlane=31128,
        farPlane=43601.5, width=15361.3, height=12998.9, cameraPosition=(11199,
        16393, -27207), cameraUpVector=(-0.978842, -0.197584, 0.0531941),
        cameraTarget=(4799.36, -593.581, 735.064))
    a = mdb.models['Model-1'].rootAssembly
    e1 = a.instances['Concrete Beam-1'].edges
    edges1 = e1.getSequenceFromMask(mask=('[#0 #800 ]', ), )
    region = a.Set(edges=edges1, name='Roller')
    mdb.models['Model-1'].DisplacementBC(name='Roller', createStepName='Step-1',
        region=region, u1=0.0, u2=0.0, u3=UNSET, ur1=UNSET, ur2=UNSET,
        ur3=UNSET, amplitude=UNSET, fixed=OFF, distributionType=UNIFORM,
        fieldName='', localCsys=None)
    session.viewports['Viewport: 1'].assemblyDisplay.setValues(loads=OFF, bcs=OFF,
        predefinedFields=OFF, connectors=OFF)
    mdb.Job(name=job, model='Model-1', description='', type=ANALYSIS,
        atTime=None, waitMinutes=0, waitHours=0, queue=None, memory=8,
        memoryUnits=GIGA_BYTES, getMemoryFromAnalysis=True,
        explicitPrecision=SINGLE, nodalOutputPrecision=SINGLE, echoPrint=OFF,
        modelPrint=OFF, contactPrint=OFF, historyPrint=OFF, userSubroutine='',
        scratch='', multiprocessingMode=DEFAULT, numCpus=4, numDomains=4,
        numGPUs=1)
    mdb.jobs[job].writeInput(consistencyChecking=OFF)
```

Example script for analysis of input files:

```
import os, glob, commands

NewInputFiles=[i[:-4] for i in glob.glob('*.inp')] # this will list all the input files in the folder

intFiles = len(NewInputFiles)
intPercentage = 0
open('_log.txt', 'w').close()
for mfile in NewInputFiles:
    intPercentage += 1
    print 'PROCESSING INPUT FILE : ' + mfile + ' - ' + str(100.0 * intPercentage / intFiles) + '%
     COMPLETED'
    logData = os.popen('abaqus job=%s int ask=off cpus=4 memory="8000 mb"' %mfile)
    output = open('_log.txt','a')
    output.write("\n" + logData.read())
    output.close()
logF = open('_log.txt', 'r')
text = logF.read()
found=text.find("error")
while found > -1:
    print "Error found at line", found, ". Check _log.txt for details"
    found=text.find("error", found+1)
print "Press Enter to end..."
raw_input()
```

Example script for extraction of nodal deflections from output database files:

```
import os
import glob
import pdb
from odbAccess import *

dicBeams = {}

OutputFiles=[i[:-4] for i in glob.glob('*.odb')]
intFiles = len(OutputFiles)
intPercentage = 0
print "Getting data from local *.odb files"

def getValue(qfile):
    odb = openOdb(mfile)
    step1 = odb.steps['Step-1']
    frame = step1.frames[-1]
    max_U2 = 0
    disp = frame.fieldOutputs['U']
    nodes = odb.rootAssembly.instances['Concrete Beam-1'].nodeSets['Load Node']
    disp_node = disp.getSubset(region=nodes)
    result = str(disp_node.values[0].data[1])
    odb.close()
    return result

for mfile in glob.glob("*.odb"):
    intPercentage += 1
    print 'PROCESSING OUTPUT FILE : ' + mfile + ' - ' + str(100.0 * intPercentage / intFiles) +
     '% COMPLETED'
    if mfile[:-4].split('-')[0] not in dicBeams.keys():
        dicBeams[mfile[:-4].split('-')[0]] = {}

    BNo = mfile[:-4].split('-')[0]
    LNo = mfile[:-4].split('-')[1]
    dicBeams[BNo][LNo] = float(getValue(mfile))

print "Done..."

open('results.txt','w').close()

allbeams = []

for keys in dicBeams.keys():
    beamresults = [keys]
    for keys2 in dicBeams[keys].keys():
        delta = dicBeams[keys][keys2]
        beamresults.append(delta)
    allbeams.append(beamresults)

for beam in allbeams:
```

```
    for value in beam:
        output = open('results.txt','a')
        output.write(str(value))
        output.write("\t")
        output.close()
    print "Writing beam " + str(beam[0]) + " to results.txt."
    output = open('results.txt','a')
    output.write("\n")
    output.close()

print "Completed!"
print "Press Enter to end..."
raw_input()
```

Appendix B - Beam Width Variation Datasets

Table B-1: Beam width variation datasets – geometric and material parameters and health indices for different widths

ID	b_w/h	h_s/h	L/h	ρ	f'_c (MPa)	ki% (b_w = 250mm)	ki% (b_w = 200mm)	ki% (b_w = 300mm)
287	0.5	0.2	10	0.005	40	0.93310	0.93272	0.93442
499	0.5	0.2	13	0.01	30	0.96354	0.96140	0.96200
685	0.7	0.28	7	0.01	40	0.97193	0.96450	0.97607
1087	0.9	0.36	7	0.005	40	0.89458	0.86946	0.89945
1186	0.9	0.36	7	0.01	50	0.95812	0.94368	0.96566
1241	0.9	0.36	10	0.005	40	0.95140	0.93995	0.95990
2064	0.5	0.2	13	0.005	30	0.96116	0.95965	0.96017
2168	0.5	0.2	13	0.01	20	0.96887	0.96915	0.97033
2180	0.5	0.2	13	0.01	20	0.95994	0.95739	0.96010
2244	0.5	0.2	13	0.01	40	0.95150	0.94857	0.95156
3140	0.9	0.36	7	0.005	40	0.86683	0.83874	0.88047
3153	0.9	0.36	7	0.005	50	0.96625	0.95814	0.97303
3242	0.9	0.36	7	0.01	40	0.97926	0.97042	0.98315
3285	0.9	0.36	7	0.01	50	0.96398	0.95297	0.97209
3667	0.9	0.36	13	0.005	50	0.94126	0.92845	0.94650
3753	0.9	0.36	13	0.01	40	0.98528	0.98122	0.98820
3847	0.5	0.2	7	0.005	20	0.96442	0.96066	0.96383
4112	0.5	0.2	10	0.005	30	0.92687	0.91990	0.92396
4125	0.5	0.2	10	0.005	30	0.98519	0.98324	0.98661
4210	0.5	0.2	10	0.01	20	0.98148	0.97824	0.98376
4394	0.5	0.2	13	0.005	40	0.97727	0.97268	0.97910
4728	0.7	0.28	7	0.01	20	0.93666	0.92502	0.93854
4792	0.7	0.28	7	0.01	40	0.92433	0.91146	0.92591
4809	0.7	0.28	7	0.01	50	0.96368	0.95523	0.96772
5304	0.7	0.28	13	0.01	40	0.94503	0.93978	0.94903
5568	0.9	0.36	7	0.01	40	0.93945	0.92446	0.94458
5625	0.9	0.36	10	0.005	20	0.96883	0.95965	0.97489
5866	0.9	0.36	13	0.005	20	0.96324	0.95255	0.96973
6066	0.9	0.36	13	0.01	40	0.96718	0.95710	0.97326
6094	0.9	0.36	13	0.01	50	0.96620	0.95611	0.97235
6187	0.5	0.2	10	0.005	20	0.98733	0.98723	0.98855

ID	b_w/h	h_s/h	L/h	ρ	f'_c (MPa)	ki% (b_w = 250mm)	ki% (b_w = 200mm)	ki% (b_w = 300mm)
6287	0.5	0.2	13	0.01	20	0.99264	0.99206	0.99281
6641	0.9	0.36	13	0.005	30	0.99471	0.99337	0.99596
6773	0.5	0.2	10	0.005	20	0.83807	0.82491	0.83652
7884	0.9	0.36	10	0.005	50	0.64344	0.59394	0.65088
8035	0.5	0.2	7	0.005	20	0.81281	0.80834	0.81856
8262	0.5	0.2	7	0.005	50	0.83080	0.83391	0.83307
8493	0.5	0.2	7	0.01	50	0.83166	0.82375	0.83388
8516	0.5	0.2	7	0.01	50	0.92406	0.92137	0.92773
9198	0.9	0.36	7	0.005	20	0.81747	0.78344	0.82754
9268	0.9	0.36	7	0.005	20	0.82873	0.79457	0.83728
9313	0.9	0.36	7	0.005	50	0.71208	0.66518	0.73020
9757	0.9	0.36	13	0.005	20	0.86163	0.83169	0.86969
9971	0.9	0.36	13	0.005	50	0.81921	0.78682	0.82923
10044	0.9	0.36	13	0.01	20	0.89576	0.86902	0.90244
10258	0.9	0.36	13	0.01	50	0.86278	0.83559	0.86925
10562	0.5	0.2	7	0.005	20	0.94965	0.94283	0.95351
10579	0.5	0.2	7	0.005	50	0.94083	0.93193	0.94452
11043	0.9	0.36	7	0.01	20	0.93014	0.91009	0.93357
11327	0.5	0.2	7	0.005	50	0.81761	0.80464	0.81959

Table B-2: Beam width variation datasets – cracking parameters

ID	b_{cr1}/L	d_{cr1}/h	w_{cr1} (mm)	b_{cr2}/L	$d_{cr2}h$	w_{cr2} (mm)	b_{cr3}/L	d_{cr3}/h	w_{cr3} (mm)	b_{cr4}/L	d_{cr4}/h	w_{cr4} (mm)	b_{cr5}/L	d_{cr5}/h	w_{cr5} (mm)
287	0.1	0	0	0.3	0	0	0.5	0	0	0.7	0.639	1	0.9	0	0
499	0.1	0	0	0.3	0.639	1	0.5	0	0	0.7	0	0	0.9	0	0
685	0.1	0	0	0.3	0	0	0.5	0	0	0.7	0.25	1	0.9	0	0
1087	0.1	0	0	0.3	0	0	0.5	0	0	0.7	0.639	1	0.9	0	0
1186	0.1	0	0	0.3	0	0	0.5	0	0	0.7	0.25	5	0.9	0	0
1241	0.1	0	0	0.3	0	0	0.5	0.25	1	0.7	0	0	0.9	0	0
2064	0.2	0.639	5	0.3	0	0	0.5	0	0	0.7	0	0	0.9	0	0
2168	0.1	0	0	0.3	0.639	5	0.5	0	0	0.7	0	0	0.9	0	0
2180	0.1	0	0	0.3	0	0	0.4	0.639	5	0.7	0	0	0.9	0	0
2244	0.1	0	0	0.3	0	0	0.4	0.639	5	0.7	0	0	0.9	0	0
3140	0.1	0	0	0.3	0	0	0.4	0.639	5	0.7	0	0	0.9	0	0
3153	0.1	0	0	0.2	0.25	1	0.5	0	0	0.7	0	0	0.9	0	0

ID	b_{cr1}/L	d_{cr1}/h	w_{cr1} (mm)	b_{cr2}/L	$d_{cr2}h$	w_{cr2} (mm)	b_{cr3}/L	d_{cr3}/h	w_{cr3} (mm)	b_{cr4}/L	d_{cr4}/h	w_{cr4} (mm)	b_{cr5}/L	d_{cr5}/h	w_{cr5} (mm)
3242	0.2	0.25	5	0.3	0	0	0.5	0	0	0.7	0	0	0.9	0	0
3285	0.1	0	0	0.3	0.25	1	0.5	0	0	0.7	0	0	0.9	0	0
3667	0.1	0	0	0.2	0.639	1	0.5	0	0	0.7	0	0	0.9	0	0
3753	0.2	0.25	1	0.3	0	0	0.5	0	0	0.7	0	0	0.9	0	0
3847	0.1	0	0	0.3	0	0	0.5	0	0	0.7	0	0	0.9	0.639	1
4112	0.1	0	0	0.3	0	0	0.6	0.639	5	0.7	0	0	0.9	0	0
4125	0.1	0	0	0.3	0	0	0.5	0	0	0.8	0.25	1	0.9	0	0
4210	0.1	0	0	0.3	0	0	0.5	0	0	0.6	0.25	5	0.9	0	0
4394	0.1	0	0	0.3	0	0	0.6	0.25	5	0.7	0	0	0.9	0	0
4728	0.1	0	0	0.3	0	0	0.5	0	0	0.7	0.639	5	0.9	0	0
4792	0.1	0	0	0.3	0	0	0.5	0	0	0.7	0.639	5	0.9	0	0
4809	0.1	0	0	0.3	0	0	0.6	0.25	1	0.7	0	0	0.9	0	0
5304	0.1	0	0	0.3	0	0	0.5	0	0	0.7	0.639	5	0.9	0	0
5568	0.1	0	0	0.3	0	0	0.5	0	0	0.8	0.639	5	0.9	0	0
5625	0.1	0	0	0.3	0	0	0.5	0	0	0.75	0.25	1	0.9	0	0
5866	0.1	0	0	0.3	0	0	0.55	0.25	5	0.7	0	0	0.9	0	0
6066	0.1	0	0	0.3	0	0	0.5	0	0	0.6	0.25	5	0.9	0	0
6094	0.1	0	0	0.3	0	0	0.6	0.25	5	0.7	0	0	0.9	0	0
6187	0.1	0.639	1	0.3	0	0	0.5	0	0	0.7	0	0	0.9	0	0
6287	0.1	0	0	0.3	0	0	0.5	0	0	0.7	0	0	0.94	0.639	1
6641	0.1	0.25	1	0.3	0	0	0.5	0	0	0.7	0	0	0.9	0	0
6773	0.1	0.5	2.5	0.3	0.5	2.5	0.5	0.5	2.5	0.7	0.5	2.5	0.9	0.5	2.5
7884	0.2	0.639	5	0.4	0.639	5	0.5	0.639	5	0.6	0.639	5	0.8	0.639	5
8035	0.2	0.1	2.5	0.4	0.639	0.05	0.6	0.639	2.5	0.79	0.639	0.05	0.9	0.1	2.5
8262	0.1	0.1	2.5	0.39	0.639	2.5	0.4	0.1	2.5	0.8	0.639	0.05	0.8	0.1	0.05
8493	0.2	0.639	0.05	0.4	0.639	2.5	0.59	0.639	0.05	0.8	0.1	2.5	0.9	0.1	0.05
8516	0.2	0.639	0.05	0.2	0.1	2.5	0.6	0.1	2.5	0.61	0.1	2.5	0.9	0.639	0.05
9198	0.2	0.1	2.5	0.4	0.639	2.5	0.59	0.1	2.5	0.8	0.639	0.05	0.9	0.1	0.05
9268	0.1	0.1	2.5	0.4	0.639	0.05	0.41	0.1	0.05	0.8	0.639	0.05	0.8	0.1	2.5
9313	0.1	0.1	2.5	0.21	0.1	0.05	0.4	0.639	2.5	0.6	0.639	0.05	0.8	0.639	2.5
9757	0.2	0.639	2.5	0.39	0.1	0.05	0.6	0.639	2.5	0.8	0.1	0.05	0.9	0.639	2.5
9971	0.2	0.639	0.05	0.2	0.639	0.05	0.6	0.639	2.5	0.6	0.1	2.5	0.94	0.1	2.5
10044	0.06	0.639	2.5	0.2	0.639	2.5	0.4	0.639	2.5	0.6	0.1	0.05	0.8	0.1	0.05
10258	0.2	0.639	2.5	0.2	0.639	0.05	0.6	0.639	0.05	0.61	0.1	0.05	0.9	0.1	2.5
10562	0.1	0.639	0.05	0.3	0.25	2.5	0.5	0	0	0.7	0	0	0.9	0.1	5
10579	0.1	0.1	5	0.3	0.25	2.5	0.5	0	0	0.7	0	0	0.9	0.639	0.05

ID	b_{cr1}/L	d_{cr1}/h	w_{cr1} (mm)	b_{cr2}/L	$d_{cr2}h$	w_{cr2} (mm)	b_{cr3}/L	d_{cr3}/h	w_{cr3} (mm)	b_{cr4}/L	d_{cr4}/h	w_{cr4} (mm)	b_{cr5}/L	d_{cr5}/h	w_{cr5} (mm)
11043	0.1	0	0	0.3	0	0	0.5	0	0	0.7	0.639	0.05	0.9	0.1	5
11327	0.1	0	0	0.3	0.639	0.05	0.5	0.25	5	0.7	0.639	2.5	0.9	0.1	5

Appendix C - Random Sample of Main Beam Database

Table C-1: Main database – geometric and material input, and nodal stiffness ratio and health index output parameters

ID	b_w/h	h_s/h	L/h	ρ	f'$_c$ (MPa)	k%$_1$	k%$_2$	k%$_3$	k%$_4$	k%$_5$	k%$_6$	k%$_7$	k%$_8$	k%$_9$	ki%	Set
15	0.5	0.2	10	0.01	40	1	1	1	1	1	1	1	1	1	1	1
17	0.5	0.2	13	0.005	20	1	1	1	1	1	1	1	1	1	1	2
31	0.7	0.28	7	0.01	40	1	1	1	1	1	1	1	1	1	1	3
75	0.5	0.2	7	0.005	20	0.91437	0.93352	0.96671	0.97932	0.98641	0.99033	0.99335	0.99541	1	0.97601	1
81	0.5	0.2	7	0.005	20	0.98882	0.97812	0.96648	0.95012	0.93419	0.94954	0.96694	0.97866	0.9951	0.9708	3
133	0.5	0.2	7	0.005	50	0.95426	0.97675	0.98895	0.99288	0.99512	0.99712	0.99815	0.99911	1	0.99045	1
169	0.5	0.2	7	0.01	20	1	0.99993	0.99947	0.9983	0.997	0.99573	0.99296	0.9858	0.97748	0.99477	1
212	0.5	0.2	7	0.01	40	0.99867	0.99597	0.99426	0.99125	0.98561	0.98055	0.96913	0.93679	0.92428	0.97765	1
249	0.5	0.2	10	0.005	20	0.99537	0.99796	0.99853	0.998	0.99756	0.99617	0.99323	0.98651	0.96254	0.99259	3
277	0.5	0.2	10	0.005	40	0.97239	0.95727	0.94404	0.96594	0.97824	0.98479	0.98898	0.99266	0.99359	0.97779	1
280	0.5	0.2	10	0.005	40	0.91836	0.87201	0.83891	0.89141	0.92779	0.94924	0.96216	0.97401	0.98046	0.93144	3
294	0.5	0.2	10	0.005	50	0.95188	0.98212	0.99183	0.99523	0.99713	0.99812	0.99848	0.99937	0.99856	0.99127	1
297	0.5	0.2	10	0.005	50	0.97143	0.95575	0.94207	0.96472	0.97745	0.98423	0.98857	0.99237	0.99341	0.977	3
312	0.5	0.2	10	0.005	50	0.99721	0.99597	0.99476	0.99246	0.98944	0.98348	0.97153	0.94139	0.87748	0.97437	1
319	0.5	0.2	10	0.01	20	0.95367	0.92701	0.9038	0.93627	0.95759	0.97048	0.9785	0.9847	0.98907	0.96011	3
323	0.5	0.2	10	0.01	20	0.97527	0.96005	0.94385	0.92366	0.8984	0.92314	0.94278	0.96032	0.97489	0.95024	2
326	0.5	0.2	10	0.01	20	0.99393	0.99384	0.99192	0.9888	0.98469	0.97569	0.95981	0.97018	0.98022	0.98391	2
332	0.5	0.2	10	0.01	20	0.99797	0.99726	0.99658	0.99499	0.993	0.98897	0.98092	0.96032	0.92864	0.98386	1
362	0.5	0.2	10	0.01	40	0.98777	0.98063	0.97128	0.96206	0.94855	0.96352	0.97422	0.98117	0.98701	0.97562	2
419	0.5	0.2	13	0.005	30	0.93536	0.90352	0.8772	0.92089	0.94783	0.96398	0.97312	0.98024	0.98729	0.94894	2
428	0.5	0.2	13	0.005	30	0.98739	0.97953	0.97222	0.96186	0.94594	0.91926	0.8732	0.89857	0.92917	0.94672	1
479	0.5	0.2	13	0.01	20	0.9604	0.93831	0.92048	0.94903	0.96671	0.97697	0.98297	0.98736	0.99231	0.96746	2
484	0.5	0.2	13	0.01	20	0.97439	0.96266	0.95134	0.93326	0.91058	0.93304	0.95018	0.96351	0.97581	0.95548	3
498	0.5	0.2	13	0.01	30	0.98366	0.97388	0.96526	0.97907	0.98668	0.9906	0.99321	0.99485	0.99702	0.98642	1
509	0.5	0.2	13	0.01	30	1	0.99994	0.99934	0.999	0.99856	0.99762	0.99577	0.99108	0.97271	0.99568	2
510	0.5	0.2	13	0.01	30	1	0.9993	0.99924	0.99879	0.99837	0.99732	0.99534	0.99012	0.97013	0.99494	1
526	0.5	0.2	13	0.01	40	0.99863	0.99506	0.99301	0.99005	0.98599	0.97808	0.96277	0.97135	0.98093	0.98559	1
541	0.5	0.2	13	0.01	50	0.99144	0.98471	0.97921	0.97166	0.95906	0.97112	0.97866	0.98434	0.9883	0.98085	1
555	0.7	0.28	7	0.005	20	0.89444	0.92481	0.96145	0.97671	0.98495	0.9897	0.9931	0.99706	0.99713	0.97194	1
573	0.7	0.28	7	0.005	30	0.94527	0.9716	0.98694	0.99192	0.9946	0.99629	0.99692	0.99876	0.99463	0.98769	3
585	0.7	0.28	7	0.005	30	0.99609	0.98863	0.98291	0.97491	0.96322	0.94299	0.91527	0.93606	0.96607	0.96662	3

ID	bw/h	hs/h	L/h	ρ	f'c (MPa)	k%1	k%2	k%3	k%4	k%5	k%6	k%7	k%8	k%9	ki%	Set
587	0.7	0.28	7	0.005	30	0.98374	0.96731	0.95038	0.9312	0.90121	0.8566	0.80009	0.84598	0.91056	0.91471	2
588	0.7	0.28	7	0.005	30	0.9849	0.9649	0.9489	0.92732	0.89687	0.852	0.7967	0.84057	0.91143	0.91236	1
611	0.7	0.28	7	0.005	40	0.99841	0.9952	0.99268	0.98842	0.98299	0.97382	0.95645	0.91592	0.87084	0.96747	2
648	0.7	0.28	7	0.01	20	0.99193	0.97748	0.96721	0.95263	0.93173	0.90017	0.86451	0.89768	0.94491	0.94282	1
678	0.7	0.28	7	0.01	40	0.97036	0.94238	0.92652	0.95014	0.96836	0.97812	0.98522	0.99193	0.9967	0.97097	1
683	0.7	0.28	7	0.01	40	0.96416	0.92815	0.89991	0.86053	0.82287	0.85903	0.89997	0.93163	0.96455	0.91308	2
687	0.7	0.28	7	0.01	40	0.98812	0.97492	0.9618	0.94653	0.92265	0.88654	0.84209	0.88044	0.93151	0.93346	1
702	0.7	0.28	7	0.01	50	0.9854	0.96838	0.95331	0.93249	0.91257	0.9316	0.95271	0.9693	0.98034	0.95861	1
724	0.7	0.28	10	0.005	20	0.95358	0.92575	0.8999	0.86068	0.82428	0.86589	0.89811	0.92602	0.95327	0.91075	3
779	0.7	0.28	10	0.005	50	0.89971	0.8488	0.80705	0.87206	0.9138	0.9378	0.95571	0.96694	0.97953	0.91814	2
799	0.7	0.28	10	0.01	20	0.94521	0.91235	0.88545	0.92492	0.9504	0.96488	0.97497	0.9817	0.98938	0.95293	3
811	0.7	0.28	10	0.01	20	1	0.9984	0.99642	0.9948	0.9922	0.98854	0.97934	0.95825	0.916	0.98242	3
856	0.7	0.28	10	0.01	50	0.89245	0.94691	0.97394	0.98536	0.99051	0.99368	0.99573	0.99756	1	0.97779	3
927	0.7	0.28	13	0.005	40	0.98273	0.97364	0.9661	0.95394	0.93412	0.90079	0.84443	0.87959	0.91159	0.93469	1
952	0.7	0.28	13	0.005	50	0.99892	0.99675	0.99559	0.99368	0.99082	0.98553	0.97499	0.94657	0.86207	0.97449	3
984	0.7	0.28	13	0.01	30	0.96268	0.94443	0.93469	0.91272	0.87517	0.90775	0.93287	0.94404	0.96415	0.93785	1
993	0.7	0.28	13	0.01	40	0.95866	0.98665	0.99412	0.99665	0.99777	0.99857	0.99899	0.99972	1	0.99311	3
1033	0.9	0.36	7	0.005	20	0.92141	0.9628	0.98053	0.98869	0.99319	0.99556	0.99709	0.99797	1	0.98414	1
1052	0.9	0.36	7	0.005	20	0.99513	0.99452	0.99016	0.98684	0.98155	0.97127	0.95358	0.90633	0.85733	0.96367	1
1097	0.9	0.36	7	0.005	50	0.95248	0.91087	0.88493	0.92138	0.94951	0.96469	0.9748	0.98278	0.99137	0.95328	2
1110	0.9	0.36	7	0.005	50	0.9965	0.99821	0.99537	0.99376	0.99156	0.98795	0.97817	0.95788	0.91695	0.98163	1
1129	0.9	0.36	7	0.01	20	0.99634	0.99916	0.99578	0.99523	0.99361	0.99064	0.9833	0.967	0.93285	0.98539	1
1154	0.9	0.36	7	0.01	40	0.92584	0.96573	0.98136	0.99003	0.99336	0.9955	0.99658	0.99804	1	0.98472	2
1176	0.9	0.36	7	0.01	50	0.86826	0.91182	0.95531	0.97295	0.98287	0.98793	0.99132	0.99473	0.99904	0.96642	1
1190	0.9	0.36	7	0.01	50	0.99667	0.99862	0.99592	0.99453	0.9927	0.98973	0.98116	0.96411	0.92885	0.98423	2
1250	0.9	0.36	10	0.005	40	0.99815	0.99796	0.99772	0.99632	0.995	0.99236	0.98633	0.97089	0.92281	0.98575	2
1265	0.9	0.36	10	0.005	50	0.989	0.9845	0.9797	0.97207	0.96064	0.93955	0.90556	0.92458	0.9492	0.96048	2
1308	0.9	0.36	10	0.01	30	0.98361	0.97397	0.96593	0.95209	0.93109	0.89885	0.85072	0.88013	0.91747	0.93538	1
1311	0.9	0.36	10	0.01	30	0.99713	0.99611	0.99512	0.99313	0.9902	0.98515	0.97389	0.94538	0.88392	0.976	1
1340	0.9	0.36	10	0.01	50	0.90709	0.8628	0.83057	0.88472	0.923	0.94571	0.96063	0.97145	0.98175	0.92677	1
1351	0.9	0.36	10	0.01	50	0.99688	0.99573	0.9946	0.99241	0.98917	0.98357	0.97108	0.93988	0.87016	0.97335	3
1390	0.9	0.36	13	0.005	30	0.99856	0.9984	0.99829	0.99748	0.99644	0.99442	0.99014	0.97879	0.93654	0.98891	1
1401	0.9	0.36	13	0.005	40	0.97585	0.96702	0.95685	0.94039	0.92016	0.94033	0.95576	0.96681	0.97599	0.95992	3
1407	0.9	0.36	13	0.005	40	0.9761	0.96985	0.95962	0.94438	0.92402	0.88424	0.8248	0.8524	0.89149	0.92269	1
1418	0.9	0.36	13	0.005	50	0.9518	0.93444	0.91853	0.94935	0.96717	0.97711	0.9831	0.98729	0.9905	0.96593	2
1419	0.9	0.36	13	0.005	50	0.88711	0.84916	0.81674	0.8796	0.91829	0.94175	0.95645	0.96701	0.97648	0.91926	1

ID	b_w/h	h_s/h	L/h	ρ	f'_c (MPa)	$k\%_1$	$k\%_2$	$k\%_3$	$k\%_4$	$k\%_5$	$k\%_6$	$k\%_7$	$k\%_8$	$k\%_9$	$k_i\%$	Set
1462	0.9	0.36	13	0.01	30	0.9779	0.97046	0.96259	0.9481	0.93062	0.94882	0.96177	0.97141	0.97931	0.9651	1
1493	0.9	0.36	13	0.01	50	0.94345	0.98172	0.99172	0.9951	0.99698	0.99784	0.99831	0.99851	0.99781	0.99014	2
1526	0.5	0.2	7	0.005	20	0.97115	0.94197	0.94526	0.96986	0.97969	0.98637	0.99031	0.99347	0.99961	0.97777	2
1547	0.5	0.2	7	0.005	30	0.89725	0.87822	0.9327	0.95944	0.97336	0.98187	0.98751	0.99268	1	0.96056	2
1556	0.5	0.2	7	0.005	30	0.90774	0.82883	0.88908	0.9308	0.95332	0.96873	0.9781	0.98567	0.99722	0.94395	1
1569	0.5	0.2	7	0.005	30	0.97992	0.96352	0.94616	0.92959	0.94871	0.96637	0.97684	0.9852	0.99964	0.9696	3
1671	0.5	0.2	7	0.01	20	0.96923	0.94495	0.91996	0.88711	0.88711	0.91929	0.94274	0.96244	0.98612	0.9419	1
1693	0.5	0.2	7	0.01	30	0.98413	0.97192	0.95867	0.94562	0.96021	0.97415	0.9825	0.98911	1	0.9768	1
1709	0.5	0.2	7	0.01	40	0.97016	0.95305	0.97144	0.98384	0.98919	0.99306	0.9955	0.99807	1	0.98603	2
1710	0.5	0.2	7	0.01	40	0.97069	0.94832	0.96959	0.98288	0.98858	0.9923	0.99476	0.99696	1	0.98468	1
1714	0.5	0.2	7	0.01	40	0.97069	0.94832	0.96959	0.98288	0.98858	0.9923	0.99476	0.99696	1	0.98468	1
1732	0.5	0.2	7	0.01	40	0.95889	0.91784	0.88053	0.84812	0.88171	0.91654	0.94181	0.95851	0.98153	0.92855	3
1745	0.5	0.2	7	0.01	50	0.96886	0.95095	0.97019	0.98312	0.98872	0.99275	0.99528	0.99791	1	0.98537	2
1769	0.5	0.2	10	0.005	20	0.96102	0.96886	0.9859	0.9919	0.99501	0.99651	0.9974	0.99869	0.99807	0.98934	2
1840	0.5	0.2	10	0.005	40	0.89175	0.84917	0.91173	0.94653	0.96563	0.97571	0.982	0.98757	0.98952	0.94996	3
1863	0.5	0.2	10	0.005	40	0.94973	0.92012	0.8916	0.85545	0.85543	0.89729	0.924	0.94425	0.96434	0.92022	1
1875	0.5	0.2	10	0.005	50	0.8952	0.84792	0.91112	0.94648	0.96511	0.97545	0.9823	0.988	0.99246	0.95041	1
1881	0.5	0.2	10	0.005	50	0.97686	0.96085	0.94436	0.94973	0.96847	0.97802	0.9842	0.98872	0.99152	0.97427	3
1909	0.5	0.2	10	0.01	20	0.98176	0.96704	0.97185	0.98406	0.99009	0.99292	0.99464	0.99606	0.99445	0.98729	1
1911	0.5	0.2	10	0.01	20	0.94649	0.91734	0.92283	0.95387	0.97056	0.97931	0.98456	0.98975	0.9913	0.9656	1
1939	0.5	0.2	10	0.01	30	0.93457	0.90113	0.94116	0.96492	0.97733	0.98423	0.9886	0.9926	0.99536	0.96799	3
1973	0.5	0.2	10	0.01	40	0.97851	0.96179	0.96743	0.98159	0.98849	0.99181	0.99385	0.99549	0.99418	0.98531	2
2075	0.5	0.2	13	0.005	30	0.94131	0.91382	0.88577	0.89476	0.92968	0.95078	0.96383	0.97281	0.98166	0.94344	2
2086	0.5	0.2	13	0.005	30	0.9855	0.97816	0.97121	0.95945	0.96083	0.97363	0.98029	0.98506	0.99054	0.97847	1
2095	0.5	0.2	13	0.005	40	0.90985	0.87168	0.9312	0.95973	0.97438	0.98173	0.98671	0.99	0.99298	0.95983	3
2114	0.5	0.2	13	0.005	40	0.98318	0.97293	0.96322	0.95065	0.96698	0.97687	0.98302	0.98718	0.99159	0.97756	2
2126	0.5	0.2	13	0.005	50	0.96808	0.95338	0.97712	0.98696	0.99154	0.99398	0.99547	0.99637	0.99694	0.98598	2
2135	0.5	0.2	13	0.005	50	0.90688	0.86915	0.88902	0.93155	0.95676	0.96862	0.9778	0.98286	0.98858	0.94712	2
2178	0.5	0.2	13	0.01	20	0.98962	0.982	0.97522	0.9666	0.97775	0.98444	0.9885	0.99121	0.99441	0.98497	2
2187	0.5	0.2	13	0.01	30	0.93421	0.94089	0.97246	0.98375	0.9897	0.99294	0.99487	0.9962	0.99906	0.98041	1
2204	0.5	0.2	13	0.01	30	0.95684	0.93589	0.91515	0.9224	0.94823	0.96381	0.97346	0.97978	0.98584	0.95814	1
2236	0.5	0.2	13	0.01	40	0.95319	0.93077	0.90855	0.91644	0.94419	0.96094	0.97133	0.97817	0.98473	0.95483	3
2241	0.5	0.2	13	0.01	40	0.98601	0.97981	0.97245	0.96235	0.97566	0.98286	0.98758	0.99062	0.99395	0.98313	3
2267	0.5	0.2	13	0.01	50	0.95292	0.92988	0.90653	0.91362	0.94274	0.95999	0.97065	0.97793	0.98532	0.95396	2
2270	0.5	0.2	13	0.01	50	0.9868	0.97805	0.97001	0.95966	0.97308	0.98116	0.98614	0.98947	0.99319	0.98176	2
2330	0.7	0.28	7	0.005	30	0.97169	0.94225	0.91334	0.92087	0.94946	0.96424	0.97585	0.98522	0.98672	0.96096	2

90

ID	b_w/h	h_s/h	L/h	ρ	f'$_c$ (MPa)	k%$_1$	k%$_2$	k%$_3$	k%$_4$	k%$_5$	k%$_6$	k%$_7$	k%$_8$	k%$_9$	ki%	Set
2358	0.7	0.28	7	0.005	40	0.96115	0.91953	0.92722	0.95732	0.97239	0.98099	0.98695	0.99244	0.9945	0.96925	1
2359	0.7	0.28	7	0.005	40	0.8986	0.81043	0.82422	0.88597	0.92464	0.94566	0.96179	0.97602	0.98853	0.92159	3
2371	0.7	0.28	7	0.005	40	0.92805	0.86828	0.81703	0.77408	0.8255	0.87445	0.90954	0.93853	0.96868	0.89041	3
2396	0.7	0.28	7	0.005	50	0.91284	0.84056	0.78101	0.79401	0.85268	0.89459	0.92276	0.94846	0.97225	0.89192	1
2402	0.7	0.28	7	0.005	50	0.97109	0.94748	0.92252	0.90081	0.92758	0.95055	0.96568	0.97805	0.98782	0.95516	2
2429	0.7	0.28	7	0.01	20	0.98483	0.96489	0.94709	0.9313	0.9502	0.96666	0.97741	0.98582	0.99046	0.96987	2
2435	0.7	0.28	7	0.01	20	0.95736	0.92017	0.88659	0.85809	0.89104	0.92311	0.94555	0.96429	0.98276	0.9329	2
2459	0.7	0.28	7	0.01	30	0.95029	0.90324	0.85991	0.86348	0.90734	0.93432	0.95303	0.96959	0.98418	0.93254	2
2465	0.7	0.28	7	0.01	30	0.98321	0.96202	0.94294	0.92612	0.94641	0.96404	0.97552	0.98447	0.98978	0.96745	2
2482	0.7	0.28	7	0.01	40	0.95701	0.93359	0.96015	0.97709	0.98485	0.98934	0.9927	0.99571	0.99427	0.97847	1
2508	0.7	0.28	7	0.01	50	0.89618	0.87549	0.93226	0.95836	0.97298	0.9813	0.9881	0.99444	0.99899	0.95981	1
2546	0.7	0.28	10	0.005	20	0.95728	0.93546	0.96598	0.98054	0.98738	0.99159	0.99383	0.99645	0.99988	0.98084	2
2569	0.7	0.28	10	0.005	30	0.94915	0.9578	0.98061	0.98879	0.99295	0.99539	0.99648	0.99833	1	0.98612	1
2596	0.7	0.28	10	0.005	30	0.93147	0.89196	0.85934	0.82259	0.86825	0.90552	0.93172	0.95138	0.9701	0.91323	3
2601	0.7	0.28	10	0.005	40	0.94687	0.95607	0.9798	0.98833	0.99265	0.99518	0.99633	0.99821	1	0.9855	3
2604	0.7	0.28	10	0.005	40	0.86407	0.87533	0.93652	0.96318	0.97574	0.98348	0.98785	0.99194	0.9968	0.95749	1
2612	0.7	0.28	10	0.005	40	0.87527	0.82232	0.89556	0.93816	0.95917	0.97121	0.97897	0.98549	0.99275	0.94189	1
2683	0.7	0.28	10	0.01	20	0.95244	0.92386	0.89474	0.90342	0.9344	0.9549	0.96663	0.97705	0.98742	0.94949	3
2692	0.7	0.28	10	0.01	20	0.95765	0.93112	0.90795	0.88256	0.91387	0.93922	0.9566	0.96965	0.98257	0.94412	3
2733	0.7	0.28	10	0.01	40	0.96228	0.94424	0.97142	0.98284	0.98927	0.99281	0.9946	0.99695	0.9998	0.98342	3
2746	0.7	0.28	10	0.01	40	0.97724	0.96034	0.94169	0.94751	0.9665	0.97721	0.98318	0.9892	0.99678	0.97397	1
2779	0.7	0.28	10	0.01	50	0.93805	0.90301	0.86741	0.87919	0.9173	0.94278	0.95737	0.97015	0.98284	0.93581	3
2780	0.7	0.28	10	0.01	50	0.9375	0.89909	0.8664	0.87527	0.91473	0.93992	0.9557	0.9694	0.98455	0.93426	1
2784	0.7	0.28	10	0.01	50	0.94496	0.91207	0.88413	0.85299	0.89162	0.92289	0.94461	0.96087	0.97659	0.92907	1
2795	0.7	0.28	13	0.005	20	0.88977	0.9116	0.95719	0.97547	0.98441	0.98915	0.99187	0.99452	0.99505	0.9689	2
2798	0.7	0.28	13	0.005	20	0.9601	0.94481	0.97276	0.98448	0.98993	0.9931	0.9949	0.99672	0.99717	0.9834	2
2812	0.7	0.28	13	0.005	20	0.93117	0.90195	0.87142	0.8795	0.91953	0.94406	0.95807	0.96819	0.97822	0.93521	3
2815	0.7	0.28	13	0.005	20	0.94496	0.92231	0.89537	0.86684	0.90668	0.93415	0.95091	0.96393	0.97462	0.93598	3
2856	0.7	0.28	13	0.005	30	0.94663	0.92267	0.89791	0.86479	0.87049	0.90563	0.93048	0.9468	0.96354	0.92489	1
2913	0.7	0.28	13	0.005	50	0.97596	0.96457	0.95217	0.93765	0.95721	0.97035	0.97833	0.9842	0.98946	0.97099	3
2921	0.7	0.28	13	0.01	20	0.96453	0.97343	0.98814	0.99322	0.99578	0.99708	0.99795	0.99901	0.99952	0.99087	2
2925	0.7	0.28	13	0.01	20	0.96863	0.95711	0.97939	0.98822	0.99221	0.99468	0.99616	0.99762	0.99841	0.98724	3
2931	0.7	0.28	13	0.01	20	0.93171	0.90795	0.95056	0.97135	0.98126	0.98706	0.99058	0.99352	0.99551	0.97095	1
2954	0.7	0.28	13	0.01	30	0.9595	0.9702	0.9868	0.99243	0.99505	0.99664	0.99751	0.99864	0.99874	0.98955	2
2996	0.7	0.28	13	0.01	40	0.91527	0.88699	0.93908	0.96411	0.97705	0.98406	0.98804	0.99213	0.99501	0.96417	1
3049	0.9	0.36	7	0.005	20	0.93208	0.93482	0.96734	0.98048	0.98716	0.99172	0.99391	0.99484	0.99586	0.97782	1

ID	bw/h	hs/h	L/h	ρ	f'c (MPa)	k%1	k%2	k%3	k%4	k%5	k%6	k%7	k%8	k%9	ki%	Set
3052	0.9	0.36	7	0.005	20	0.85529	0.842	0.91198	0.94644	0.96472	0.97519	0.98254	0.98768	0.99343	0.94593	3
3093	0.9	0.36	7	0.005	30	0.94165	0.89794	0.908	0.94594	0.96505	0.97585	0.98275	0.9892	0.9958	0.96022	3
3109	0.9	0.36	7	0.005	30	0.96727	0.94658	0.92151	0.89187	0.89468	0.92714	0.94789	0.9645	0.9792	0.94406	1
3290	0.9	0.36	7	0.01	50	0.96409	0.93192	0.899	0.90567	0.93851	0.95783	0.96991	0.98159	0.99057	0.95391	2
3299	0.9	0.36	7	0.01	50	0.93348	0.87786	0.83033	0.79474	0.84197	0.8851	0.91503	0.94307	0.96683	0.89884	2
3308	0.9	0.36	10	0.005	20	0.85192	0.87179	0.93559	0.96237	0.97497	0.98301	0.98725	0.99069	0.99243	0.955	1
3313	0.9	0.36	10	0.005	20	0.93635	0.91757	0.95641	0.97499	0.98361	0.98861	0.99175	0.99409	0.99656	0.97399	1
3322	0.9	0.36	10	0.005	20	0.95858	0.93774	0.91603	0.92308	0.95012	0.96523	0.97481	0.98165	0.98728	0.95945	1
3337	0.9	0.36	10	0.005	30	0.92749	0.94405	0.97438	0.98482	0.99034	0.99326	0.99525	0.9963	0.99645	0.98023	1
3338	0.9	0.36	10	0.005	30	0.92354	0.94108	0.97293	0.98415	0.98977	0.993	0.99502	0.99639	0.99665	0.97925	2
3382	0.9	0.36	10	0.005	40	0.94233	0.91123	0.92595	0.9573	0.97205	0.98008	0.98598	0.98945	0.99193	0.96563	1
3404	0.9	0.36	10	0.005	50	0.82193	0.84783	0.92245	0.95443	0.96966	0.97933	0.98451	0.98868	0.99114	0.946	1
3413	0.9	0.36	10	0.005	50	0.94193	0.91239	0.92657	0.95786	0.97226	0.98093	0.9862	0.99008	0.99405	0.96623	2
3509	0.9	0.36	10	0.01	40	0.95185	0.92672	0.93864	0.96507	0.97698	0.98427	0.98864	0.99191	0.99529	0.97194	2
3525	0.9	0.36	10	0.01	40	0.97266	0.95912	0.94553	0.92416	0.92647	0.94884	0.96269	0.97295	0.98256	0.9595	3
3535	0.9	0.36	10	0.01	50	0.88527	0.84563	0.90862	0.94516	0.96415	0.97492	0.98241	0.98745	0.99141	0.9485	3
3539	0.9	0.36	10	0.01	50	0.88527	0.84563	0.90862	0.94516	0.96415	0.97492	0.98241	0.98745	0.99141	0.9485	2
3550	0.9	0.36	10	0.01	50	0.96655	0.94918	0.93182	0.91288	0.93833	0.95687	0.96828	0.977	0.98557	0.95865	1
3602	0.9	0.36	13	0.005	30	0.94129	0.92516	0.96198	0.97794	0.98582	0.99019	0.99274	0.99462	0.99742	0.97672	2
3635	0.9	0.36	13	0.005	40	0.86579	0.83024	0.90711	0.94396	0.96308	0.97383	0.98141	0.98566	0.98846	0.94395	2
3643	0.9	0.36	13	0.005	40	0.90598	0.86841	0.82884	0.84913	0.89768	0.92654	0.94522	0.95755	0.96778	0.91471	3
3689	0.9	0.36	13	0.01	20	0.94831	0.96331	0.98358	0.99044	0.99385	0.99573	0.99667	0.99732	0.99764	0.98668	2
3716	0.9	0.36	13	0.01	20	0.94802	0.92984	0.90645	0.88179	0.91755	0.9402	0.95691	0.9669	0.97607	0.94237	1
3717	0.9	0.36	13	0.01	20	0.97817	0.97007	0.96034	0.94538	0.94774	0.96384	0.97298	0.97942	0.98417	0.97021	3
3733	0.9	0.36	13	0.01	30	0.95623	0.94185	0.95268	0.97264	0.98233	0.98772	0.99088	0.9931	0.99438	0.97718	1
3751	0.9	0.36	13	0.01	30	0.9522	0.93633	0.91617	0.88912	0.89038	0.92063	0.94157	0.95466	0.96582	0.93669	3
3764	0.9	0.36	13	0.01	40	0.89703	0.86842	0.92782	0.95772	0.9724	0.98116	0.9856	0.98906	0.99161	0.95708	1
3766	0.9	0.36	13	0.01	40	0.95535	0.93721	0.94963	0.97104	0.98101	0.98686	0.99016	0.99262	0.99443	0.97583	1
3769	0.9	0.36	13	0.01	40	0.96668	0.954	0.93888	0.94461	0.96436	0.9751	0.98163	0.98603	0.98973	0.9701	1
3802	0.9	0.36	13	0.01	50	0.96359	0.9505	0.93442	0.94078	0.96165	0.97328	0.9803	0.9854	0.99048	0.96804	1
3828	0.5	0.2	7	0.005	20	0.97676	0.95164	0.92992	0.90465	0.86814	0.81535	0.85069	0.9047	0.95557	0.91574	1
3850	0.5	0.2	7	0.005	30	0.98723	0.97879	0.96861	0.95328	0.93226	0.93137	0.95355	0.97022	0.99128	0.96666	1
3854	0.5	0.2	7	0.005	30	0.99261	0.98344	0.97581	0.96413	0.9466	0.92532	0.94305	0.96323	0.98538	0.96796	2
3858	0.5	0.2	7	0.005	30	0.99261	0.98344	0.97581	0.96413	0.9466	0.92532	0.94305	0.96323	0.98538	0.96796	1
3863	0.5	0.2	7	0.005	30	0.98146	0.96069	0.94265	0.92162	0.88701	0.8359	0.83273	0.88597	0.94454	0.91926	2
3882	0.5	0.2	7	0.005	40	0.98675	0.97779	0.96718	0.9513	0.92921	0.92813	0.95134	0.96872	0.99048	0.96509	1

ID	bw/h	hs/h	L/h	ρ	f'c (MPa)	k%1	k%2	k%3	k%4	k%5	k%6	k%7	k%8	k%9	ki%	Set
3900	0.5	0.2	7	0.005	40	0.98663	0.97539	0.9641	0.94804	0.92621	0.89422	0.83873	0.83726	0.91595	0.92865	1
3944	0.5	0.2	7	0.005	50	0.99632	0.99105	0.98567	0.97781	0.96768	0.95251	0.92147	0.86454	0.88846	0.95455	1
4006	0.5	0.2	7	0.01	30	0.99829	0.99774	0.99633	0.99506	0.99286	0.98927	0.98202	0.96428	0.96358	0.98794	1
4015	0.5	0.2	7	0.01	40	0.98508	0.96423	0.94566	0.92359	0.89036	0.85658	0.88709	0.92268	0.96563	0.93409	3
4035	0.5	0.2	7	0.01	40	0.99501	0.98936	0.98343	0.9772	0.96565	0.94698	0.91343	0.88152	0.9392	0.95918	1
4090	0.5	0.2	10	0.005	20	0.99661	0.99539	0.99337	0.99016	0.98633	0.97865	0.96158	0.95495	0.97279	0.98298	1
4133	0.5	0.2	10	0.005	30	0.99765	0.99779	0.99734	0.99619	0.99471	0.99156	0.98535	0.96808	0.96015	0.98888	2
4156	0.5	0.2	10	0.005	40	0.98722	0.98105	0.97437	0.96448	0.9498	0.92386	0.87505	0.85999	0.91101	0.94268	3
4169	0.5	0.2	10	0.005	50	0.98931	0.98208	0.97524	0.96531	0.9489	0.94687	0.9629	0.97378	0.98236	0.97267	2
4177	0.5	0.2	10	0.005	50	0.99275	0.98625	0.98088	0.97248	0.96039	0.94184	0.9557	0.96901	0.97931	0.97386	1
4195	0.5	0.2	10	0.005	50	0.99156	0.98663	0.98209	0.97517	0.96449	0.94685	0.9107	0.84559	0.89306	0.94961	3
4206	0.5	0.2	10	0.01	20	0.98766	0.9892	0.98658	0.98104	0.97331	0.96022	0.97064	0.9796	0.98659	0.98148	1
4227	0.5	0.2	10	0.01	20	0.99492	0.99201	0.98962	0.98543	0.97925	0.96851	0.94633	0.91053	0.94119	0.97078	1
4266	0.5	0.2	10	0.01	40	0.99069	0.98611	0.98073	0.97309	0.95998	0.95847	0.97079	0.97997	0.98681	0.97866	1
4273	0.5	0.2	10	0.01	40	0.99504	0.98982	0.98584	0.97932	0.97012	0.9559	0.96651	0.97684	0.98421	0.98036	1
4275	0.5	0.2	10	0.01	40	0.98145	0.96779	0.956	0.94097	0.91562	0.88495	0.90978	0.93353	0.95791	0.9448	1
4276	0.5	0.2	10	0.01	40	0.97616	0.96781	0.95512	0.93914	0.91443	0.88235	0.90747	0.93223	0.95742	0.94321	3
4306	0.5	0.2	10	0.01	50	0.98662	0.98724	0.98382	0.9772	0.96776	0.95212	0.96456	0.97514	0.9838	0.97783	1
4333	0.5	0.2	13	0.005	20	0.9941	0.9896	0.9859	0.98059	0.97208	0.95855	0.96831	0.97621	0.98492	0.98103	1
4335	0.5	0.2	13	0.005	20	0.9805	0.96827	0.95741	0.94236	0.91821	0.88557	0.90965	0.9322	0.95252	0.94467	1
4337	0.5	0.2	13	0.005	20	0.9941	0.9896	0.9859	0.98059	0.97208	0.95855	0.96831	0.97621	0.98492	0.98103	2
4364	0.5	0.2	13	0.005	30	0.97237	0.95503	0.94076	0.92051	0.88627	0.88482	0.91405	0.93487	0.95649	0.93652	1
4377	0.5	0.2	13	0.005	30	0.99833	0.99567	0.99381	0.99114	0.98769	0.9807	0.96573	0.9585	0.9733	0.98449	3
4435	0.5	0.2	13	0.005	50	0.97526	0.96066	0.94749	0.92925	0.89995	0.86094	0.88977	0.91681	0.94127	0.93214	3
4470	0.5	0.2	13	0.01	20	0.99773	0.99402	0.99124	0.98805	0.98296	0.97309	0.97072	0.97873	0.98659	0.98631	1
4530	0.5	0.2	13	0.01	40	0.99406	0.99048	0.98703	0.98217	0.97458	0.9621	0.97097	0.97837	0.98573	0.98255	1
4584	0.5	0.2	13	0.01	50	0.99676	0.99573	0.99352	0.99126	0.98754	0.98075	0.96688	0.92951	0.9171	0.97591	1
4594	0.7	0.28	7	0.005	20	0.99277	0.97907	0.96959	0.95608	0.93612	0.9126	0.93073	0.95501	0.97831	0.96103	1
4619	0.7	0.28	7	0.005	30	0.96624	0.92903	0.89474	0.85722	0.8025	0.79842	0.84894	0.8933	0.94123	0.89316	2
4642	0.7	0.28	7	0.005	30	0.99877	0.99428	0.99243	0.98808	0.98278	0.97276	0.95354	0.92504	0.94662	0.97543	1
4719	0.7	0.28	7	0.01	20	0.97918	0.96338	0.94608	0.92337	0.89066	0.85747	0.88782	0.92542	0.95932	0.93327	1
4720	0.7	0.28	7	0.01	20	0.98236	0.96197	0.94307	0.92155	0.88743	0.85503	0.88418	0.92023	0.95671	0.93125	3
4745	0.7	0.28	7	0.01	30	0.99302	0.98012	0.96911	0.9549	0.93338	0.932	0.95196	0.97036	0.98318	0.9668	2
4750	0.7	0.28	7	0.01	30	0.99463	0.98237	0.97433	0.96265	0.94544	0.92509	0.94098	0.96219	0.98228	0.967	1
4765	0.7	0.28	7	0.01	30	0.99959	0.99667	0.9944	0.9912	0.98686	0.97945	0.96257	0.93989	0.96436	0.9815	1
4805	0.7	0.28	7	0.01	40	0.99704	0.99624	0.99552	0.99422	0.99103	0.98654	0.9773	0.9539	0.94737	0.98392	2

ID	b_w/h	h_s/h	L/h	ρ	f'_c (MPa)	k%_1	k%_2	k%_3	k%_4	k%_5	k%_6	k%_7	k%_8	k%_9	ki%	Set
4834	0.7	0.28	7	0.01	50	0.99919	0.99502	0.99352	0.98958	0.98496	0.97613	0.95923	0.93456	0.95281	0.9785	1
4843	0.7	0.28	10	0.005	20	0.96621	0.94356	0.92192	0.89569	0.85584	0.85321	0.88899	0.91831	0.95014	0.91939	3
4850	0.7	0.28	10	0.005	20	0.99129	0.98351	0.97593	0.96654	0.95122	0.93058	0.94532	0.96123	0.97686	0.96825	2
4868	0.7	0.28	10	0.005	20	0.99328	0.98836	0.98217	0.9753	0.9644	0.94654	0.90954	0.85	0.89341	0.9503	1
4884	0.7	0.28	10	0.005	30	0.96912	0.95079	0.9311	0.90715	0.87066	0.82313	0.86077	0.89375	0.93149	0.9138	1
4942	0.7	0.28	10	0.005	50	0.98962	0.98099	0.97256	0.962	0.94466	0.92153	0.93813	0.95584	0.97326	0.96386	1
4950	0.7	0.28	10	0.005	50	0.9922	0.98532	0.97866	0.97041	0.95771	0.93396	0.9267	0.9485	0.96855	0.9662	1
4967	0.7	0.28	10	0.005	50	0.99722	0.99246	0.98811	0.98334	0.97621	0.96349	0.9379	0.87831	0.86254	0.95796	2
4972	0.7	0.28	10	0.01	20	0.97813	0.96114	0.94414	0.92374	0.89425	0.89297	0.92061	0.94116	0.96606	0.94222	3
4988	0.7	0.28	10	0.01	20	0.9931	0.98598	0.98076	0.97084	0.95972	0.94037	0.90093	0.88875	0.93078	0.95512	1
5016	0.7	0.28	10	0.01	30	0.98609	0.97398	0.9618	0.94675	0.92664	0.88748	0.88074	0.90961	0.94402	0.94171	1
5036	0.7	0.28	10	0.01	40	0.97234	0.95262	0.93267	0.9085	0.87395	0.87236	0.90458	0.92855	0.95759	0.93032	1
5043	0.7	0.28	10	0.01	40	0.97857	0.96328	0.94841	0.93151	0.90143	0.86674	0.8922	0.92105	0.95124	0.93544	1
5060	0.7	0.28	10	0.01	40	0.9946	0.99039	0.98495	0.97913	0.96985	0.95465	0.9228	0.8723	0.91129	0.958	1
5080	0.7	0.28	10	0.01	50	0.98336	0.96995	0.95633	0.93932	0.91682	0.87289	0.86502	0.89702	0.93553	0.93362	3
5091	0.7	0.28	10	0.01	50	0.99498	0.99009	0.98503	0.97918	0.96994	0.95363	0.92116	0.86582	0.9092	0.9569	1
5099	0.7	0.28	13	0.005	20	0.9697	0.95329	0.93832	0.91548	0.88225	0.88191	0.90919	0.93156	0.95145	0.93331	2
5121	0.7	0.28	13	0.005	20	0.99849	0.99642	0.99525	0.99342	0.99016	0.98477	0.97349	0.94597	0.95964	0.98376	3
5135	0.7	0.28	13	0.005	30	0.97202	0.95967	0.94575	0.92639	0.89762	0.85679	0.88648	0.91323	0.93979	0.92977	2
5184	0.7	0.28	13	0.005	40	0.99238	0.98754	0.9831	0.97712	0.96724	0.94985	0.91392	0.84437	0.88152	0.94971	1
5207	0.7	0.28	13	0.005	50	0.97358	0.96255	0.95035	0.9332	0.90445	0.86079	0.84923	0.88151	0.91653	0.92322	2
5225	0.7	0.28	13	0.01	20	0.99138	0.98608	0.98096	0.97385	0.96186	0.96062	0.97171	0.97925	0.98606	0.97918	2
5258	0.7	0.28	13	0.01	30	0.99053	0.98462	0.97886	0.97082	0.9576	0.95625	0.96862	0.97669	0.98363	0.97676	2
5259	0.7	0.28	13	0.01	30	0.97683	0.96366	0.95178	0.93359	0.90689	0.90649	0.92856	0.94666	0.96255	0.9477	1
5291	0.7	0.28	13	0.01	40	0.97484	0.96076	0.94801	0.9285	0.89993	0.89954	0.9231	0.94242	0.95944	0.94365	2
5297	0.7	0.28	13	0.01	40	0.99234	0.98748	0.9831	0.97676	0.9663	0.94971	0.96255	0.97225	0.98105	0.97715	2
5334	0.7	0.28	13	0.01	50	0.99372	0.98929	0.98559	0.98021	0.97095	0.95512	0.95022	0.96349	0.97487	0.97635	1
5379	0.9	0.36	7	0.005	20	0.99197	0.98423	0.97187	0.96284	0.94688	0.92202	0.87241	0.813	0.87851	0.93437	1
5448	0.9	0.36	7	0.005	40	0.99364	0.98835	0.97981	0.97207	0.96003	0.93913	0.90023	0.82162	0.83217	0.93871	1
5462	0.9	0.36	7	0.005	50	0.9866	0.97657	0.96348	0.94951	0.92843	0.89113	0.88265	0.91914	0.95986	0.94574	2
5491	0.9	0.36	7	0.01	20	0.97223	0.95311	0.93051	0.90647	0.87133	0.8313	0.86324	0.90398	0.94765	0.91798	3
5499	0.9	0.36	7	0.01	20	0.98777	0.97801	0.96799	0.95637	0.93998	0.90884	0.8554	0.85158	0.91754	0.93635	1
5546	0.9	0.36	7	0.01	40	0.98234	0.96842	0.95141	0.9338	0.90311	0.90194	0.9303	0.95247	0.97487	0.94987	2
5594	0.9	0.36	7	0.01	50	0.98646	0.98795	0.98208	0.9765	0.96629	0.94826	0.9134	0.90329	0.95063	0.96149	2
5597	0.9	0.36	7	0.01	50	0.99692	0.99548	0.98995	0.98599	0.97998	0.96896	0.94717	0.91117	0.94122	0.97169	2
5605	0.9	0.36	7	0.01	50	0.99785	0.99758	0.99376	0.99172	0.98848	0.98236	0.96982	0.93955	0.94163	0.98028	1

ID	b_w/h	h_s/h	L/h	ρ	f'_c (MPa)	$k\%_1$	$k\%_2$	$k\%_3$	$k\%_4$	$k\%_5$	$k\%_6$	$k\%_7$	$k\%_8$	$k\%_9$	$ki\%$	Set
5659	0.9	0.36	10	0.005	30	0.98397	0.97539	0.96703	0.95521	0.93556	0.90378	0.84445	0.82127	0.87617	0.92628	3
5660	0.9	0.36	10	0.005	30	0.98279	0.97377	0.9657	0.95268	0.93427	0.90057	0.83979	0.81786	0.87212	0.92396	1
5675	0.9	0.36	10	0.005	40	0.94492	0.91812	0.89076	0.85662	0.80415	0.79785	0.84532	0.884	0.92091	0.88627	2
5691	0.9	0.36	10	0.005	40	0.98286	0.97376	0.9648	0.95224	0.93136	0.89771	0.83536	0.81072	0.86826	0.92171	1
5735	0.9	0.36	10	0.005	50	0.98985	0.98804	0.9853	0.97953	0.97138	0.95558	0.92672	0.85304	0.82927	0.94787	2
5793	0.9	0.36	10	0.01	30	0.99694	0.99449	0.99302	0.99014	0.98551	0.97811	0.96173	0.92879	0.949	0.97777	3
5803	0.9	0.36	10	0.01	40	0.96031	0.94046	0.91988	0.8937	0.85228	0.84752	0.88519	0.91516	0.94296	0.91575	3
5825	0.9	0.36	10	0.01	40	0.99679	0.99426	0.99271	0.98973	0.98491	0.97719	0.96017	0.926	0.94678	0.97685	2
5834	0.9	0.36	10	0.01	50	0.98021	0.97	0.95997	0.94478	0.92118	0.91806	0.94072	0.9562	0.97246	0.95636	2
5842	0.9	0.36	10	0.01	50	0.98361	0.97668	0.96854	0.95651	0.93842	0.91289	0.93181	0.94945	0.96675	0.95847	1
5877	0.9	0.36	13	0.005	20	0.9881	0.98451	0.98012	0.97287	0.9613	0.94016	0.93287	0.94975	0.96417	0.96739	3
5932	0.9	0.36	13	0.005	40	0.94862	0.93157	0.90937	0.88003	0.83601	0.83503	0.87149	0.90129	0.9278	0.90412	3
5938	0.9	0.36	13	0.005	40	0.98254	0.97837	0.97147	0.96086	0.94473	0.91936	0.93778	0.95272	0.9666	0.96144	1
5963	0.9	0.36	13	0.005	50	0.95024	0.93234	0.9114	0.88049	0.83578	0.83284	0.86993	0.90179	0.92705	0.90418	2
5980	0.9	0.36	13	0.005	50	0.98334	0.9773	0.96961	0.95908	0.94095	0.9135	0.85344	0.82968	0.87168	0.92986	3
5993	0.9	0.36	13	0.01	20	0.9849	0.97979	0.97339	0.96338	0.94727	0.94614	0.96014	0.96993	0.97857	0.97035	2
5998	0.9	0.36	13	0.01	20	0.98616	0.98349	0.97823	0.96997	0.95746	0.9373	0.95209	0.96377	0.9748	0.97033	1
6026	0.9	0.36	13	0.01	30	0.98363	0.97734	0.97062	0.96026	0.94243	0.94043	0.95675	0.96728	0.97745	0.96762	2
6082	0.9	0.36	13	0.01	40	0.99593	0.99508	0.99384	0.99141	0.98763	0.98092	0.9666	0.93377	0.9503	0.97955	1
6127	0.5	0.2	7	0.005	20	0.99961	0.99828	0.99694	0.99445	0.99162	0.98796	0.97934	0.95981	0.92001	0.9828	3
6173	0.5	0.2	7	0.01	40	0.99518	0.9995	0.99712	0.99721	0.99698	0.99576	0.99396	0.98748	0.9751	0.99383	2
6210	0.5	0.2	10	0.005	50	0.96689	0.99038	0.99551	0.9973	0.99853	0.99893	0.99908	0.99986	0.99797	0.99444	1
6216	0.5	0.2	10	0.005	50	0.99921	0.99838	0.99766	0.99649	0.99515	0.99231	0.98633	0.97132	0.91434	0.98512	1
6272	0.5	0.2	13	0.005	40	1	0.99913	0.99836	0.99761	0.99664	0.99469	0.99075	0.97987	0.93336	0.98913	1
6282	0.5	0.2	13	0.01	20	0.9891	0.99682	0.99868	0.9991	0.99952	0.99962	0.99978	0.99985	1	0.99825	2
6284	0.5	0.2	13	0.01	20	0.95492	0.98626	0.9935	0.99629	0.9977	0.99839	0.99877	0.99908	1	0.99249	1
6292	0.5	0.2	13	0.01	30	0.95216	0.98541	0.99311	0.99607	0.99757	0.9983	0.9987	0.99902	0.99995	0.99203	3
6309	0.5	0.2	13	0.01	50	1	1	0.99983	0.99951	0.9994	0.99894	0.99808	0.99567	0.98418	0.99784	3
6339	0.7	0.28	7	0.005	50	0.8924	0.94883	0.97431	0.9848	0.99077	0.99368	0.99604	0.99963	1	0.97805	1
6351	0.7	0.28	7	0.01	20	0.99851	0.99747	0.99689	0.99391	0.992	0.98725	0.97852	0.9567	0.90832	0.98096	1
6414	0.7	0.28	10	0.01	20	1	1	0.99964	0.99922	0.99872	0.99829	0.99632	0.99241	0.97349	0.99602	1
6418	0.7	0.28	10	0.01	30	0.97326	0.99268	0.99651	0.99798	0.9987	0.99941	0.99947	1	1	0.99604	1
6425	0.7	0.28	10	0.01	40	0.97223	0.99211	0.99608	0.99775	0.99862	0.9994	0.99945	1	1	0.99579	2
6460	0.7	0.28	13	0.005	40	0.92356	0.97649	0.98916	0.99406	0.9961	0.99735	0.99811	0.99917	0.99973	0.98737	3
6464	0.7	0.28	13	0.005	40	1	0.99855	0.99828	0.99731	0.99589	0.99381	0.9893	0.97648	0.92143	0.98711	1
6496	0.7	0.28	13	0.01	40	1	0.99889	0.99875	0.99795	0.99679	0.99521	0.99179	0.9818	0.93807	0.98996	3

ID	b_w/h	h_s/h	L/h	ρ	f'_c (MPa)	$k\%_1$	$k\%_2$	$k\%_3$	$k\%_4$	$k\%_5$	$k\%_6$	$k\%_7$	$k\%_8$	$k\%_9$	$ki\%$	Set
6516	0.9	0.36	7	0.005	30	0.8593	0.93806	0.96723	0.98026	0.9875	0.99113	0.99276	0.99614	0.99312	0.97055	1
6521	0.9	0.36	7	0.005	40	0.92135	0.97145	0.98468	0.99137	0.99419	0.9961	0.99621	0.99678	0.99439	0.98465	2
6544	0.9	0.36	7	0.01	20	1	0.99647	0.99518	0.99283	0.98903	0.98453	0.972	0.94639	0.88449	0.97635	3
6561	0.9	0.36	7	0.01	50	0.92942	0.97468	0.98625	0.9923	0.99479	0.99652	0.99648	0.99697	0.99444	0.98619	3
6578	0.9	0.36	10	0.005	30	0.94893	0.98376	0.9931	0.99595	0.99724	0.99835	0.99877	0.99896	0.99924	0.99143	2
6606	0.9	0.36	10	0.01	20	0.99741	0.99888	0.99908	0.99833	0.99791	0.99662	0.99445	0.98813	0.96015	0.9931	1
6625	0.9	0.36	10	0.01	50	0.95606	0.9856	0.99396	0.99636	0.99762	0.99856	0.99903	0.99937	1	0.99268	1
6656	0.9	0.36	13	0.005	40	0.99835	0.99821	0.99789	0.9969	0.99561	0.99309	0.98775	0.97437	0.91324	0.98554	1
6681	0.9	0.36	13	0.01	40	0.97059	0.99203	0.99669	0.99805	0.99871	0.99902	0.99919	0.99938	0.99976	0.99534	3
6697	0.5	0.2	7	0.005	20	0.92893	0.90829	0.88915	0.89083	0.88405	0.89047	0.88862	0.90878	0.93446	0.91236	1
6712	0.5	0.2	7	0.005	30	0.808	0.74234	0.70128	0.70282	0.68868	0.70196	0.70003	0.74754	0.81606	0.76087	3
6720	0.5	0.2	7	0.005	40	0.81528	0.7663	0.72655	0.73226	0.71679	0.72917	0.72668	0.76909	0.82562	0.78077	1
6741	0.5	0.2	7	0.01	20	0.86939	0.79676	0.77476	0.77379	0.76643	0.77772	0.7812	0.80535	0.86293	0.82083	3
6757	0.5	0.2	7	0.01	40	0.85032	0.78983	0.75609	0.756	0.74464	0.75536	0.75539	0.79404	0.85862	0.80603	1
6781	0.5	0.2	10	0.005	30	0.82912	0.8179	0.79198	0.80288	0.78742	0.80252	0.79263	0.81816	0.82819	0.82708	1
6812	0.5	0.2	10	0.01	20	0.86442	0.84398	0.82402	0.8306	0.82099	0.83215	0.81865	0.84555	0.86143	0.85418	1
6856	0.5	0.2	13	0.005	30	0.80544	0.8105	0.78756	0.79954	0.78476	0.80258	0.78377	0.81137	0.80512	0.81907	3
6909	0.5	0.2	13	0.01	50	0.86057	0.8647	0.8466	0.85762	0.84538	0.85791	0.84689	0.86584	0.85919	0.87047	3
6915	0.7	0.28	7	0.005	20	0.89487	0.87082	0.84931	0.8515	0.83895	0.85035	0.84768	0.87043	0.89419	0.87681	1
6933	0.7	0.28	7	0.005	40	0.88423	0.85882	0.83578	0.83811	0.82537	0.83731	0.83433	0.85833	0.88355	0.86558	3
6943	0.7	0.28	7	0.005	50	0.78468	0.73219	0.69285	0.69588	0.67834	0.69491	0.69281	0.73389	0.78683	0.74924	3
7005	0.7	0.28	10	0.005	40	0.88484	0.88326	0.86471	0.87331	0.86073	0.87426	0.86587	0.88471	0.88851	0.88802	3
7048	0.7	0.28	10	0.01	50	0.90961	0.90626	0.88991	0.89685	0.8869	0.89604	0.88828	0.9052	0.90986	0.90889	3
7059	0.7	0.28	13	0.005	20	0.90576	0.91187	0.89752	0.90663	0.8949	0.90567	0.89698	0.91038	0.90396	0.91337	1
7074	0.7	0.28	13	0.005	30	0.76392	0.77169	0.744	0.75963	0.73897	0.75873	0.74492	0.77219	0.7655	0.78196	1
7095	0.7	0.28	13	0.01	20	0.92485	0.92918	0.91674	0.92457	0.91382	0.92375	0.91681	0.92735	0.92313	0.93002	1
7109	0.7	0.28	13	0.01	30	0.82799	0.83317	0.80953	0.8231	0.80816	0.82245	0.81303	0.83358	0.82527	0.83963	2
7191	0.9	0.36	7	0.01	40	0.76319	0.7077	0.67206	0.67573	0.65624	0.67576	0.67203	0.70714	0.76208	0.72919	1
7229	0.9	0.36	10	0.005	50	0.85122	0.85211	0.8314	0.84113	0.83015	0.84213	0.83194	0.85239	0.85284	0.85853	2
7250	0.9	0.36	10	0.01	30	0.79976	0.79354	0.76894	0.78067	0.76321	0.77904	0.76958	0.79552	0.79853	0.80488	2
7264	0.9	0.36	10	0.01	50	0.86999	0.873	0.85499	0.86353	0.85244	0.86293	0.85436	0.87314	0.87324	0.87776	3
7329	0.9	0.36	13	0.01	40	0.88395	0.89217	0.87753	0.88712	0.87692	0.88704	0.87722	0.89286	0.88504	0.89599	3
7374	0.5	0.2	7	0.005	50	0.91775	0.85769	0.84383	0.8184	0.80992	0.81864	0.84617	0.85895	0.9203	0.86916	1
7378	0.5	0.2	7	0.005	50	0.79995	0.66897	0.63543	0.59309	0.57977	0.59127	0.64045	0.66819	0.80416	0.69813	1
7379	0.5	0.2	7	0.005	50	0.79385	0.66045	0.63372	0.58486	0.57338	0.5885	0.6304	0.66626	0.79946	0.69309	2
7397	0.5	0.2	7	0.01	30	0.866	0.76036	0.73441	0.69367	0.68383	0.69811	0.7331	0.76663	0.87186	0.7808	2

ID	b_w/h	h_s/h	L/h	ρ	f'_c (MPa)	$k\%_1$	$k\%_2$	$k\%_3$	$k\%_4$	$k\%_5$	$k\%_6$	$k\%_7$	$k\%_8$	$k\%_9$	$k_i\%$	Set
7409	0.5	0.2	7	0.01	50	0.94409	0.89288	0.88103	0.85604	0.85189	0.85807	0.87975	0.89138	0.94103	0.89962	2
7410	0.5	0.2	7	0.01	50	0.93395	0.88481	0.87106	0.84926	0.84266	0.84988	0.87319	0.88573	0.93655	0.89271	1
7472	0.5	0.2	10	0.01	40	0.94068	0.90834	0.90847	0.89164	0.88638	0.89141	0.90759	0.91068	0.94279	0.9188	1
7507	0.5	0.2	13	0.005	40	0.93173	0.90348	0.9049	0.88785	0.88297	0.88751	0.90503	0.90381	0.93187	0.91391	3
7532	0.5	0.2	13	0.01	20	0.88154	0.83471	0.83162	0.80296	0.80173	0.80778	0.83136	0.83243	0.87966	0.85038	1
7535	0.5	0.2	13	0.01	30	0.95066	0.92687	0.92684	0.91386	0.91019	0.91388	0.92769	0.92603	0.94744	0.93435	2
7551	0.5	0.2	13	0.01	40	0.85376	0.80022	0.79603	0.77008	0.75606	0.7667	0.79897	0.79832	0.85358	0.81937	1
7554	0.5	0.2	13	0.01	50	0.94255	0.91658	0.91808	0.9027	0.89858	0.90283	0.91761	0.9173	0.94163	0.92579	1
7555	0.5	0.2	13	0.01	50	0.87774	0.82916	0.829	0.80462	0.79639	0.80547	0.82955	0.82828	0.87605	0.84763	3
7567	0.7	0.28	7	0.005	20	0.79993	0.6732	0.64415	0.60498	0.58792	0.6025	0.64482	0.67509	0.79673	0.70293	3
7600	0.7	0.28	7	0.01	20	0.87396	0.78738	0.76124	0.73095	0.71703	0.72809	0.7653	0.78817	0.8779	0.803	3
7612	0.7	0.28	7	0.01	30	0.84122	0.72872	0.70021	0.66456	0.64822	0.66266	0.70076	0.73077	0.83848	0.75156	3
7686	0.7	0.28	10	0.01	30	0.82661	0.75035	0.7437	0.70915	0.69712	0.70976	0.74352	0.7476	0.8262	0.7754	1
7688	0.7	0.28	10	0.01	40	0.9176	0.87696	0.87475	0.85284	0.8478	0.85303	0.87515	0.87711	0.91865	0.88939	1
7689	0.7	0.28	10	0.01	40	0.91641	0.87315	0.87237	0.85069	0.843	0.84929	0.87084	0.87464	0.91802	0.88684	3
7690	0.7	0.28	10	0.01	40	0.84706	0.77804	0.77393	0.74265	0.7313	0.74007	0.77302	0.77711	0.84604	0.80092	1
7709	0.7	0.28	13	0.005	20	0.83215	0.77819	0.77907	0.75105	0.74164	0.74768	0.78225	0.77816	0.83166	0.80219	2
7710	0.7	0.28	13	0.005	20	0.82825	0.77435	0.77514	0.74328	0.73516	0.74216	0.77654	0.77403	0.82924	0.79782	1
7720	0.7	0.28	13	0.005	30	0.78509	0.72019	0.72494	0.68957	0.67685	0.69034	0.72328	0.72359	0.78421	0.75181	3
7759	0.7	0.28	13	0.01	40	0.9243	0.89541	0.89828	0.88119	0.87452	0.88029	0.89697	0.89526	0.92242	0.90686	3
7778	0.9	0.36	7	0.005	20	0.87823	0.8034	0.78642	0.75666	0.74725	0.75738	0.78629	0.80363	0.88314	0.82024	2
7793	0.9	0.36	7	0.005	30	0.72743	0.60456	0.57531	0.53407	0.51851	0.53264	0.57489	0.60346	0.73309	0.6404	2
7813	0.9	0.36	7	0.01	20	0.89943	0.83617	0.81925	0.79325	0.78436	0.79383	0.81988	0.83551	0.90395	0.84856	1
7826	0.9	0.36	7	0.01	30	0.81676	0.71239	0.68751	0.65171	0.63763	0.64983	0.69014	0.71447	0.81506	0.73755	2
7834	0.9	0.36	7	0.01	40	0.80467	0.70074	0.67692	0.63865	0.62921	0.63845	0.67893	0.70363	0.8051	0.72763	1
7838	0.9	0.36	7	0.01	40	0.7797	0.66718	0.638	0.59918	0.58352	0.59781	0.63767	0.66638	0.78415	0.69536	2
7840	0.9	0.36	7	0.01	50	0.88516	0.81587	0.79827	0.77045	0.76099	0.77094	0.79889	0.81517	0.88938	0.83051	3
7863	0.9	0.36	10	0.005	30	0.74988	0.67442	0.66687	0.62624	0.61744	0.62882	0.66889	0.6728	0.75315	0.70585	1
7874	0.9	0.36	10	0.005	40	0.71107	0.61901	0.61519	0.57704	0.56339	0.57243	0.61985	0.62561	0.71075	0.66143	2
7916	0.9	0.36	10	0.01	50	0.79003	0.72079	0.71523	0.6781	0.66815	0.67902	0.71389	0.7177	0.79061	0.74735	1
7918	0.9	0.36	10	0.01	50	0.76651	0.69185	0.68329	0.64821	0.63493	0.64732	0.68818	0.68754	0.76772	0.72155	1
7921	0.9	0.36	13	0.005	20	0.88649	0.85063	0.85417	0.83197	0.82584	0.83177	0.85402	0.85031	0.88848	0.86737	1
8001	0.5	0.2	7	0.005	20	0.84995	0.76063	0.74832	0.72896	0.74203	0.74299	0.78517	0.84094	0.91863	0.81176	3
8010	0.5	0.2	7	0.005	20	0.87865	0.80969	0.8277	0.83457	0.82669	0.79903	0.83411	0.87456	0.93816	0.86232	1
8027	0.5	0.2	7	0.005	20	0.81657	0.76026	0.76752	0.76641	0.81172	0.84819	0.88631	0.90917	0.95432	0.85205	2
8028	0.5	0.2	7	0.005	20	0.81373	0.75633	0.76458	0.76268	0.80972	0.85018	0.88538	0.91113	0.95789	0.85116	1

ID	b_w/h	h_s/h	L/h	ρ	f'c (MPa)	$k\%_1$	$k\%_2$	$k\%_3$	$k\%_4$	$k\%_5$	$k\%_6$	$k\%_7$	$k\%_8$	$k\%_9$	$k_i\%$	Set
8075	0.5	0.2	7	0.005	20	0.88087	0.78912	0.79807	0.80066	0.76835	0.72414	0.77557	0.84232	0.90391	0.8283	2
8079	0.5	0.2	7	0.005	20	0.89144	0.80234	0.8258	0.83755	0.82161	0.7887	0.82529	0.87261	0.92837	0.85937	1
8109	0.5	0.2	7	0.005	20	0.90576	0.83855	0.7784	0.72732	0.76534	0.79541	0.79752	0.78514	0.88548	0.82789	3
8131	0.5	0.2	7	0.005	20	0.84996	0.82247	0.7813	0.73857	0.79046	0.84624	0.87994	0.90256	0.95135	0.85628	3
8132	0.5	0.2	7	0.005	20	0.85067	0.823	0.78183	0.73578	0.79362	0.84444	0.87743	0.89982	0.95147	0.85581	1
8143	0.5	0.2	7	0.005	50	0.81851	0.71526	0.70333	0.68119	0.69723	0.70474	0.75277	0.81074	0.90097	0.77847	3
8159	0.5	0.2	7	0.005	50	0.88499	0.9091	0.92163	0.91656	0.90977	0.89167	0.86173	0.81212	0.88995	0.89975	2
8184	0.5	0.2	7	0.005	50	0.89326	0.80993	0.74689	0.69531	0.69923	0.676	0.70153	0.71719	0.82931	0.77686	1
8192	0.5	0.2	7	0.005	50	0.88738	0.81535	0.86944	0.8922	0.91042	0.91669	0.92066	0.90881	0.88844	0.90094	1
8198	0.5	0.2	7	0.005	50	0.94376	0.89423	0.86297	0.826	0.77868	0.72828	0.72888	0.71921	0.78727	0.82693	2
8223	0.5	0.2	7	0.005	50	0.86653	0.76445	0.79426	0.80765	0.78917	0.75077	0.79192	0.84749	0.9128	0.83251	1
8224	0.5	0.2	7	0.005	50	0.85961	0.76486	0.7943	0.81286	0.7902	0.75139	0.79266	0.8487	0.91302	0.83276	3
8264	0.5	0.2	7	0.005	50	0.89789	0.92528	0.92894	0.91743	0.9191	0.90637	0.86515	0.8063	0.88607	0.90525	1
8271	0.5	0.2	7	0.005	50	0.90265	0.85135	0.79334	0.74004	0.76361	0.77433	0.75008	0.70576	0.82277	0.81039	1
8328	0.5	0.2	7	0.01	20	0.93639	0.88356	0.84074	0.80738	0.80696	0.79241	0.80807	0.82391	0.9018	0.86012	1
8371	0.5	0.2	7	0.01	20	0.92787	0.8779	0.90866	0.93581	0.94159	0.93932	0.94382	0.93624	0.91158	0.93228	3
8383	0.5	0.2	7	0.01	20	0.90056	0.82437	0.83716	0.86182	0.84912	0.83663	0.87382	0.9088	0.94772	0.884	3
8392	0.5	0.2	7	0.01	20	0.88132	0.88514	0.86727	0.8377	0.86077	0.8774	0.87264	0.85196	0.92451	0.88587	3
8411	0.5	0.2	7	0.01	20	0.91294	0.93986	0.94692	0.93958	0.94235	0.93487	0.91031	0.87539	0.93557	0.93378	2
8451	0.5	0.2	7	0.01	50	0.91446	0.8609	0.81947	0.77222	0.76801	0.75188	0.76821	0.78139	0.87911	0.83156	1
8473	0.5	0.2	7	0.01	50	0.93427	0.88396	0.85128	0.8197	0.84244	0.85008	0.84434	0.83225	0.90189	0.87602	1
8513	0.5	0.2	7	0.01	50	0.90058	0.82267	0.83864	0.854	0.83851	0.80221	0.83904	0.88379	0.93067	0.87101	2
8528	0.5	0.2	7	0.01	50	0.86608	0.77663	0.80119	0.82576	0.81438	0.79487	0.83922	0.88475	0.93168	0.85345	1
8536	0.5	0.2	7	0.01	50	0.86694	0.86391	0.83837	0.79987	0.83013	0.85072	0.84533	0.81742	0.8999	0.86126	3
8545	0.5	0.2	7	0.01	50	0.92631	0.8877	0.8433	0.80677	0.83812	0.85336	0.84199	0.82329	0.90905	0.87299	1
8561	0.5	0.2	7	0.01	50	0.93075	0.88547	0.83896	0.7937	0.8165	0.82634	0.80087	0.77707	0.87627	0.85459	2
8587	0.5	0.2	13	0.005	20	0.92359	0.95113	0.95995	0.95642	0.9556	0.94484	0.92896	0.88393	0.91135	0.94158	3
8595	0.5	0.2	13	0.005	20	0.91672	0.88699	0.8647	0.82778	0.83213	0.81217	0.82619	0.81426	0.85978	0.86407	1
8597	0.5	0.2	13	0.005	20	0.9173	0.88714	0.86278	0.82821	0.83116	0.81177	0.82501	0.81121	0.85766	0.86322	2
8623	0.5	0.2	13	0.005	20	0.91155	0.88329	0.92807	0.94419	0.95525	0.9563	0.9597	0.95086	0.92359	0.94128	3
8667	0.5	0.2	13	0.005	20	0.94574	0.91999	0.91377	0.89378	0.8541	0.80087	0.83788	0.8684	0.8695	0.8904	1
8695	0.5	0.2	13	0.005	20	0.92965	0.96121	0.96141	0.95414	0.95724	0.95022	0.92812	0.87437	0.90356	0.94199	3
8704	0.5	0.2	13	0.005	20	0.93499	0.91032	0.8837	0.84961	0.87227	0.87765	0.85419	0.79409	0.84322	0.882	3
8728	0.5	0.2	13	0.005	50	0.87268	0.82768	0.86823	0.87742	0.86712	0.8354	0.8638	0.88662	0.91985	0.88188	3
8769	0.5	0.2	13	0.005	50	0.89362	0.861	0.91682	0.93561	0.94933	0.95129	0.95492	0.94495	0.91555	0.93231	3
8779	0.5	0.2	13	0.005	50	0.831	0.77934	0.79343	0.77811	0.7997	0.79631	0.83675	0.8647	0.90167	0.8381	3

ID	b_w/h	h_s/h	L/h	ρ	f'_c (MPa)	$k\%_1$	$k\%_2$	$k\%_3$	$k\%_4$	$k\%_5$	$k\%_6$	$k\%_7$	$k\%_8$	$k\%_9$	$k_i\%$	Set
8782	0.5	0.2	13	0.005	50	0.83072	0.78055	0.79649	0.78063	0.80198	0.79837	0.84077	0.86628	0.90262	0.83984	1
8825	0.5	0.2	13	0.005	50	0.87452	0.88487	0.86322	0.82525	0.85959	0.87674	0.87097	0.82054	0.85972	0.87354	2
8831	0.5	0.2	13	0.005	50	0.88512	0.84726	0.8011	0.75616	0.80353	0.83357	0.83233	0.79715	0.84985	0.84061	2
8844	0.5	0.2	13	0.005	50	0.91925	0.95531	0.9568	0.94829	0.95143	0.94358	0.91715	0.85282	0.88411	0.93287	1
8867	0.5	0.2	13	0.01	20	0.90277	0.8645	0.87388	0.86248	0.87592	0.87047	0.89462	0.91252	0.94023	0.89974	2
8880	0.5	0.2	13	0.01	20	0.93865	0.95963	0.96776	0.96502	0.9651	0.95731	0.94703	0.91572	0.93673	0.95529	1
8893	0.5	0.2	13	0.01	20	0.92638	0.8975	0.92286	0.92334	0.91775	0.90033	0.91726	0.92428	0.91451	0.92442	1
8918	0.5	0.2	13	0.01	20	0.96668	0.95212	0.94575	0.93119	0.91428	0.88733	0.88834	0.86836	0.87777	0.92318	2
8945	0.5	0.2	13	0.01	20	0.92269	0.88951	0.91662	0.92454	0.91649	0.89237	0.91367	0.93267	0.95076	0.92593	2
8976	0.5	0.2	13	0.01	20	0.93449	0.91028	0.88335	0.85206	0.88544	0.90349	0.9003	0.87778	0.91386	0.90611	1
9009	0.5	0.2	13	0.01	50	0.87463	0.83082	0.84437	0.82967	0.84592	0.83879	0.86794	0.89215	0.9247	0.8749	3
9026	0.5	0.2	13	0.01	50	0.92476	0.89715	0.87672	0.84382	0.84684	0.82987	0.84343	0.8315	0.87326	0.87674	2
9053	0.5	0.2	13	0.01	50	0.94156	0.91532	0.89855	0.87774	0.90132	0.90394	0.89891	0.86802	0.90124	0.91066	2
9075	0.5	0.2	13	0.01	50	0.89869	0.86497	0.90271	0.90896	0.89381	0.86986	0.89586	0.91136	0.903	0.90492	1
9118	0.5	0.2	13	0.01	50	0.91758	0.88773	0.8526	0.81675	0.85559	0.87805	0.8746	0.84631	0.8889	0.88181	1
9123	0.5	0.2	13	0.01	50	0.93984	0.91669	0.89183	0.86636	0.8953	0.90618	0.89574	0.85815	0.89832	0.90684	1
9163	0.9	0.36	7	0.005	20	0.85064	0.89433	0.9095	0.90659	0.90275	0.88216	0.84712	0.79407	0.86073	0.88479	3
9182	0.9	0.36	7	0.005	20	0.83384	0.75176	0.78373	0.78208	0.75876	0.72747	0.76947	0.79269	0.80503	0.80049	2
9188	0.9	0.36	7	0.005	20	0.8701	0.78472	0.71992	0.66613	0.6667	0.64923	0.66816	0.67739	0.7821	0.74845	1
9201	0.9	0.36	7	0.005	20	0.86201	0.79825	0.85009	0.88267	0.9041	0.9099	0.91105	0.89474	0.85813	0.88709	3
9208	0.9	0.36	7	0.005	20	0.92571	0.87968	0.84775	0.80808	0.761	0.70269	0.70078	0.68266	0.73169	0.804	3
9211	0.9	0.36	7	0.005	20	0.78181	0.67835	0.67287	0.65485	0.67327	0.67319	0.73369	0.78785	0.86305	0.75189	3
9214	0.9	0.36	7	0.005	20	0.7862	0.68181	0.67264	0.65539	0.67754	0.67757	0.73382	0.78868	0.85953	0.75332	1
9215	0.9	0.36	7	0.005	20	0.78728	0.68167	0.67698	0.65749	0.6765	0.67426	0.72907	0.78626	0.86277	0.75323	2
9295	0.9	0.36	7	0.005	50	0.74175	0.63102	0.62378	0.60308	0.62415	0.62018	0.67514	0.74433	0.84449	0.71079	3
9359	0.9	0.36	7	0.005	50	0.74655	0.63255	0.62853	0.60742	0.6281	0.6254	0.68578	0.75062	0.83898	0.71439	2
9440	0.9	0.36	7	0.01	20	0.83402	0.74784	0.73901	0.72281	0.73914	0.73864	0.78465	0.83407	0.90371	0.80439	1
9461	0.9	0.36	7	0.01	20	0.89549	0.83683	0.79164	0.74488	0.74132	0.72679	0.74237	0.74949	0.84281	0.80716	2
9526	0.9	0.36	7	0.01	20	0.90026	0.84681	0.89206	0.92265	0.93127	0.92845	0.93367	0.92392	0.88218	0.91613	1
9528	0.9	0.36	7	0.01	20	0.89642	0.8449	0.89193	0.9212	0.92931	0.92782	0.93217	0.92749	0.88655	0.91578	1
9536	0.9	0.36	7	0.01	20	0.85182	0.76923	0.79723	0.82221	0.81226	0.7943	0.83324	0.87655	0.91626	0.84731	1
9548	0.9	0.36	7	0.01	20	0.89744	0.84263	0.78829	0.74865	0.78437	0.81597	0.81248	0.80252	0.8813	0.83737	1
9599	0.9	0.36	7	0.01	50	0.8587	0.89858	0.91361	0.9106	0.90636	0.88841	0.8602	0.80896	0.87492	0.89204	2
9608	0.9	0.36	7	0.01	50	0.74956	0.70535	0.72004	0.7225	0.77307	0.81845	0.85855	0.88847	0.93657	0.81726	1
9653	0.9	0.36	7	0.01	50	0.85272	0.77896	0.81382	0.81486	0.78873	0.75404	0.79405	0.82426	0.82006	0.82415	2
9669	0.9	0.36	7	0.01	50	0.8792	0.81637	0.87639	0.91199	0.92244	0.92107	0.92487	0.91968	0.86875	0.90408	3

ID	b_w/h	h_s/h	L/h	ρ	f'_c (MPa)	k%_1	k%_2	k%_3	k%_4	k%_5	k%_6	k%_7	k%_8	k%_9	ki%	Set
9688	0.9	0.36	7	0.01	50	0.82198	0.82492	0.79612	0.75963	0.79143	0.81878	0.80996	0.7739	0.85053	0.82473	3
9694	0.9	0.36	7	0.01	50	0.87859	0.80786	0.74571	0.69508	0.74646	0.77702	0.77563	0.76252	0.85152	0.80404	1
9729	0.9	0.36	13	0.005	20	0.80484	0.75499	0.7735	0.75716	0.77507	0.76853	0.80726	0.84252	0.8829	0.81668	3
9730	0.9	0.36	13	0.005	20	0.80759	0.75582	0.77671	0.75649	0.77776	0.77085	0.80871	0.84373	0.88427	0.81819	1
9857	0.9	0.36	13	0.005	20	0.91204	0.88691	0.85062	0.81004	0.8353	0.84529	0.81236	0.7335	0.78488	0.84709	2
9882	0.9	0.36	13	0.005	50	0.82131	0.77197	0.82652	0.84067	0.82685	0.78594	0.82318	0.85332	0.89305	0.84428	1
9911	0.9	0.36	13	0.005	50	0.85919	0.81376	0.77557	0.72809	0.73933	0.7134	0.73257	0.71374	0.76753	0.78432	2
9920	0.9	0.36	13	0.005	50	0.84243	0.81479	0.88967	0.9172	0.93489	0.93942	0.94355	0.93231	0.88877	0.9103	1
10000	0.9	0.36	13	0.005	50	0.89368	0.86253	0.82621	0.78143	0.80763	0.81258	0.78086	0.69064	0.74387	0.81994	3
10003	0.9	0.36	13	0.005	50	0.79268	0.79069	0.75429	0.70859	0.77902	0.83072	0.86579	0.88045	0.91189	0.83141	3
10008	0.9	0.36	13	0.005	50	0.78651	0.78825	0.75097	0.70605	0.77663	0.82928	0.86365	0.88058	0.91187	0.82938	1
10017	0.9	0.36	13	0.01	20	0.85479	0.8149	0.82916	0.81623	0.8307	0.82492	0.85606	0.88177	0.91358	0.86221	3
10055	0.9	0.36	13	0.01	20	0.91243	0.88236	0.85858	0.82546	0.83352	0.81499	0.82873	0.81574	0.85439	0.86262	2
10116	0.9	0.36	13	0.01	20	0.84085	0.80397	0.86207	0.88445	0.87937	0.85995	0.89307	0.91633	0.93636	0.88764	1
10141	0.9	0.36	13	0.01	20	0.9354	0.91556	0.89032	0.86202	0.87952	0.88529	0.86289	0.80472	0.8446	0.88803	1
10147	0.9	0.36	13	0.01	20	0.868	0.8722	0.84856	0.81707	0.86524	0.89805	0.91845	0.92328	0.94436	0.89552	3
10169	0.9	0.36	13	0.01	50	0.86604	0.8278	0.86708	0.87446	0.86856	0.83604	0.86427	0.88549	0.9163	0.8806	2
10196	0.9	0.36	13	0.01	50	0.89142	0.85413	0.82505	0.78798	0.79398	0.77705	0.79007	0.77241	0.82478	0.83169	1
10238	0.9	0.36	13	0.01	50	0.86614	0.82556	0.87122	0.8846	0.87204	0.8374	0.86366	0.89528	0.9197	0.88356	2
10256	0.9	0.36	13	0.01	50	0.80442	0.75887	0.8324	0.85751	0.85147	0.82905	0.86539	0.89457	0.92151	0.86152	1
10276	0.9	0.36	13	0.01	50	0.92108	0.89847	0.86856	0.83787	0.87328	0.88753	0.87381	0.83138	0.86976	0.88618	3
10303	0.5	0.2	7	0.005	20	0.97985	0.98773	0.99066	0.9886	0.98535	0.9786	0.96647	0.93451	0.9202	0.9732	3
10344	0.5	0.2	7	0.01	20	0.98319	0.96735	0.95346	0.94727	0.93247	0.90089	0.88076	0.90949	0.9578	0.94327	1
10348	0.5	0.2	7	0.01	50	0.92674	0.88283	0.85003	0.88568	0.92213	0.94611	0.96218	0.9753	0.9917	0.93427	3
10352	0.5	0.2	7	0.01	50	0.98437	0.98878	0.99084	0.98766	0.98457	0.9787	0.96448	0.93314	0.92311	0.97356	1
10375	0.5	0.2	13	0.005	20	0.98114	0.97067	0.96073	0.95874	0.94742	0.92434	0.88519	0.90945	0.93552	0.94732	3
10413	0.5	0.2	13	0.01	50	0.91368	0.96405	0.98279	0.98981	0.99323	0.9948	0.99532	0.99399	0.98729	0.9815	3
10497	0.9	0.36	13	0.005	20	0.901	0.86412	0.83714	0.88637	0.91739	0.94037	0.9564	0.96632	0.97513	0.92443	3
10575	0.5	0.2	7	0.005	50	0.94449	0.90947	0.88281	0.88712	0.8783	0.843	0.80057	0.84504	0.92313	0.89139	1
10596	0.5	0.2	7	0.01	20	0.97271	0.95293	0.94437	0.95867	0.96628	0.96726	0.96371	0.93468	0.93789	0.95985	1
10628	0.5	0.2	13	0.005	20	0.96669	0.96276	0.95368	0.97025	0.97699	0.97851	0.97343	0.95459	0.89709	0.9634	1
10672	0.5	0.2	13	0.01	50	0.95965	0.95265	0.94065	0.94766	0.94294	0.92398	0.89078	0.91424	0.93997	0.94125	3
10712	0.9	0.36	7	0.005	50	0.94682	0.93546	0.91513	0.88616	0.85457	0.87193	0.87872	0.85266	0.81326	0.89547	1
10741	0.9	0.36	7	0.01	50	0.85271	0.87911	0.8986	0.89029	0.87296	0.90087	0.92747	0.94271	0.95177	0.91165	1
10765	0.9	0.36	13	0.005	50	0.80425	0.87979	0.8923	0.9316	0.95204	0.96096	0.9624	0.97099	0.97908	0.93334	1
10767	0.9	0.36	13	0.005	50	0.91711	0.9037	0.8832	0.89727	0.89117	0.86103	0.8057	0.83757	0.88062	0.88774	1

ID	b_w/h	h_s/h	L/h	ρ	f'$_c$ (MPa)	k%$_1$	k%$_2$	k%$_3$	k%$_4$	k%$_5$	k%$_6$	k%$_7$	k%$_8$	k%$_9$	ki%	Set
10794	0.9	0.36	13	0.01	50	0.84909	0.89961	0.90583	0.93528	0.94803	0.96325	0.97264	0.97935	0.98571	0.94388	1
10823	0.5	0.2	7	0.005	50	0.88402	0.79692	0.74428	0.7626	0.76566	0.76473	0.74783	0.80698	0.90317	0.81762	2
10824	0.5	0.2	7	0.005	50	0.88162	0.79598	0.733	0.7588	0.76434	0.75799	0.73508	0.80173	0.89531	0.81239	1
10828	0.5	0.2	7	0.005	50	0.8978	0.82253	0.77904	0.82513	0.86055	0.86569	0.84627	0.84453	0.85614	0.85977	3
10867	0.5	0.2	13	0.005	20	0.91261	0.8886	0.86417	0.89452	0.90315	0.9242	0.93538	0.92913	0.88681	0.91386	3
10923	0.9	0.36	7	0.005	50	0.85727	0.77067	0.71671	0.77774	0.81212	0.81644	0.78994	0.78859	0.78243	0.81119	1
10927	0.9	0.36	7	0.005	50	0.83882	0.74627	0.69547	0.7346	0.75508	0.79801	0.82672	0.81928	0.79666	0.80109	3
10951	0.9	0.36	7	0.01	50	0.87478	0.799	0.75474	0.78331	0.79698	0.83322	0.8581	0.85281	0.84178	0.83947	3
11008	0.5	0.2	7	0.005	50	0.98319	0.96556	0.94862	0.9273	0.89492	0.84935	0.79789	0.84045	0.90533	0.91126	3
11018	0.5	0.2	13	0.005	20	0.99878	0.99566	0.99387	0.99138	0.98794	0.98097	0.96698	0.9507	0.90189	0.97682	2
11022	0.5	0.2	13	0.005	50	0.99827	0.99498	0.99297	0.99015	0.98624	0.97835	0.96244	0.94263	0.88183	0.97278	1
11023	0.5	0.2	13	0.005	50	0.9865	0.97805	0.97012	0.9599	0.94194	0.91116	0.86425	0.88764	0.90868	0.94082	3
11030	0.5	0.2	13	0.01	50	0.99904	0.99599	0.99431	0.99199	0.98879	0.98229	0.96925	0.95456	0.91152	0.97877	2
11041	0.9	0.36	7	0.01	20	1	0.99545	0.98886	0.98338	0.97642	0.96276	0.94006	0.9118	0.88813	0.9649	1
11049	0.9	0.36	13	0.005	20	0.9943	0.99428	0.99249	0.98948	0.98482	0.97673	0.96017	0.93731	0.85973	0.96893	3
11050	0.9	0.36	13	0.005	20	0.99441	0.99392	0.99217	0.98914	0.98429	0.97592	0.95837	0.9379	0.86258	0.96887	1
11057	0.9	0.36	13	0.01	20	0.99503	0.99537	0.99395	0.99149	0.98768	0.9811	0.96741	0.95095	0.89508	0.97581	2
11071	0.5	0.2	7	0.005	50	0.95777	0.9155	0.87972	0.83379	0.78703	0.83112	0.86345	0.90037	0.95144	0.89202	3
11078	0.5	0.2	7	0.01	50	0.98194	0.96967	0.95384	0.93444	0.90705	0.88024	0.84746	0.88602	0.94118	0.93018	2
11079	0.5	0.2	7	0.01	50	0.97021	0.93888	0.91102	0.8761	0.83968	0.87208	0.89576	0.92473	0.96434	0.91928	1
11091	0.5	0.2	13	0.01	20	0.97336	0.96165	0.94983	0.9333	0.90981	0.92883	0.93989	0.95354	0.96712	0.95173	1
11102	0.9	0.36	7	0.005	50	0.96673	0.9442	0.91878	0.88804	0.84832	0.79936	0.74111	0.79178	0.87585	0.87742	2
11167	0.9	0.36	7	0.005	50	0.91888	0.86153	0.80939	0.75948	0.70236	0.72928	0.74546	0.79646	0.87304	0.81959	3
11185	0.9	0.36	13	0.01	20	0.98678	0.98262	0.97708	0.96833	0.95533	0.94345	0.91669	0.91133	0.86916	0.95108	1
11233	0.9	0.36	7	0.01	20	0.97135	0.97597	0.96969	0.96063	0.94581	0.91862	0.87703	0.86426	0.86614	0.93495	1
11234	0.9	0.36	7	0.01	20	0.97736	0.97788	0.97057	0.96194	0.94656	0.91953	0.87946	0.86845	0.86369	0.93654	2
11239	0.9	0.36	7	0.01	50	0.86439	0.90565	0.93659	0.94406	0.93913	0.91982	0.89	0.91035	0.94339	0.92534	3
11247	0.9	0.36	13	0.005	50	0.83622	0.93038	0.95621	0.96154	0.95746	0.94362	0.91331	0.92828	0.93592	0.9363	1
11259	0.5	0.2	7	0.005	20	0.93609	0.87295	0.83418	0.86834	0.89787	0.90447	0.89964	0.92285	0.9561	0.90925	1
11261	0.5	0.2	7	0.005	50	0.98766	0.96936	0.95475	0.95318	0.94479	0.92182	0.88503	0.86973	0.86568	0.9352	2
11306	0.9	0.36	13	0.005	20	0.97881	0.9718	0.9631	0.96367	0.95612	0.93883	0.90403	0.89529	0.83957	0.94112	2
11315	0.9	0.36	13	0.01	20	0.92858	0.90026	0.87834	0.91311	0.93005	0.93063	0.91634	0.93097	0.93882	0.92671	2
11344	0.5	0.2	13	0.005	50	0.89904	0.85377	0.81952	0.84534	0.84644	0.84595	0.81713	0.85212	0.88427	0.86636	3
11347	0.5	0.2	13	0.01	20	0.94092	0.91444	0.8901	0.90545	0.90237	0.90395	0.88847	0.90933	0.92874	0.91838	3
11355	0.9	0.36	7	0.005	20	0.86976	0.77457	0.71137	0.72687	0.72657	0.72552	0.7085	0.76188	0.848	0.7853	1
11358	0.9	0.36	7	0.005	50	0.91256	0.83752	0.77887	0.72967	0.67308	0.69708	0.70834	0.73012	0.74928	0.78165	1

Table C-2: Main database – cracking input parameters

ID	b_{cr1}/L	d_{cr1}/h	w_{cr1} (mm)	b_{cr2}/L	$d_{cr2}h$	w_{cr2} (mm)	b_{cr3}/L	d_{cr3}/h	w_{cr3} (mm)	b_{cr4}/L	d_{cr4}/h	w_{cr4} (mm)	b_{cr5}/L	d_{cr5}/h	w_{cr5} (mm)
15	0.1	0	0	0.3	0	0	0.5	0	0	0.7	0	0	0.9	0	0
17	0.1	0	0	0.3	0	0	0.5	0	0	0.7	0	0	0.9	0	0
31	0.1	0	0	0.3	0	0	0.5	0	0	0.7	0	0	0.9	0	0
75	0.1	0.639	1	0.3	0	0	0.5	0	0	0.7	0	0	0.9	0	0
81	0.1	0	0	0.3	0	0	0.5	0.25	1	0.7	0	0	0.9	0	0
133	0.1	0.25	1	0.3	0	0	0.5	0	0	0.7	0	0	0.9	0	0
169	0.1	0	0	0.3	0	0	0.5	0	0	0.7	0	0	0.9	0.25	1
212	0.1	0	0	0.3	0	0	0.5	0	0	0.7	0	0	0.9	0.639	5
249	0.1	0	0	0.3	0	0	0.5	0	0	0.7	0	0	0.9	0.25	1
277	0.1	0	0	0.3	0.25	1	0.5	0	0	0.7	0	0	0.9	0	0
280	0.1	0	0	0.3	0.639	5	0.5	0	0	0.7	0	0	0.9	0	0
294	0.1	0.25	5	0.3	0	0	0.5	0	0	0.7	0	0	0.9	0	0
297	0.1	0	0	0.3	0.25	1	0.5	0	0	0.7	0	0	0.9	0	0
312	0.1	0	0	0.3	0	0	0.5	0	0	0.7	0	0	0.9	0.639	5
319	0.1	0	0	0.3	0.639	1	0.5	0	0	0.7	0	0	0.9	0	0
323	0.1	0	0	0.3	0	0	0.5	0.639	1	0.7	0	0	0.9	0	0
326	0.1	0	0	0.3	0	0	0.5	0	0	0.7	0.25	5	0.9	0	0
332	0.1	0	0	0.3	0	0	0.5	0	0	0.7	0	0	0.9	0.639	5
362	0.1	0	0	0.3	0	0	0.5	0.25	5	0.7	0	0	0.9	0	0
419	0.1	0	0	0.3	0.639	1	0.5	0	0	0.7	0	0	0.9	0	0
428	0.1	0	0	0.3	0	0	0.5	0	0	0.7	0.639	5	0.9	0	0
479	0.1	0	0	0.3	0.639	1	0.5	0	0	0.7	0	0	0.9	0	0
484	0.1	0	0	0.3	0	0	0.5	0.639	5	0.7	0	0	0.9	0	0
498	0.1	0	0	0.3	0.25	5	0.5	0	0	0.7	0	0	0.9	0	0
509	0.1	0	0	0.3	0	0	0.5	0	0	0.7	0	0	0.9	0.25	1
510	0.1	0	0	0.3	0	0	0.5	0	0	0.7	0	0	0.9	0.25	5
526	0.1	0	0	0.3	0	0	0.5	0	0	0.7	0.25	5	0.9	0	0
541	0.1	0	0	0.3	0	0	0.5	0.25	1	0.7	0	0	0.9	0	0
555	0.1	0.639	1	0.3	0	0	0.5	0	0	0.7	0	0	0.9	0	0
573	0.1	0.25	1	0.3	0	0	0.5	0	0	0.7	0	0	0.9	0	0
585	0.1	0	0	0.3	0	0	0.5	0	0	0.7	0.25	1	0.9	0	0

ID	b_{cr1}/L	d_{cr1}/h	w_{cr1} (mm)	b_{cr2}/L	$d_{cr2}h$	w_{cr2} (mm)	b_{cr3}/L	d_{cr3}/h	w_{cr3} (mm)	b_{cr4}/L	d_{cr4}/h	w_{cr4} (mm)	b_{cr5}/L	d_{cr5}/h	w_{cr5} (mm)
587	0.1	0	0	0.3	0	0	0.5	0	0	0.7	0.639	1	0.9	0	0
588	0.1	0	0	0.3	0	0	0.5	0	0	0.7	0.639	5	0.9	0	0
611	0.1	0	0	0.3	0	0	0.5	0	0	0.7	0	0	0.9	0.639	1
648	0.1	0	0	0.3	0	0	0.5	0	0	0.7	0.639	5	0.9	0	0
678	0.1	0	0	0.3	0.25	5	0.5	0	0	0.7	0	0	0.9	0	0
683	0.1	0	0	0.3	0	0	0.5	0.639	1	0.7	0	0	0.9	0	0
687	0.1	0	0	0.3	0	0	0.5	0	0	0.7	0.639	1	0.9	0	0
702	0.1	0	0	0.3	0	0	0.5	0.25	5	0.7	0	0	0.9	0	0
724	0.1	0	0	0.3	0	0	0.5	0.639	5	0.7	0	0	0.9	0	0
779	0.1	0	0	0.3	0.639	1	0.5	0	0	0.7	0	0	0.9	0	0
799	0.1	0	0	0.3	0.639	1	0.5	0	0	0.7	0	0	0.9	0	0
811	0.1	0	0	0.3	0	0	0.5	0	0	0.7	0	0	0.9	0.639	1
856	0.1	0.639	5	0.3	0	0	0.5	0	0	0.7	0	0	0.9	0	0
927	0.1	0	0	0.3	0	0	0.5	0	0	0.7	0.639	1	0.9	0	0
952	0.1	0	0	0.3	0	0	0.5	0	0	0.7	0	0	0.9	0.639	5
984	0.1	0	0	0.3	0	0	0.5	0.639	5	0.7	0	0	0.9	0	0
993	0.1	0.25	1	0.3	0	0	0.5	0	0	0.7	0	0	0.9	0	0
1033	0.1	0.25	1	0.3	0	0	0.5	0	0	0.7	0	0	0.9	0	0
1052	0.1	0	0	0.3	0	0	0.5	0	0	0.7	0	0	0.9	0.639	5
1097	0.1	0	0	0.3	0.25	1	0.5	0	0	0.7	0	0	0.9	0	0
1110	0.1	0	0	0.3	0	0	0.5	0	0	0.7	0	0	0.9	0.25	5
1129	0.1	0	0	0.3	0	0	0.5	0	0	0.7	0	0	0.9	0.25	1
1154	0.1	0.25	5	0.3	0	0	0.5	0	0	0.7	0	0	0.9	0	0
1176	0.1	0.639	5	0.3	0	0	0.5	0	0	0.7	0	0	0.9	0	0
1190	0.1	0	0	0.3	0	0	0.5	0	0	0.7	0	0	0.9	0.25	5
1250	0.1	0	0	0.3	0	0	0.5	0	0	0.7	0	0	0.9	0.25	5
1265	0.1	0	0	0.3	0	0	0.5	0	0	0.7	0.25	1	0.9	0	0
1308	0.1	0	0	0.3	0	0	0.5	0	0	0.7	0.639	5	0.9	0	0
1311	0.1	0	0	0.3	0	0	0.5	0	0	0.7	0	0	0.9	0.639	1
1340	0.1	0	0	0.3	0.639	5	0.5	0	0	0.7	0	0	0.9	0	0
1351	0.1	0	0	0.3	0	0	0.5	0	0	0.7	0	0	0.9	0.639	1
1390	0.1	0	0	0.3	0	0	0.5	0	0	0.7	0	0	0.9	0.25	5
1401	0.1	0	0	0.3	0	0	0.5	0.25	1	0.7	0	0	0.9	0	0
1407	0.1	0	0	0.3	0	0	0.5	0	0	0.7	0.639	1	0.9	0	0
1418	0.1	0	0	0.3	0.25	5	0.5	0	0	0.7	0	0	0.9	0	0
1419	0.1	0	0	0.3	0.639	1	0.5	0	0	0.7	0	0	0.9	0	0

ID	b_{cr1}/L	d_{cr1}/h	w_{cr1} (mm)	b_{cr2}/L	$d_{cr2}h$	w_{cr2} (mm)	b_{cr3}/L	d_{cr3}/h	w_{cr3} (mm)	b_{cr4}/L	d_{cr4}/h	w_{cr4} (mm)	b_{cr5}/L	d_{cr5}/h	w_{cr5} (mm)
1462	0.1	0	0	0.3	0	0	0.5	0.25	5	0.7	0	0	0.9	0	0
1493	0.1	0.25	1	0.3	0	0	0.5	0	0	0.7	0	0	0.9	0	0
1526	0.1	0	0	0.25	0.25	5	0.5	0	0	0.7	0	0	0.9	0	0
1547	0.15	0.639	1	0.3	0	0	0.5	0	0	0.7	0	0	0.9	0	0
1556	0.1	0	0	0.2	0.639	5	0.5	0	0	0.7	0	0	0.9	0	0
1569	0.1	0	0	0.3	0	0	0.4	0.25	1	0.7	0	0	0.9	0	0
1671	0.1	0	0	0.3	0	0	0.45	0.639	1	0.7	0	0	0.9	0	0
1693	0.1	0	0	0.4	0.25h	1	0.5	0	0	0.7	0	0	0.9	0	0
1709	0.2	0.25	1	0.3	0	0	0.5	0	0	0.7	0	0	0.9	0	0
1710	0.2	0.25	5	0.3	0	0	0.5	0	0	0.7	0	0	0.9	0	0
1714	0.1	0	0	0.2	0.25	5	0.5	0	0	0.7	0	0	0.9	0	0
1732	0.1	0	0	0.3	0	0	0.4	0.639	5	0.7	0	0	0.9	0	0
1745	0.1	0	0	0.2	0.25	1	0.5	0	0	0.7	0	0	0.9	0	0
1769	0.15	0.25	1	0.3	0	0	0.5	0	0	0.7	0	0	0.9	0	0
1840	0.2	0.639	5	0.3	0	0	0.5	0	0	0.7	0	0	0.9	0	0
1863	0.1	0	0	0.3	0	0	0.45	0.639	1	0.7	0	0	0.9	0	0
1875	0.1	0	0	0.2	0.639	1	0.5	0	0	0.7	0	0	0.9	0	0
1881	0.1	0	0	0.35	0.25	1	0.5	0	0	0.7	0	0	0.9	0	0
1909	0.1	0	0	0.25	0.25	1	0.5	0	0	0.7	0	0	0.9	0	0
1911	0.1	0	0	0.25	0.639	1	0.5	0	0	0.7	0	0	0.9	0	0
1939	0.1	0	0	0.2	0.639	1	0.5	0	0	0.7	0	0	0.9	0	0
1973	0.1	0	0	0.25	0.25	1	0.5	0	0	0.7	0	0	0.9	0	0
2075	0.1	0	0	0.35	0.639	1	0.5	0	0	0.7	0	0	0.9	0	0
2086	0.1	0	0	0.3	0	0	0.45	0.25	5	0.7	0	0	0.9	0	0
2095	0.2	0.639	1	0.3	0	0	0.5	0	0	0.7	0	0	0.9	0	0
2114	0.1	0	0	0.3	0	0	0.4	0.25	5	0.7	0	0	0.9	0	0
2126	0.2	0.25	5	0.3	0	0	0.5	0	0	0.7	0	0	0.9	0	0
2135	0.1	0	0	0.25	0.639	1	0.5	0	0	0.7	0	0	0.9	0	0
2178	0.1	0	0	0.3	0	0	0.4	0.25h	5	0.7	0	0	0.9	0	0
2187	0.15	0.639	1	0.3	0	0	0.5	0	0	0.7	0	0	0.9	0	0
2204	0.1	0	0	0.35	0.639	5	0.5	0	0	0.7	0	0	0.9	0	0
2236	0.1	0	0	0.35	0.639	5	0.5	0	0	0.7	0	0	0.9	0	0
2241	0.1	0	0	0.3	0	0	0.4	0.25	1	0.7	0	0	0.9	0	0
2267	0.1	0	0	0.35	0.639	1	0.5	0	0	0.7	0	0	0.9	0	0
2270	0.1	0	0	0.4	0.25	5	0.5	0	0	0.7	0	0	0.9	0	0
2330	0.1	0	0	0.35	0.25	5	0.5	0	0	0.7	0	0	0.9	0	0

ID	b_{cr1}/L	d_{cr1}/h	w_{cr1} (mm)	b_{cr2}/L	$d_{cr2}h$	w_{cr2} (mm)	b_{cr3}/L	d_{cr3}/h	w_{cr3} (mm)	b_{cr4}/L	d_{cr4}/h	w_{cr4} (mm)	b_{cr5}/L	d_{cr5}/h	w_{cr5} (mm)
2358	0.1	0	0	0.25	0.25	5	0.5	0	0	0.7	0	0	0.9	0	0
2359	0.1	0	0	0.25	0.639	1	0.5	0	0	0.7	0	0	0.9	0	0
2371	0.1	0	0	0.3	0	0	0.4	0.639	1	0.7	0	0	0.9	0	0
2396	0.1	0	0	0.35	0.639	5	0.5	0	0	0.7	0	0	0.9	0	0
2402	0.1	0	0	0.3	0	0	0.4	0.25	5	0.7	0	0	0.9	0	0
2429	0.1	0	0	0.4	0.25	1	0.5	0	0	0.7	0	0	0.9	0	0
2435	0.1	0	0	0.3	0	0	0.4	0.639	1	0.7	0	0	0.9	0	0
2459	0.1	0	0	0.35	0.639	1	0.5	0	0	0.7	0	0	0.9	0	0
2465	0.1	0	0	0.3	0	0	0.4	0.25	1	0.7	0	0	0.9	0	0
2482	0.1	0	0	0.2	0.25	5	0.5	0	0	0.7	0	0	0.9	0	0
2508	0.15	0.639	5	0.3	0	0	0.5	0	0	0.7	0	0	0.9	0	0
2546	0.1	0	0	0.2	0.25	5	0.5	0	0	0.7	0	0	0.9	0	0
2569	0.15	0.25	1	0.3	0	0	0.5	0	0	0.7	0	0	0.9	0	0
2596	0.1	0	0	0.3	0	0	0.4	0.639	5	0.7	0	0	0.9	0	0
2601	0.15	0.25	1	0.3	0	0	0.5	0	0	0.7	0	0	0.9	0	0
2604	0.15	0.639	5	0.3	0	0	0.5	0	0	0.7	0	0	0.9	0	0
2612	0.1	0	0	0.2	0.639	5	0.5	0	0	0.7	0	0	0.9	0	0
2683	0.1	0	0	0.35	0.639	1	0.5	0	0	0.7	0	0	0.9	0	0
2692	0.1	0	0	0.3	0	0	0.4	0.639	5	0.7	0	0	0.9	0	0
2733	0.2	0.25	1	0.3	0	0	0.5	0	0	0.7	0	0	0.9	0	0
2746	0.1	0	0	0.35	0.25	5	0.5	0	0	0.7	0	0	0.9	0	0
2779	0.1	0	0	0.35	0.639	1	0.5	0	0	0.7	0	0	0.9	0	0
2780	0.1	0	0	0.35	0.639	5	0.5	0	0	0.7	0	0	0.9	0	0
2784	0.1	0	0	0.4	0.639	5	0.5	0	0	0.7	0	0	0.9	0	0
2795	0.15	0.639	1	0.3	0	0	0.5	0	0	0.7	0	0	0.9	0	0
2798	0.2	0.25	5	0.3	0	0	0.5	0	0	0.7	0	0	0.9	0	0
2812	0.1	0	0	0.35	0.639	5	0.5	0	0	0.7	0	0	0.9	0	0
2815	0.1	0	0	0.4	0.639	1	0.5	0	0	0.7	0	0	0.9	0	0
2856	0.1	0	0	0.3	0	0	0.45	0.639	5	0.7	0	0	0.9	0	0
2913	0.1	0	0	0.3	0	0	0.4	0.25	1	0.7	0	0	0.9	0	0
2921	0.15	0.25	1	0.3	0	0	0.5	0	0	0.7	0	0	0.9	0	0
2925	0.2	0.25	1	0.3	0	0	0.5	0	0	0.7	0	0	0.9	0	0
2931	0.1	0	0	0.2	0.639	1	0.5	0	0	0.7	0	0	0.9	0	0
2954	0.15	0.25	5	0.3	0	0	0.5	0	0	0.7	0	0	0.9	0	0
2996	0.1	0	0	0.2	0.639	5	0.5	0	0	0.7	0	0	0.9	0	0
3049	0.15	0.25	1	0.3	0	0	0.5	0	0	0.7	0	0	0.9	0	0

ID	b_{cr1}/L	d_{cr1}/h	w_{cr1} (mm)	b_{cr2}/L	$d_{cr2}h$	w_{cr2} (mm)	b_{cr3}/L	d_{cr3}/h	w_{cr3} (mm)	b_{cr4}/L	d_{cr4}/h	w_{cr4} (mm)	b_{cr5}/L	d_{cr5}/h	w_{cr5} (mm)
3052	0.15	0.639	5	0.3	0	0	0.5	0	0	0.7	0	0	0.9	0	0
3093	0.1	0	0	0.25	0.25	1	0.5	0	0	0.7	0	0	0.9	0	0
3109	0.1	0	0	0.3	0	0	0.45	0.25	1	0.7	0	0	0.9	0	0
3290	0.1	0	0	0.35	0.25	5	0.5	0	0	0.7	0	0	0.9	0	0
3299	0.1	0	0	0.3	0	0	0.4	0.639	1	0.7	0	0	0.9	0	0
3308	0.15	0.639	5	0.3	0	0	0.5	0	0	0.7	0	0	0.9	0	0
3313	0.1	0	0	0.2	0.25	1	0.5	0	0	0.7	0	0	0.9	0	0
3322	0.1	0	0	0.35	0.25h	5	0.5	0	0	0.7	0	0	0.9	0	0
3337	0.15	0.25	1	0.3	0	0	0.5	0	0	0.7	0	0	0.9	0	0
3338	0.15	0.25	5	0.3	0	0	0.5	0	0	0.7	0	0	0.9	0	0
3382	0.1	0	0	0.25	0.25	5	0.5	0	0	0.7	0	0	0.9	0	0
3404	0.15	0.639	5	0.3	0	0	0.5	0	0	0.7	0	0	0.9	0	0
3413	0.1	0	0	0.25	0.25	1	0.5	0	0	0.7	0	0	0.9	0	0
3509	0.1	0	0	0.25	0.25	1	0.5	0	0	0.7	0	0	0.9	0	0
3525	0.1	0	0	0.3	0	0	0.45	0.25	1	0.7	0	0	0.9	0	0
3535	0.2	0.639	1	0.3	0	0	0.5	0	0	0.7	0	0	0.9	0	0
3539	0.1	0	0	0.2	0.639	1	0.5	0	0	0.7	0	0	0.9	0	0
3550	0.1	0	0	0.4	0.25	5	0.5	0	0	0.7	0	0	0.9	0	0
3602	0.1	0	0	0.2	0.25	5	0.5	0	0	0.7	0	0	0.9	0	0
3635	0.1	0	0	0.2	0.639	1	0.5	0	0	0.7	0	0	0.9	0	0
3643	0.1	0	0	0.35	0.639	1	0.5	0	0	0.7	0	0	0.9	0	0
3689	0.15	0.25	1	0.3	0	0	0.5	0	0	0.7	0	0	0.9	0	0
3716	0.1	0	0	0.3	0	0	0.4	0.639	5	0.7	0	0	0.9	0	0
3717	0.1	0	0	0.3	0	0	0.45	0.25	1	0.7	0	0	0.9	0	0
3733	0.1	0	0	0.25	0.25	1	0.5	0	0	0.7	0	0	0.9	0	0
3751	0.1	0	0	0.3	0	0	0.45	0.639	1	0.7	0	0	0.9	0	0
3764	0.1	0	0	0.2	0.639	5	0.5	0	0	0.7	0	0	0.9	0	0
3766	0.1	0	0	0.25	0.25	5	0.5	0	0	0.7	0	0	0.9	0	0
3769	0.1	0	0	0.35	0.25	1	0.5	0	0	0.7	0	0	0.9	0	0
3802	0.1	0	0	0.35	0.25	5	0.5	0	0	0.7	0	0	0.9	0	0
3828	0.1	0	0	0.3	0	0	0.5	0	0	0.6	0.639	5	0.9	0	0
3850	0.1	0	0	0.3	0	0	0.55	0.25	5	0.7	0	0	0.9	0	0
3854	0.1	0	0	0.3	0	0	0.6	0.25	5	0.7	0	0	0.9	0	0
3858	0.1	0	0	0.3	0L	0	0.5	0	0	0.6	0.25	5	0.9	0	0
3863	0.1	0	0	0.3	0	0	0.5	0	0	0.65	0.639	1	0.9	0	0
3882	0.1	0	0	0.3	0	0	0.55	0.25	5	0.7	0	0	0.9	0	0

ID	b_{cr1}/L	d_{cr1}/h	w_{cr1} (mm)	b_{cr2}/L	$d_{cr2}h$	w_{cr2} (mm)	b_{cr3}/L	d_{cr3}/h	w_{cr3} (mm)	b_{cr4}/L	d_{cr4}/h	w_{cr4} (mm)	b_{cr5}/L	d_{cr5}/h	w_{cr5} (mm)
3900	0.1	0	0	0.3	0	0	0.5	0	0	0.75	0.639	5	0.9	0	0
3944	0.1	0	0	0.3	0	0	0.5	0	0	0.7	0	0	0.85	0.639	5
4006	0.1	0	0	0.3	0	0	0.5	0	0	0.7	0	0	0.85	0.25	5
4015	0.1	0	0	0.3	0	0	0.6	0.639	1	0.7	0	0	0.9	0	0
4035	0.1	0	0	0.3	0	0	0.5	0	0	0.7	0	0	0.8	0.639	1
4090	0.1	0	0	0.3	0	0	0.5	0	0	0.75	0.25	5	0.9	0	0
4133	0.1	0	0	0.3	0	0	0.5	0	0	0.7	0	0	0.85	0.25	1
4156	0.1	0	0	0.3	0	0	0.5	0	0	0.75	0.639	5	0.9	0	0
4169	0.1	0	0	0.3	0	0	0.55	0.25	1	0.7	0	0	0.9	0	0
4177	0.1	0	0	0.3	0	0	0.5	0	0	0.6	0.25	1	0.9	0	0
4195	0.1	0	0	0.3	0	0	0.5	0	0	0.7	0	0	0.8	0.639	1
4206	0.1	0	0	0.3	0	0	0.6	0.25	5	0.7	0	0	0.9	0	0
4227	0.1	0	0	0.3	0	0	0.5	0	0	0.7	0	0	0.8	0.639	1
4266	0.1	0	0	0.3	0	0	0.55	0.25	5	0.7	0	0	0.9	0	0
4273	0.1	0	0	0.3	0	0	0.5	0	0	0.6	0.25	1	0.9	0	0
4275	0.1	0	0	0.3	0	0	0.5	0	0	0.6	0.639	1	0.9	0	0
4276	0.1	0	0	0.3	0	0	0.5	0	0	0.6	0.639	5	0.9	0	0
4306	0.1	0	0	0.3	0	0	0.5	0	0	0.6	0.25	5	0.9	0	0
4333	0.1	0	0	0.3	0	0	0.6	0.25	1	0.7	0	0	0.9	0	0
4335	0.1	0	0	0.3	0	0	0.6	0.639	1	0.7	0	0	0.9	0	0
4337	0.1	0	0	0.3	0	0	0.5	0	0	0.6	0.25	1	0.9	0	0
4364	0.1	0	0	0.3	0	0	0.55	0.639	5	0.7	0	0	0.9	0	0
4377	0.1	0	0	0.3	0	0	0.5	0	0	0.75	0.25	1	0.9	0	0
4435	0.1	0	0	0.3	0	0	0.5	0	0	0.6	0.639	1	0.9	0	0
4470	0.1	0	0	0.3	0	0	0.5	0	0	0.65	0.25	5	0.9	0	0
4530	0.1	0	0	0.3	0	0	0.5	0	0	0.6	0.25	5	0.9	0	0
4584	0.1	0	0	0.3	0	0	0.5	0	0	0.7	0	0	0.85	0.639	5
4594	0.1	0	0	0.3	0	0	0.5	0	0	0.6	0.25	5	0.9	0	0
4619	0.1	0	0	0.3	0	0	0.55	0.639	1	0.7	0	0	0.9	0	0
4642	0.1	0	0	0.3	0	0	0.5	0	0	0.7	0	0	0.8	0.25	5
4719	0.1	0	0	0.3	0	0	0.6	0.639	1	0.7	0	0	0.9	0	0
4720	0.1	0	0	0.3	0	0	0.6	0.639	5	0.7	0	0	0.9	0	0
4745	0.1	0	0	0.3	0	0	0.55	0.25	1	0.7	0	0	0.9	0	0
4750	0.1	0	0	0.3	0	0	0.6	0.25	5	0.7	0	0	0.9	0	0
4765	0.1	0	0	0.3	0	0	0.5	0	0	0.8	0.25	1	0.9	0	0
4805	0.1	0	0	0.3	0	0	0.5	0	0	0.7	0	0	0.85	0.25	1

ID	b_{cr1}/L	d_{cr1}/h	w_{cr1} (mm)	b_{cr2}/L	$d_{cr2}h$	w_{cr2} (mm)	b_{cr3}/L	d_{cr3}/h	w_{cr3} (mm)	b_{cr4}/L	d_{cr4}/h	w_{cr4} (mm)	b_{cr5}/L	d_{cr5}/h	w_{cr5} (mm)
4834	0.1	0	0	0.3	0	0	0.5	0	0	0.7	0	0	0.8	0.25	5
4843	0.1	0	0	0.3	0	0	0.55	0.639	1	0.7	0	0	0.9	0	0
4850	0.1	0	0	0.3	0	0	0.5	0	0	0.6	0.25	5	0.9	0	0
4868	0.1	0	0	0.3	0	0	0.5	0	0	0.7	0	0	0.8	0.639	5
4884	0.1	0	0	0.3	0	0	0.5	0	0	0.6	0.639	5	0.9	0	0
4942	0.1	0	0	0.3	0	0	0.6	0.25	5	0.7	0	0	0.9	0	0
4950	0.1	0	0	0.3	0	0	0.5	0	0	0.65	0.25	5	0.9	0	0
4967	0.1	0	0	0.3	0	0	0.5	0	0	0.7	0	0	0.85	0.639	1
4972	0.1	0	0	0.3	0	0	0.55	0.639	5	0.7	0	0	0.9	0	0
4988	0.1	0	0	0.3	0	0	0.5	0	0	0.75	0.639	5	0.9	0	0
5016	0.1	0	0	0.3	0	0	0.5	0	0	0.65	0.639	5	0.9	0	0
5036	0.1	0	0	0.3	0	0	0.55	0.639	5	0.7	0	0	0.9	0	0
5043	0.1	0	0	0.3	0	0	0.5	0	0	0.6	0.639	1	0.9	0	0
5060	0.1	0	0	0.3	0	0	0.5	0	0	0.7	0	0	0.8	0.639	5
5080	0.1	0	0	0.3	0	0	0.5	0	0	0.65	0.639	5	0.9	0	0
5091	0.1	0	0	0.3	0	0	0.5	0	0	0.7	0	0	0.8	0.639	1
5099	0.1	0	0	0.3	0	0	0.55	0.639	1	0.7	0	0	0.9	0	0
5121	0.1	0	0	0.3	0	0	0.5	0	0	0.7	0	0	0.8	0.25	1
5135	0.1	0	0	0.3	0	0	0.6	0.639	1	0.7	0	0	0.9	0	0
5184	0.1	0	0	0.3	0	0	0.5	0	0	0.8	0.639	5	0.9	0	0
5207	0.1	0	0	0.3	0	0	0.5	0	0	0.65	0.639	1	0.9	0	0
5225	0.1	0	0	0.3	0	0	0.55	0.25	1	0.7	0	0	0.9	0	0
5258	0.1	0	0	0.3	0	0	0.55	0.25	5	0.7	0	0	0.9	0	0
5259	0.1	0	0	0.3	0	0	0.55	0.639	1	0.7	0	0	0.9	0	0
5291	0.1	0	0	0.3	0	0	0.55	0.639	1	0.7	0	0	0.9	0	0
5297	0.1	0	0	0.3	0	0	0.5	0	0	0.6	0.25	1	0.9	0	0
5334	0.1	0	0	0.3	0	0	0.5	0	0	0.65	0.25	5	0.9	0	0
5379	0.1	0	0	0.3	0	0	0.5	0	0	0.7	0	0	0.8	0.639	1
5448	0.1	0	0	0.3	0	0	0.5	0	0	0.7	0	0	0.85	0.639	5
5462	0.1	0	0	0.3	0	0	0.5	0	0	0.65	0.25	5	0.9	0	0
5491	0.1	0	0	0.3	0	0	0.5	0	0	0.6	0.639	1	0.9	0	0
5499	0.1	0	0	0.3	0	0	0.5	0	0	0.75	0.639	1	0.9	0	0
5546	0.1	0	0	0.3	0	0	0.55	0.25	5	0.7	0	0	0.9	0	0
5594	0.1	0	0	0.3	0	0	0.5	0	0	0.75	0.25	5	0.9	0	0
5597	0.1	0	0	0.3	0	0	0.5	0	0	0.8	0.25	1	0.9	0	0
5605	0.1	0	0	0.3	0	0	0.5	0	0	0.7	0	0	0.85	0.25	1

ID	b_{cr1}/L	d_{cr1}/h	w_{cr1} (mm)	b_{cr2}/L	$d_{cr2}h$	w_{cr2} (mm)	b_{cr3}/L	d_{cr3}/h	w_{cr3} (mm)	b_{cr4}/L	d_{cr4}/h	w_{cr4} (mm)	b_{cr5}/L	d_{cr5}/h	w_{cr5} (mm)
5659	0.1	0	0	0.3	0	0	0.5	0	0	0.75	0.639	1	0.9	0	0
5660	0.1	0	0	0.3	0	0	0.5	0	0	0.75	0.639	5	0.9	0	0
5675	0.1	0	0	0.3	0	0	0.55	0.639	1	0.7	0	0	0.9	0	0
5691	0.1	0	0	0.3	0	0	0.5	0	0	0.75	0.639	1	0.9	0	0
5735	0.1	0	0	0.3	0	0	0.5	0	0	0.7	0	0	0.85	0.639	1
5793	0.1	0	0	0.3	0	0	0.5	0	0	0.7	0	0	0.8	0.25	1
5803	0.1	0	0	0.3	0	0	0.55	0.639	1	0.7	0	0	0.9	0	0
5825	0.1	0	0	0.3	0	0	0.5	0	0	0.7	0	0	0.8	0.25	1
5834	0.1	0	0	0.3	0	0	0.55	0.25	5	0.7	0	0	0.9	0	0
5842	0.1	0	0	0.3	0	0	0.5	0	0	0.6	0.25	5	0.9	0	0
5877	0.1	0	0	0.3	0	0	0.5	0	0	0.65	0.25	1	0.9	0	0
5932	0.1	0	0	0.3	0	0	0.55	0.639	5	0.7	0	0	0.9	0	0
5938	0.1	0	0	0.3	0	0	0.5	0	0	0.6	0.25	5	0.9	0	0
5963	0.1	0	0	0.3	0	0	0.55	0.639	1	0.7	0	0	0.9	0	0
5980	0.1	0	0	0.3	0	0	0.5	0	0	0.75	0.639	5	0.9	0	0
5993	0.1	0	0	0.3	0	0	0.55	0.25	1	0.7	0	0	0.9	0	0
5998	0.1	0	0	0.3	0	0	0.6	0.25	5	0.7	0	0	0.9	0	0
6026	0.1	0	0	0.3	0	0	0.55	0.25	5	0.7	0	0	0.9	0	0
6082	0.1	0	0	0.3	0	0	0.5	0	0	0.7	0	0	0.8	0.25	5
6127	0.1	0	0	0.3	0	0	0.5	0	0	0.7	0	0	0.94	0.639	1
6173	0.1	0	0	0.3	0	0	0.5	0	0	0.7	0	0	0.94	0.25	1
6210	0.06	0.25	5	0.3	0	0	0.5	0	0	0.7	0	0	0.9	0	0
6216	0.1	0	0	0.3	0	0	0.5	0	0	0.7	0	0	0.94	0.639	5
6272	0.1	0	0	0.3	0	0	0.5	0	0	0.7	0	0	0.94	0.639	5
6282	0.06	0.25	5	0.3	0	0	0.5	0	0	0.7	0	0	0.9	0	0
6284	0.06	0.639	5	0.3	0	0	0.5	0	0	0.7	0	0	0.9	0	0
6292	0.06	0.639	5	0.3	0	0	0.5	0	0	0.7	0	0	0.9	0	0
6309	0.1	0	0	0.3	0	0	0.5	0	0	0.7	0	0	0.94	0.25	1
6339	0.06	0.639	1	0.3	0	0	0.5	0	0	0.7	0	0	0.9	0	0
6351	0.1	0	0	0.3	0	0	0.5	0	0	0.7	0	0	0.94	0.639	1
6414	0.1	0	0	0.3	0	0	0.5	0	0	0.7	0	0	0.94	0.25	5
6418	0.06	0.25	5	0.3	0	0	0.5	0	0	0.7	0	0	0.9	0	0
6425	0.06	0.25	1	0.3	0	0	0.5	0	0	0.7	0	0	0.9	0	0
6460	0.06	0.639	5	0.3	0	0	0.5	0	0	0.7	0	0	0.9	0	0
6464	0.1	0	0	0.3	0	0	0.5	0	0	0.7	0	0	0.94	0.639	5
6496	0.1	0	0	0.3	0	0	0.5	0	0	0.7	0	0	0.94	0.639	5

ID	b_{cr1}/L	d_{cr1}/h	w_{cr1} (mm)	b_{cr2}/L	$d_{cr2}h$	w_{cr2} (mm)	b_{cr3}/L	d_{cr3}/h	w_{cr3} (mm)	b_{cr4}/L	d_{cr4}/h	w_{cr4} (mm)	b_{cr5}/L	d_{cr5}/h	w_{cr5} (mm)
6516	0.06	0.639	5	0.3	0	0	0.5	0	0	0.7	0	0	0.9	0	0
6521	0.06	0.25	1	0.3	0	0	0.5	0	0	0.7	0	0	0.9	0	0
6544	0.1	0	0	0.3	0	0	0.5	0	0	0.7	0	0	0.94	0.639	5
6561	0.06	0.25	1	0.3	0	0	0.5	0	0	0.7	0	0	0.9	0	0
6578	0.06	0.25	5	0.3	0	0	0.5	0	0	0.7	0	0	0.9	0	0
6606	0.1	0	0	0.3	0	0	0.5	0	0	0.7	0	0	0.94	0.25	5
6625	0.06	0.25	1	0.3	0	0	0.5	0	0	0.7	0	0	0.9	0	0
6656	0.1	0	0	0.3	0	0	0.5	0	0	0.7	0	0	0.94	0.639	5
6681	0.06	0.25	1	0.3	0	0	0.5	0	0	0.7	0	0	0.9	0	0
6697	0.1	0.25	1	0.3	0.25	1	0.5	0.25	1	0.7	0.25	1	0.9	0.25	1
6712	0.1	0.639	1	0.3	0.639	1	0.5	0.639	1	0.7	0.639	1	0.9	0.639	1
6720	0.1	0.5	5	0.3	0.5	5	0.5	0.5	5	0.7	0.5	5	0.9	0.5	5
6741	0.1	0.639	5	0.3	0.639	5	0.5	0.639	5	0.7	0.639	5	0.9	0.639	5
6757	0.1	0.639	1	0.3	0.639	1	0.5	0.639	1	0.7	0.639	1	0.9	0.639	1
6781	0.1	0.5	1	0.3	0.5	1	0.5	0.5	1	0.7	0.5	1	0.9	0.5	1
6812	0.1	0.639	2.5	0.3	0.639	2.5	0.5	0.639	2.5	0.7	0.639	2.5	0.9	0.639	2.5
6856	0.1	0.639	1	0.3	0.639	1	0.5	0.639	1	0.7	0.639	1	0.9	0.639	1
6909	0.1	0.5	5	0.3	0.5	5	0.5	0.5	5	0.7	0.5	5	0.9	0.5	5
6915	0.1	0.25	5	0.3	0.25	5	0.5	0.25	5	0.7	0.25	5	0.9	0.25	5
6933	0.1	0.25	5	0.3	0.25	5	0.5	0.25	5	0.7	0.25	5	0.9	0.25	5
6943	0.1	0.5	1	0.3	0.5	1	0.5	0.5	1	0.7	0.5	1	0.9	0.5	1
7005	0.1	0.25	5	0.3	0.25	5	0.5	0.25	5	0.7	0.25	5	0.9	0.25	5
7048	0.1	0.25	1	0.3	0.25	1	0.5	0.25	1	0.7	0.25	1	0.9	0.25	1
7059	0.1	0.25	5	0.3	0.25	5	0.5	0.25	5	0.7	0.25	5	0.9	0.25	5
7074	0.1	0.639	5	0.3	0.639	5	0.5	0.639	5	0.7	0.639	5	0.9	0.639	5
7095	0.1	0.25	5	0.3	0.25	5	0.5	0.25	5	0.7	0.25	5	0.9	0.25	5
7109	0.1	0.639	2.5	0.3	0.639	2.5	0.5	0.639	2.5	0.7	0.639	2.5	0.9	0.639	2.5
7191	0.1	0.639	5	0.3	0.639	5	0.5	0.639	5	0.7	0.639	5	0.9	0.639	5
7229	0.1	0.25	2.5	0.3	0.25	2.5	0.5	0.25	2.5	0.7	0.25	2.5	0.9	0.25	2.5
7250	0.1	0.5	2.5	0.3	0.5	2.5	0.5	0.5	2.5	0.7	0.5	2.5	0.9	0.5	2.5
7264	0.1	0.25	1	0.3	0.25	1	0.5	0.25	1	0.7	0.25	1	0.9	0.25	1
7329	0.1	0.25	5	0.3	0.25	5	0.5	0.25	5	0.7	0.25	5	0.9	0.25	5
7374	0.2	0.25	5	0.4	0.25	5	0.5	0.25	5	0.6	0.25	5	0.8	0.25	5
7378	0.2	0.639	1	0.4	0.639	1	0.5	0.639	1	0.6	0.639	1	0.8	0.639	1
7379	0.2	0.639	2.5	0.4	0.639	2.5	0.5	0.639	2.5	0.6	0.639	2.5	0.8	0.639	2.5
7397	0.2	0.639	2.5	0.4	0.639	2.5	0.5	0.639	2.5	0.6	0.639	2.5	0.8	0.639	2.5

ID	b_{cr1}/L	d_{cr1}/h	w_{cr1} (mm)	b_{cr2}/L	$d_{cr2}h$	w_{cr2} (mm)	b_{cr3}/L	d_{cr3}/h	w_{cr3} (mm)	b_{cr4}/L	d_{cr4}/h	w_{cr4} (mm)	b_{cr5}/L	d_{cr5}/h	w_{cr5} (mm)
7409	0.2	0.25	2.5	0.4	0.25	2.5	0.5	0.25	2.5	0.6	0.25	2.5	0.8	0.25	2.5
7410	0.2	0.25	5	0.4	0.25	5	0.5	0.25	5	0.6	0.25	5	0.8	0.25	5
7472	0.2	0.25	2.5	0.4	0.25	2.5	0.5	0.25	2.5	0.6	0.25	2.5	0.8	0.25	2.5
7507	0.2	0.25	1	0.4	0.25	1	0.5	0.25	1	0.6	0.25	1	0.8	0.25	1
7532	0.2	0.639	2.5	0.4	0.639	2.5	0.5	0.639	2.5	0.6	0.639	2.5	0.8	0.639	2.5
7535	0.2	0.25	2.5	0.4	0.25	2.5	0.5	0.25	2.5	0.6	0.25	2.5	0.8	0.25	2.5
7551	0.2	0.639	5	0.4	0.639	5	0.5	0.639	5	0.6	0.639	5	0.8	0.639	5
7554	0.2	0.25h	5	0.4	0.25h	5	0.5	0.25	5	0.6	0.25	5	0.8	0.25	5
7555	0.2	0.5	1	0.4	0.5	1	0.5	0.5	1	0.6	0.5	1	0.8	0.5	1
7567	0.2	0.639	1	0.4	0.639	1	0.5	0.639	1	0.6	0.639	1	0.8	0.639	1
7600	0.2	0.5	1	0.4	0.5	1	0.5	0.5	1	0.6	0.5	1	0.8	0.5	1
7612	0.2	0.639	1	0.4	0.639	1	0.5	0.639	1	0.6	0.639	1	0.8	0.639	1
7686	0.2	0.639	5	0.4	0.639	5	0.5	0.639	5	0.6	0.639	5	0.8	0.639	5
7688	0.2	0.25	2.5	0.4	0.25	2.5	0.5	0.25	2.5	0.6	0.25	2.5	0.8	0.25	2.5
7689	0.2	0.25	5	0.4	0.25	5	0.5	0.25	5	0.6	0.25	5	0.8	0.25	5
7690	0.2	0.5	1	0.4	0.5	1	0.5	0.5	1	0.6	0.5	1	0.8	0.5	1
7709	0.2	0.5	2.5	0.4	0.5	2.5	0.5	0.5	2.5	0.6	0.5	2.5	0.8	0.5	2.5
7710	0.2	0.5	5	0.4	0.5	5	0.5	0.5	5	0.6	0.5	5	0.8	0.5	5
7720	0.2	0.639	1	0.4	0.639	1	0.5	0.639	1	0.6	0.639	1	0.8	0.639	1
7759	0.2	0.25	1	0.4	0.25	1	0.5	0.25	1	0.6	0.25	1	0.8	0.25	1
7778	0.2	0.25h	2.5	0.4	0.25h	2.5	0.5	0.25	2.5	0.6	0.25h	2.5	0.8	0.25h	2.5
7793	0.2	0.639	2.5	0.4	0.639	2.5	0.5	0.639	2.5	0.6	0.639	2.5	0.8	0.639	2.5
7813	0.2	0.25	1	0.4	0.25	1	0.5	0.25	1	0.6	0.25	1	0.8	0.25	1
7826	0.2	0.5	2.5	0.4	0.5	2.5	0.5	0.5	2.5	0.6	0.5	2.5	0.8	0.5	2.5
7834	0.2	0.5	1	0.4	0.5	1	0.5	0.5	1	0.6	0.5	1	0.8	0.5	1
7838	0.2	0.639	2.5	0.4	0.639	2.5	0.5	0.639	2.5	0.6	0.639	2.5	0.8	0.639	2.5
7840	0.2	0.25	1	0.4	0.25	1	0.5	0.25	1	0.6	0.25	1	0.8	0.25	1
7863	0.2	0.5	5	0.4	0.5	5	0.5	0.5	5	0.6	0.5	5	0.8	0.5	5
7874	0.2	0.639	2.5	0.4	0.639	2.5	0.5	0.639	2.5	0.6	0.639	2.5	0.8	0.639	2.5
7916	0.2	0.5	2.5	0.4	0.5	2.5	0.5	0.5	2.5	0.6	0.5	2.5	0.8	0.5	2.5
7918	0.2	0.639	1	0.4	0.639	1	0.5	0.639	1	0.6	0.639	1	0.8	0.639	1
7921	0.2	0.25	1	0.4	0.25	1	0.5	0.25	1	0.6	0.25	1	0.8	0.25	1
8001	0.06	0.1	0.05	0.21	0.639	2.5	0.41	0.639	0.05	0.61	0.639	2.5	0.81	0.1	0.05
8010	0.06	0.1	2.5	0.21	0.639	2.5	0.41	0.1	2.5	0.61	0.639	0.05	0.81	0.1	0.05
8027	0.06	0.639	0.05	0.21	0.639	0.05	0.41	0.639	2.5	0.61	0.1	2.5	0.81	0.1	2.5
8028	0.06	0.639	2.5	0.21	0.639	2.5	0.41	0.639	2.5	0.61	0.1	0.05	0.81	0.1	0.05

ID	b_{cr1}/L	d_{cr1}/h	w_{cr1} (mm)	b_{cr2}/L	$d_{cr2}h$	w_{cr2} (mm)	b_{cr3}/L	d_{cr3}/h	w_{cr3} (mm)	b_{cr4}/L	d_{cr4}/h	w_{cr4} (mm)	b_{cr5}/L	d_{cr5}/h	w_{cr5} (mm)
8075	0.19	0.1	0.05	0.21	0.639	0.05	0.59	0.639	2.5	0.61	0.639	2.5	0.94	0.1	2.5
8079	0.19	0.1	0.05	0.21	0.639	2.5	0.59	0.1	0.05	0.61	0.639	2.5	0.94	0.1	0.05
8109	0.06	0.1	0.05	0.39	0.639	2.5	0.41	0.639	0.05	0.79	0.639	2.5	0.81	0.1	0.05
8131	0.06	0.639	2.5	0.39	0.639	0.05	0.41	0.639	2.5	0.79	0.1	0.05	0.81	0.1	2.5
8132	0.06	0.639	0.05	0.39	0.639	2.5	0.41	0.639	2.5	0.79	0.1	2.5	0.81	0.1	0.05
8143	0.06	0.1	2.5	0.21	0.639	0.05	0.41	0.639	2.5	0.61	0.639	0.05	0.81	0.1	2.5
8159	0.06	0.639	0.05	0.21	0.1	0.05	0.41	0.1	2.5	0.61	0.1	2.5	0.81	0.639	2.5
8184	0.19	0.1/h	2.5	0.39	0.639h	2.5	0.59	0.639/h	2.5	0.79	0.639	0.05	0.94	0.1	0.05
8192	0.19	0.639	0.05	0.39	0.1	2.5	0.59	0.1	2.5	0.79	0.1	2.5	0.94	0.639	0.05
8198	0.19	0.1	0.05	0.39	0.1	2.5	0.59	0.639	2.5	0.79	0.639	2.5	0.94	0.639	0.05
8223	0.19	0.1	0.05	0.21	0.639	2.5	0.59	0.1	0.05	0.61	0.639	2.5	0.94	0.1	0.05
8224	0.19	0.1	2.5	0.21	0.639	0.05	0.59	0.1	0.05	0.61	0.639	0.05	0.94	0.1	2.5
8264	0.06	0.639	0.05	0.39	0.1h	2.5	0.41	0.1	2.5	0.79	0.1	2.5	0.81	0.639	0.05
8271	0.06	0.1	0.05	0.39	0.1	2.5	0.41	0.639	0.05	0.79	0.639	2.5	0.81	0.639	0.05
8328	0.19	0.1	2.5	0.39	0.639	2.5	0.59	0.639	2.5	0.79	0.639	0.05	0.94	0.1	0.05
8371	0.19	0.639	2.5	0.21	0.1	0.05	0.59	0.1	2.5	0.61	0.1	0.05	0.94	0.639	2.5
8383	0.19	0.639	2.5	0.21	0.639	0.05	0.59	0.639	2.5	0.61	0.1	0.05	0.94	0.1	2.5
8392	0.06	0.639	2.5	0.39	0.1	0.05	0.41	0.639	0.05	0.79	0.1	0.05	0.81	0.639	2.5
8411	0.06	0.639	0.05	0.39	0.1	0.05	0.41	0.1	2.5	0.79	0.1	2.5	0.81	0.639	2.5
8451	0.06	0.1	0.05	0.21	0.1	2.5	0.41	0.639	0.05	0.61	0.639	2.5	0.81	0.639	0.05
8473	0.19	0.1	2.5	0.39	0.639	0.05	0.59	0.1	2.5	0.79	0.639	0.05	0.94	0.1	2.5
8513	0.19	0.1	0.05	0.21	0.639	0.05	0.59	0.1	2.5	0.61	0.639	2.5	0.94	0.1	2.5
8528	0.19	0.639	0.05	0.21	0.639	2.5	0.59	0.639	2.5	0.61	0.1	2.5	0.94	0.1	0.05
8536	0.06	0.639	2.5	0.39	0.1	0.05	0.41	0.639	0.05	0.79	0.1	0.05	0.81	0.639	2.5
8545	0.06	0.1	2.5	0.39	0.639	0.05	0.41	0.1	2.5	0.79	0.639	0.05	0.81	0.1	2.5
8561	0.06	0.1	0.05	0.39	0.1	0.05	0.41	0.639	2.5	0.79	0.639	2.5	0.81	0.639	2.5
8587	0.06	0.639	2.5	0.21	0.1	0.05	0.41	0.1	2.5	0.61	0.1	0.05	0.81	0.639	2.5
8595	0.06	0.1	0.05	0.21	0.1	2.5	0.41	0.639	0.05	0.61	0.639	2.5	0.81	0.639	0.05
8597	0.06	0.1	0.05	0.21	0.1	0.05	0.41	0.639	2.5	0.61	0.639	2.5	0.81	0.639	2.5
8623	0.19	0.639	2.5	0.39	0.1	0.05	0.59	0.1	2.5	0.79	0.1	0.05	0.94	0.639	2.5
8667	0.19	0.1	0.05	0.21	0.1	2.5	0.59	0.639	0.05	0.61	0.639	2.5	0.94	0.639	0.05
8695	0.06	0.639	2.5	0.39	0.1	0.05	0.41	0.1	2.5	0.79	0.1	0.05	0.81	0.639	2.5
8704	0.06	0.1	2.5	0.39	0.1	0.05	0.41	0.639	0.05	0.79	0.639	0.05	0.81	0.639	2.5
8728	0.06	0.1/h	2.5	0.21	0.639	0.05	0.41	0.1/h	0.05	0.61	0.639	0.05	0.81	0.1	2.5
8769	0.19	0.639	0.05	0.39	0.1	2.5	0.59	0.1	0.05	0.79	0.1	2.5	0.94	0.639	0.05
8779	0.19	0.639	2.5	0.39	0.639	0.05	0.59	0.639	2.5	0.79	0.1	0.05	0.94	0.1	2.5

ID	bcr1/L	dcr1/h	wcr1 (mm)	bcr2/L	dcr2h	wcr2 (mm)	bcr3/L	dcr3/h	wcr3 (mm)	bcr4/L	dcr4/h	wcr4 (mm)	bcr5/L	dcr5/h	wcr5 (mm)
8782	0.19	0.639	2.5	0.39	0.639	0.05	0.59	0.639	0.05	0.79	0.1	0.05	0.94	0.1	2.5
8825	0.06	0.639	0.05	0.39	0.1	0.05	0.41	0.639	2.5	0.79	0.1	2.5	0.81	0.639	2.5
8831	0.06	0.1	0.05	0.39	0.639	0.05	0.41	0.639	2.5	0.79	0.639	2.5	0.81	0.1	2.5
8844	0.06	0.639	2.5	0.39	0.1	2.5	0.41	0.1	2.5	0.79	0.1	0.05	0.81	0.639	0.05
8867	0.06	0.1	0.05	0.21	0.639	0.05	0.41	0.639	2.5	0.61	0.639	2.5	0.81	0.1	2.5
8880	0.06	0.639	2.5	0.21	0.1	2.5	0.41	0.1	2.5	0.61	0.1	0.05	0.81	0.639	0.05
8893	0.19	0.639	2.5	0.39	0.1	0.05	0.59	0.639	2.5	0.79	0.1	0.05	0.94	0.639	2.5
8918	0.19	0.1	0.05	0.39	0.1	2.5	0.59	0.639	2.5	0.79	0.639	2.5	0.94	0.639	0.05
8945	0.19	0.1	0.05	0.21	0.639	0.05	0.59	0.1	2.5	0.61	0.639	2.5	0.94	0.1	2.5
8976	0.06	0.1	2.5	0.39	0.639	2.5	0.41	0.639	2.5	0.79	0.639	0.05	0.81	0.1	0.05
9009	0.06	0.1	0.05	0.21	0.639	2.5	0.41	0.639	0.05	0.61	0.639	2.5	0.81	0.1	0.05
9026	0.06	0.1	0.05	0.21	0.1	2.5	0.41	0.639	2.5	0.61	0.639	2.5	0.81	0.639	0.05
9053	0.19	0.1	0.05	0.39	0.639	0.05	0.59	0.1	2.5	0.79	0.639	2.5	0.94	0.1	2.5
9075	0.19	0.639	0.05	0.21	0.1	2.5	0.59	0.639	0.05	0.61	0.1	2.5	0.94	0.639	0.05
9118	0.06	0.1	2.5	0.39	0.639	0.05	0.41	0.639	0.05	0.79	0.639	0.05	0.81	0.1	2.5
9123	0.06	0.1	0.05	0.39	0.639	2.5	0.41	0.1	0.05	0.79	0.639	2.5	0.81	0.1	0.05
9163	0.06	0.639	2.5	0.21	0.1	0.05	0.41	0.1	2.5	0.61	0.1	0.05	0.81	0.639	2.5
9182	0.19	0.639	0.05	0.39	0.1	2.5	0.59	0.639	2.5	0.79	0.1	2.5	0.94	0.639	0.05
9188	0.19	0.1	0.05	0.39	0.639	2.5	0.59	0.639	2.5	0.79	0.639	2.5	0.94	0.1	0.05
9201	0.19	0.639	0.05	0.39	0.1	2.5	0.59	0.1	0.05	0.79	0.1	2.5	0.94	0.639	0.05
9208	0.19	0.1	2.5	0.39	0.1	0.05	0.59	0.639	0.05	0.79	0.639	0.05	0.94	0.639	2.5
9211	0.19	0.639	2.5	0.39	0.639	0.05	0.59	0.639	2.5	0.79	0.1	0.05	0.94	0.1	2.5
9214	0.19	0.639	2.5	0.39	0.639	0.05	0.59	0.639	0.05	0.79	0.1	0.05	0.94	0.1	2.5
9215	0.19	0.639	0.05	0.39	0.639	0.05	0.59	0.639	2.5	0.79	0.1	2.5	0.94	0.1	2.5
9295	0.06	0.1	2.5	0.21	0.639	0.05	0.41	0.639	2.5	0.61	0.639	0.05	0.81	0.1	2.5
9359	0.19	0.639	0.05	0.39	0.639	0.05	0.59	0.639	2.5	0.79	0.1	2.5	0.94	0.1	2.5
9440	0.06	0.1	0.05	0.21	0.639	2.5	0.41	0.639	2.5	0.61	0.639	2.5	0.81	0.1	0.05
9461	0.06	0.1	0.05	0.21	0.1	0.05	0.41	0.639	2.5	0.61	0.639	2.5	0.81	0.639	2.5
9526	0.19	0.639	2.5	0.21	0.1	0.05	0.59	0.1	0.05	0.61	0.1	0.05	0.94	0.639	2.5
9528	0.19	0.639	2.5	0.21	0.1	2.5	0.59	0.1	2.5	0.61	0.1	0.05	0.94	0.639	0.05
9536	0.19	0.639	0.05	0.21	0.639	2.5	0.59	0.639	2.5	0.61	0.1	2.5	0.94	0.1	0.05
9548	0.06	0.1	0.05	0.39	0.639	2.5	0.41	0.639	2.5	0.79	0.639	2.5	0.81	0.1	0.05
9599	0.06	0.639	0.05	0.21	0.1	0.05	0.41	0.1	2.5	0.61	0.1	2.5	0.81	0.639	2.5
9608	0.06	0.639	0.05	0.21	0.639	2.5	0.41	0.639	2.5	0.61	0.1	2.5	0.81	0.1	0.05
9653	0.19	0.639	0.05	0.21	0.1	0.05	0.59	0.639	2.5	0.61	0.1	2.5	0.94	0.639	2.5
9669	0.19	0.639	0.05	0.21	0.1	2.5	0.59	0.1	0.05	0.61	0.1	2.5	0.94	0.639	0.05

ID	b_{cr1}/L	d_{cr1}/h	w_{cr1} (mm)	b_{cr2}/L	$d_{cr2}h$	w_{cr2} (mm)	b_{cr3}/L	d_{cr3}/h	w_{cr3} (mm)	b_{cr4}/L	d_{cr4}/h	w_{cr4} (mm)	b_{cr5}/L	d_{cr5}/h	w_{cr5} (mm)
9688	0.06	0.639	2.5	0.39	0.1	0.05	0.41	0.639	0.05	0.79	0.1	0.05	0.81	0.639	2.5
9694	0.06	0.1	2.5	0.39	0.639	0.05	0.41	0.639	0.05	0.79	0.639	0.05	0.81	0.1	2.5
9729	0.06	0.1	0.05	0.21	0.639	2.5	0.41	0.639	0.05	0.61	0.639	2.5	0.81	0.1	0.05
9730	0.06	0.1	2.5	0.21	0.639	0.05	0.41	0.639	0.05	0.61	0.639	0.05	0.81	0.1	2.5
9857	0.06	0.1	0.05	0.39	0.1	0.05	0.41	0.639	2.5	0.79	0.639	2.5	0.81	0.639	2.5
9882	0.06	0.1	2.5	0.21	0.639	2.5	0.41	0.1	2.5	0.61	0.639	0.05	0.81	0.1	0.05
9911	0.19	0.1	0.05	0.39	0.639	0.05	0.59	0.639	2.5	0.79	0.639	2.5	0.94	0.1	2.5
9920	0.19	0.639	0.05	0.39	0.1	2.5	0.59	0.1	2.5	0.79	0.1	2.5	0.94	0.639	0.05
10000	0.06	0.1	2.5	0.39	0.1	0.05	0.41	0.639	0.05	0.79	0.639	0.05	0.81	0.639	2.5
10003	0.06	0.639	2.5	0.39	0.639	0.05	0.41	0.639	2.5	0.79	0.1	0.05	0.81	0.1	2.5
10008	0.06	0.639	2.5	0.39	0.639	2.5	0.41	0.639	2.5	0.79	0.1	0.05	0.81	0.1	0.05
10017	0.06	0.1	0.05	0.21	0.639	2.5	0.41	0.639	0.05	0.61	0.639	2.5	0.81	0.1	0.05
10055	0.19	0.1	0.05	0.39	0.639	0.05	0.59	0.639	2.5	0.79	0.639	2.5	0.94	0.1	2.5
10116	0.19	0.639	2.5	0.21	0.639	2.5	0.59	0.639	2.5	0.61	0.1	0.05	0.94	0.1	0.05
10141	0.06	0.1	2.5	0.39	0.1	0.05	0.41	0.639	2.5	0.79	0.639	0.05	0.81	0.639	2.5
10147	0.06	0.639	2.5	0.39	0.639	0.05	0.41	0.639	2.5	0.79	0.1	0.05	0.81	0.1	2.5
10169	0.06	0.1	0.05	0.21	0.639	0.05	0.41	0.1	2.5	0.61	0.639	2.5	0.81	0.1	2.5
10196	0.19	0.1	0.05	0.39	0.639	2.5	0.59	0.639	2.5	0.79	0.639	2.5	0.94	0.1	0.05
10238	0.19	0.1	0.05	0.21	0.639	2.5	0.59	0.1	2.5	0.61	0.639	2.5	0.94	0.1	0.05
10256	0.19	0.639	0.05	0.21	0.639	2.5	0.59	0.639	2.5	0.61	0.1	2.5	0.94	0.1	0.05
10276	0.06	0.1	2.5	0.39	0.639	0.05	0.41	0.1	0.05	0.79	0.639	0.05	0.81	0.1	2.5
10303	0.1	0.1	5	0.3	0	0	0.5	0	0	0.7	0	0	0.9	0.639	0.05
10344	0.1	0	0	0.3	0.1	0.05	0.5	0	0	0.7	0.639	5	0.9	0	0
10348	0.1	0.1	0.05	0.3	0.639	5	0.5	0	0	0.7	0	0	0.9	0	0
10352	0.1	0.1	0.05	0.3	0	0	0.5	0	0	0.7	0	0	0.9	0.639	5
10375	0.1	0	0	0.3	0.1	5	0.5	0	0	0.7	0.639	0.05	0.9	0	0
10413	0.1	0.639	5	0.3	0	0	0.5	0	0	0.7	0	0	0.9	0.1	0.05
10497	0.1	0	0	0.3	0.639	5	0.5	0.1	0.05	0.7	0	0	0.9	0	0
10575	0.1	0.1	5	0.3	0.25	2.5	0.5	0	0	0.7	0.639	0.05	0.9	0	0
10596	0.1	0.1	0.05	0.3	0.25	2.5	0.5	0	0	0.7	0	0	0.9	0.639	5
10628	0.1	0.1	0.05	0.3	0.25	2.5	0.5	0	0	0.7	0	0	0.9	0.639	5
10672	0.1	0.1	0.05	0.3	0.25	2.5	0.5	0	0	0.7	0.639	5	0.9	0	0
10712	0.1	0.1	0.05	0.3	0	0	0.5	0.25	2.5	0.7	0	0	0.9	0.639	5
10741	0.1	0.639	5	0.3	0	0	0.5	0.25	2.5	0.7	0	0	0.9	0.1	0.05
10765	0.1	0.639	5	0.3	0.25	2.5	0.5	0	0	0.7	0.1	0.05	0.9	0	0
10767	0.1	0.1	5	0.3	0.25	2.5	0.5	0	0	0.7	0.639	0.05	0.9	0	0

ID	b_{cr1}/L	d_{cr1}/h	w_{cr1} (mm)	b_{cr2}/L	$d_{cr2}h$	w_{cr2} (mm)	b_{cr3}/L	d_{cr3}/h	w_{cr3} (mm)	b_{cr4}/L	d_{cr4}/h	w_{cr4} (mm)	b_{cr5}/L	d_{cr5}/h	w_{cr5} (mm)
10794	0.1	0.639	0.05	0.3	0.25	2.5	0.5	0.1	5	0.7	0	0	0.9	0	0
10823	0.1	0.1	5	0.3	0.639	2.5	0.5	0.25	5	0.7	0.639	0.05	0.9	0	0
10824	0.1	0.1	0.05	0.3	0.639	5	0.5	0.25	2.5	0.7	0.639	5	0.9	0	0
10828	0.1	0.1	0.05	0.3	0.639	5	0.5	0	0	0.7	0.25	2.5	0.9	0.639	5
10867	0.1	0.1	5	0.3	0.639	2.5	0.5	0.25	5	0.7	0	0	0.9	0.639	0.05
10923	0.1	0.1	5	0.3	0.639	2.5	0.5	0	0	0.7	0.25	5	0.9	0.639	0.05
10927	0.1	0.1	5	0.3	0.639	2.5	0.5	0.25	5	0.7	0	0	0.9	0.639	0.05
10951	0.1	0.1	5	0.3	0.639h	2.5	0.5	0.25h	5	0.7L	0	0	0.9	0.639	0.05
11008	0.1	0	0	0.3	0	0	0.5	0	0	0.7	0.639	5	0.9	0.1	0.05
11018	0.1	0	0	0.3	0	0	0.5	0	0	0.7	0.1	5	0.9	0.639	0.05
11022	0.1	0	0	0.3	0	0	0.5	0	0	0.7	0.1	5	0.9	0.639	0.05
11023	0.1	0	0	0.3	0	0	0.5	0	0	0.7	0.639	0.05	0.9	0.1	5
11030	0.1	0	0	0.3	0	0	0.5	0	0	0.7	0.1	5	0.9	0.639	0.05
11041	0.1	0	0	0.3	0	0	0.5	0	0	0.7	0.1	0.05	0.9	0.639	5
11049	0.1	0	0	0.3	0	0	0.5	0	0	0.7	0.1	0.05	0.9	0.639	5
11050	0.1	0	0	0.3	0	0	0.5	0	0	0.7	0.1	5	0.9	0.639	0.05
11057	0.1	0	0	0.3	0	0	0.5	0	0	0.7	0.1	0.05	0.9	0.639	5
11071	0.1	0	0	0.3	0	0	0.5	0.639	0.05	0.7	0.1	5	0.9	0	0
11078	0.1	0	0	0.3	0	0	0.5	0.1	5	0.7	0.639	0.05	0.9	0	0
11079	0.1	0	0	0.3	0	0	0.5	0.639	0.05	0.7	0.1	5	0.9	0	0
11091	0.1	0	0	0.3	0	0	0.5	0.639h	0.05	0.7L	0.1	5	0.9L	0	0
11102	0.1	0	0	0.3	0	0	0.5	0.1	5	0.7	0.639	0.05	0.9	0	0
11167	0.1	0	0	0.3	0	0	0.5	0.639	0.05	0.7	0.25	2.5	0.9	0.1	5
11185	0.1	0	0	0.3	0	0	0.5	0.1	0.05	0.7	0.25	2.5	0.9	0.639	5
11233	0.1	0.1	0.05	0.3	0	0	0.5	0	0	0.7	0.25	2.5	0.9	0.639	5
11234	0.1	0.1	5	0.3	0	0	0.5	0	0	0.7	0.25	2.5	0.9	0.639	0.05
11239	0.1	0.639	0.05	0.3	0	0	0.5	0	0	0.7	0.25	2.5	0.9	0.1	5
11247	0.1	0.639	0.05	0.3	0	0	0.5	0	0	0.7	0.25	2.5	0.9	0.1	5
11259	0.1	0	0	0.3	0.639	0.05	0.5	0	0	0.7	0.25	2.5	0.9	0.1	5
11261	0.1	0	0	0.3	0.1	0.05	0.5	0	0	0.7	0.25	2.5	0.9	0.639	5
11306	0.1	0	0	0.3	0.1	5	0.5	0	0	0.7	0.25	2.5	0.9	0.639	0.05
11315	0.1	0	0	0.3	0.639	0.05	0.5	0	0	0.7	0.25	2.5	0.9	0.1	5
11344	0.1	0	0	0.3	0.639	5	0.5	0.25	2.5	0.7	0.639	5	0.9	0.1	0.05
11347	0.1	0	0	0.3	0.639	0.05	0.5	0.25	5	0.7	0.639	2.5	0.9	0.1	5
11355	0.1	0	0	0.3	0.639	0.05	0.5	0.25	5	0.7	0.639	2.5	0.9	0.1	5

Appendix D - Randomly Generated Testing Datasets

Table D-1: Randomly generated testing datasets – geometric and material input, and nodal stiffness ratio and health index output parameters

ID	b_w/h	h_s/h	L/h	ρ	f'_c (MPa)	$k\%_1$	$k\%_2$	$k\%_3$	$k\%_4$	$k\%_5$	$k\%_6$	$k\%_7$	$k\%_8$	$k\%_9$	$k_i\%$
43115	0.723	0.325	11.44	0.00912	29.108	0.99812	0.99645	0.99566	0.99393	0.99145	0.98663	0.97727	0.95106	0.91444	0.9805
43116	0.791	0.241	9.926	0.00579	29.599	0.99772	0.99798	0.99720	0.99610	0.99438	0.99128	0.98492	0.96675	0.93651	0.98629
43117	0.745	0.333	10.11	0.00951	34.113	0.99814	0.99306	0.99112	0.98884	0.98442	0.97549	0.95794	0.91531	0.92100	0.97253
43118	0.693	0.208	11.57	0.00819	34.731	0.98636	0.98319	0.97648	0.96843	0.95510	0.93075	0.88699	0.89981	0.93136	0.95185
43119	0.658	0.215	10.31	0.00505	29.917	0.99312	0.98922	0.98566	0.98020	0.97210	0.95768	0.92380	0.91758	0.94711	0.96665
43120	0.888	0.331	12.31	0.00552	37.149	0.90306	0.90006	0.95313	0.97271	0.98240	0.98789	0.99117	0.99336	0.99790	0.96817
43121	0.894	0.246	8.197	0.00564	38.045	0.99171	0.98704	0.98075	0.97338	0.96181	0.94092	0.89730	0.88710	0.93184	0.95519
43122	0.507	0.204	7.502	0.00981	40.451	0.99348	0.99367	0.99215	0.98935	0.98540	0.97686	0.96105	0.93329	0.95638	0.97816
43123	0.76	0.28	9.381	0.01	23.781	0.99716	0.99945	0.99891	0.99854	0.99791	0.99677	0.99473	0.98848	0.98559	0.99576
43124	0.539	0.312	10.26	0.00916	33.094	0.97746	0.96341	0.94942	0.93069	0.90187	0.90976	0.93367	0.95124	0.96675	0.94843
43125	0.808	0.265	9.984	0.00611	39.488	0.98228	0.97181	0.96205	0.94790	0.92761	0.89231	0.91633	0.93582	0.95982	0.94959
43126	0.898	0.276	7.963	0.00854	23.446	0.98512	0.97978	0.97111	0.96126	0.94427	0.91466	0.87102	0.89379	0.93262	0.94536
43127	0.898	0.252	9.126	0.00809	43.415	0.91797	0.89937	0.94970	0.97080	0.98092	0.98696	0.99032	0.99490	0.99634	0.96873
43128	0.714	0.334	9.989	0.00858	35.001	0.92143	0.94022	0.97112	0.98351	0.98930	0.99253	0.99446	0.99618	0.99764	0.97864
43129	0.585	0.206	8.112	0.00772	49.568	0.92020	0.92581	0.96481	0.97869	0.98632	0.99014	0.99310	0.99650	0.99801	0.97536
43130	0.529	0.229	9.086	0.00885	38.757	0.98946	0.98517	0.97720	0.96770	0.95299	0.92707	0.91194	0.88898	0.90042	0.95009
43131	0.804	0.31	9.259	0.00719	33.853	0.97711	0.96634	0.95108	0.93882	0.92570	0.89739	0.90866	0.93402	0.95862	0.94577
43132	0.758	0.302	12.33	0.00927	49.279	0.90025	0.85984	0.84548	0.86820	0.90822	0.93441	0.95134	0.96387	0.97715	0.92088
43133	0.686	0.201	7.6	0.00592	47.535	0.95696	0.91176	0.87139	0.82906	0.83319	0.87517	0.88833	0.87304	0.87016	0.8909
43134	0.897	0.216	7.279	0.00564	26.524	0.90290	0.93884	0.94546	0.93467	0.91429	0.87250	0.84078	0.88339	0.93861	0.91714
43135	0.719	0.268	8.22	0.00536	36.45	0.97746	0.95635	0.93836	0.91545	0.87628	0.85439	0.89101	0.91967	0.94049	0.92695
43136	0.806	0.302	7.554	0.00839	35.966	0.99238	0.99156	0.98835	0.98240	0.97457	0.95919	0.93962	0.91100	0.91905	0.96581
43137	0.513	0.236	8.625	0.0084	41.072	0.96199	0.94060	0.91725	0.88578	0.84523	0.80971	0.82243	0.86920	0.92503	0.89772
43138	0.806	0.242	10.91	0.00757	20.083	0.93724	0.91005	0.94996	0.96949	0.97667	0.97880	0.97506	0.97974	0.98908	0.96661
43139	0.894	0.294	9.333	0.00517	48.914	0.92958	0.94590	0.97144	0.97843	0.97934	0.97511	0.96241	0.92915	0.95048	0.96218
43140	0.759	0.325	9.513	0.00593	39.641	0.96408	0.93882	0.91493	0.89895	0.92717	0.94142	0.94320	0.92551	0.93780	0.93919
43141	0.898	0.346	10.75	0.00964	41.486	0.96239	0.94250	0.92239	0.90125	0.92549	0.93886	0.93860	0.91395	0.89879	0.93442
43142	0.589	0.227	10.03	0.00871	29.309	0.97882	0.97037	0.96007	0.94509	0.92251	0.91128	0.93252	0.94234	0.96510	0.95281
43143	0.803	0.278	9.445	0.00916	33.182	0.93194	0.89969	0.86303	0.86735	0.90709	0.92494	0.92863	0.91361	0.94455	0.91808

ID	b_w/h	h_s/h	L/h	ρ	f'_c (MPa)	$k\%_1$	$k\%_2$	$k\%_3$	$k\%_4$	$k\%_5$	$k\%_6$	$k\%_7$	$k\%_8$	$k\%_9$	$k_i\%$
43144	0.651	0.242	12.86	0.00907	27.869	0.94172	0.94520	0.96713	0.97119	0.96731	0.96175	0.97337	0.97999	0.98766	0.96953
43145	0.753	0.326	11.64	0.00826	43.162	0.95796	0.93928	0.91968	0.89222	0.85151	0.79451	0.80901	0.85087	0.89232	0.89074
43146	0.649	0.263	7.106	0.00806	45.741	0.96660	0.94381	0.92017	0.89256	0.85257	0.81334	0.84096	0.88844	0.93868	0.90571
43147	0.739	0.278	8.992	0.00873	33.644	0.94824	0.91734	0.88999	0.89972	0.89272	0.87911	0.87802	0.89370	0.93744	0.91363
43148	0.873	0.215	8.351	0.00965	34.386	0.87403	0.79444	0.78910	0.78670	0.79933	0.79940	0.84149	0.88526	0.93304	0.85028
43149	0.753	0.231	8.647	0.00964	25.082	0.96137	0.94049	0.91674	0.88752	0.84417	0.82796	0.80514	0.83866	0.86492	0.8887
43150	0.805	0.35	8.132	0.00647	45.194	0.98171	0.96817	0.97038	0.96886	0.96178	0.95035	0.92103	0.91968	0.95119	0.95932
43151	0.506	0.298	12.22	0.008	39.801	0.97043	0.96391	0.95381	0.93791	0.92911	0.94243	0.94511	0.95719	0.97144	0.95714
43152	0.676	0.354	8.167	0.0081	37.545	0.92759	0.92191	0.91015	0.88475	0.84483	0.80210	0.78524	0.82870	0.89608	0.88013
43153	0.701	0.27	10.87	0.00791	38.047	0.99605	0.99271	0.98904	0.98510	0.97835	0.97498	0.96723	0.95051	0.93303	0.9767
43154	0.718	0.241	7.742	0.00641	41.017	0.92021	0.86722	0.89156	0.90019	0.88639	0.85539	0.87235	0.89076	0.92055	0.90046
43155	0.737	0.319	10.51	0.00773	47.528	0.97656	0.96312	0.94862	0.95344	0.96506	0.96729	0.96030	0.95339	0.92617	0.9614
43156	0.594	0.344	11.23	0.00742	44.184	0.91649	0.87495	0.88863	0.91361	0.91591	0.90086	0.91107	0.92204	0.93291	0.91765
43157	0.526	0.346	11.97	0.00865	20.681	0.97108	0.97113	0.97043	0.96368	0.95198	0.92779	0.91368	0.89503	0.90848	0.94733
43158	0.84	0.278	11.62	0.00896	26.517	0.95584	0.93479	0.93943	0.93981	0.93341	0.92674	0.89770	0.90985	0.93825	0.93758
43159	0.779	0.282	8.219	0.00785	48.003	0.90504	0.92453	0.96123	0.97431	0.97815	0.97767	0.96907	0.95806	0.95038	0.95984
43160	0.524	0.227	8.688	0.00766	42.391	0.90424	0.90480	0.88480	0.89958	0.92286	0.94445	0.95970	0.97307	0.98355	0.93771
43161	0.684	0.318	7.428	0.00526	23.652	0.97748	0.95087	0.92944	0.93647	0.94994	0.95266	0.94959	0.93781	0.91919	0.95035
43162	0.744	0.304	9.277	0.00757	23.071	0.84547	0.78916	0.79657	0.81577	0.81968	0.79657	0.82383	0.83860	0.88699	0.84126
43163	0.516	0.225	11.03	0.00597	37.171	0.89696	0.89778	0.92721	0.94508	0.94879	0.93910	0.91131	0.85428	0.89244	0.9213
43164	0.839	0.208	7.587	0.00818	42.934	0.85437	0.80480	0.80629	0.85481	0.87233	0.86010	0.80986	0.76202	0.84278	0.84674
43165	0.645	0.327	11.62	0.0053	46.943	0.84118	0.82196	0.87115	0.90457	0.91037	0.89731	0.85534	0.80155	0.82249	0.87259
43166	0.636	0.24	7.439	0.0079	29.407	0.92211	0.87701	0.85192	0.81336	0.81908	0.80573	0.81735	0.86747	0.92829	0.87023
43167	0.82	0.228	9.304	0.00884	35.657	0.82546	0.75230	0.77870	0.78186	0.77978	0.79005	0.83537	0.87612	0.92133	0.8341
43168	0.55	0.227	7.936	0.00964	47.58	0.87862	0.84138	0.86146	0.90735	0.93095	0.93980	0.93634	0.93917	0.95325	0.91883
43169	0.772	0.277	7.432	0.00571	47.017	0.81186	0.70828	0.70445	0.73121	0.77939	0.83068	0.87319	0.90958	0.94485	0.82935
43170	0.59	0.26	10.14	0.008	49.604	0.88080	0.82295	0.85378	0.85421	0.87270	0.90016	0.90770	0.92698	0.95533	0.89746
43171	0.599	0.244	12.65	0.00613	22.862	0.94092	0.93286	0.92146	0.90502	0.92665	0.93170	0.91765	0.87792	0.90298	0.92572
43172	0.761	0.259	7.003	0.00944	48.086	0.84177	0.76065	0.74242	0.77348	0.81117	0.86196	0.89706	0.92079	0.93045	0.85397
43173	0.799	0.212	10.75	0.00706	23.949	0.95355	0.94290	0.93191	0.91268	0.90307	0.92141	0.91859	0.90211	0.92277	0.9309
43174	0.574	0.262	12.08	0.00804	41.699	0.98217	0.97778	0.96969	0.95890	0.94059	0.92300	0.90940	0.87181	0.89761	0.94309
43175	0.552	0.242	11.19	0.00895	49.573	0.96845	0.96689	0.98110	0.98553	0.98592	0.98266	0.97353	0.96235	0.95485	0.97613
43176	0.602	0.349	7.056	0.00646	28.196	0.95691	0.91197	0.87962	0.89006	0.90579	0.91719	0.91178	0.92914	0.95316	0.92556
43177	0.854	0.32	11.11	0.00557	40.582	0.84519	0.79368	0.82436	0.83053	0.80335	0.77365	0.80200	0.82861	0.81180	0.83132
43178	0.542	0.344	8.743	0.00539	47.235	0.79462	0.73112	0.74584	0.78103	0.81546	0.85459	0.87212	0.86449	0.86444	0.83237
43179	0.547	0.263	11.97	0.00705	44.136	0.88147	0.86763	0.88199	0.90385	0.89965	0.90415	0.89283	0.85783	0.88802	0.89774

ID	b_w/h	h_s/h	L/h	ρ	f'$_c$ (MPa)	k%$_1$	k%$_2$	k%$_3$	k%$_4$	k%$_5$	k%$_6$	k%$_7$	k%$_8$	k%$_9$	ki%
43180	0.503	0.24	11.72	0.00632	40.274	0.92469	0.92239	0.92979	0.92506	0.90565	0.87487	0.89978	0.92257	0.94794	0.92528
43181	0.806	0.35	7.041	0.00618	37.821	0.85511	0.79907	0.78903	0.80403	0.78548	0.75064	0.74568	0.73885	0.82564	0.80935
43182	0.67	0.276	10.5	0.00826	43.876	0.93023	0.93227	0.92865	0.91372	0.89262	0.87203	0.86209	0.87579	0.87929	0.90867
43183	0.604	0.345	8.816	0.00784	41.409	0.86850	0.85857	0.84429	0.86286	0.88073	0.89568	0.88780	0.86605	0.86781	0.88323
43184	0.664	0.216	10.5	0.00674	48.659	0.88097	0.85786	0.87012	0.89133	0.88429	0.85903	0.86824	0.88298	0.90368	0.88985
43185	0.633	0.297	11.75	0.00825	33.443	0.94767	0.96490	0.96188	0.95195	0.93379	0.92525	0.91966	0.93702	0.95266	0.94948
43186	0.504	0.292	7.514	0.00719	23.068	0.87946	0.83708	0.81774	0.78505	0.79736	0.80670	0.83122	0.84242	0.89821	0.84952
43187	0.659	0.339	10.26	0.00646	22.631	0.84761	0.82709	0.83271	0.85195	0.85994	0.85834	0.85176	0.88362	0.88923	0.87022
43188	0.524	0.23	9.802	0.00933	20.785	0.96657	0.94827	0.93501	0.92921	0.94298	0.94619	0.94913	0.94066	0.93596	0.9494
43189	0.608	0.258	10.11	0.00908	31.692	0.94815	0.92737	0.91898	0.91960	0.90024	0.87024	0.86150	0.82730	0.85025	0.90236

Table D-2: Randomly generated testing datasets – cracking input parameters

ID	b_{cr1}/L	d_{cr1}/h	w_{cr1} (mm)	b_{cr2}/L	$d_{cr2}h$	w_{cr2} (mm)	b_{cr3}/L	d_{cr3}/h	w_{cr3} (mm)	b_{cr4}/L	d_{cr4}/h	w_{cr4} (mm)	b_{cr5}/L	d_{cr5}/h	w_{cr5} (mm)
43115	0.1	0	0	0.3	0	0	0.4	0	0	0.6	0	0	0.9	0.494	1.706
43116	0.2	0	0	0.2	0	0	0.5	0	0	0.8	0	0	0.9	0.267	0.342
43117	0.1	0	0	0.4	0	0	0.5	0	0	0.6	0	0	0.8	0.434	3.211
43118	0.126	0	0	0.3	0	0	0.5	0	0	0.7	0.568	1.713	0.9	0	0
43119	0.1	0	0	0.3	0	0	0.515	0	0	0.7	0.335	2.941	0.8	0	0
43120	0.172	0.414	0.382	0.2	0	0	0.5	0	0	0.7	0	0	0.9	0	0
43121	0.1	0	0	0.3	0	0	0.4	0	0	0.7	0.306	3.108	0.924	0	0
43122	0.2	0	0	0.3	0	0	0.5	0	0	0.8	0	0	0.805	0.335	4.528
43123	0.1	0	0	0.3	0	0	0.5	0	0	0.7	0	0	0.855	0.099	3.882
43124	0.1	0	0	0.225	0	0	0.5	0.507	0.676	0.7	0	0	0.9	0	0
43125	0.1	0	0	0.272	0	0	0.6	0	0	0.6	0.329	1.168	0.8	0	0
43126	0.084	0	0	0.4	0	0	0.5	0	0	0.7	0.38	2.517	0.8	0	0
43127	0.2	0.332	3.488	0.35	0	0	0.5	0	0	0.8	0	0	0.9	0	0
43128	0.1	0.446	1.13	0.3	0	0	0.5	0	0	0.6	0	0	0.805	0	0
43129	0.1	0.445	4.902	0.346	0	0	0.6	0	0	0.7	0	0	0.9	0	0
43130	0.1	0	0	0.3	0	0	0.491	0	0	0.6	0.269	4.326	0.9	0.617	1.38
43131	0.1	0	0	0.4	0.095	2.032	0.6	0	0	0.625	0.311	3.517	0.8	0	0
43132	0.2	0	0	0.3	0.507	4.734	0.4	0.296	3.706	0.7	0	0	0.803	0	0
43133	0.2	0	0	0.3	0	0	0.442	0.508	3.27	0.7	0	0	0.9	0.446	2.516
43134	0.1	0.317	0.499	0.315	0	0	0.6	0	0	0.7	0.4	2.826	0.8	0	0
43135	0.1	0	0	0.3	0	0	0.6	0.41	2.577	0.632	0	0	0.9	0.091	3.704

ID	b_cr1/L	d_cr1/h	w_cr1 (mm)	b_cr2/L	d_cr2h	w_cr2 (mm)	b_cr3/L	d_cr3/h	w_cr3 (mm)	b_cr4/L	d_cr4/h	w_cr4 (mm)	b_cr5/L	d_cr5/h	w_cr5 (mm)
43136	0.2	0	0	0.239	0	0	0.6	0	0	0.7	0.104	0.044	0.8	0.356	2.023
43137	0.1	0	0	0.4	0	0	0.566	0.572	2.53	0.7	0.433	4.621	0.8	0	0
43138	0.1	0	0	0.206	0.359	0.979	0.6	0	0	0.7	0.095	4.276	0.8	0	0
43139	0.1	0.216	1.625	0.4	0	0	0.5	0	0	0.7	0	0	0.808	0.187	3.879
43140	0.1	0	0	0.4	0.306	1.177	0.5	0	0	0.8	0	0	0.829	0.224	0.435
43141	0.1	0	0	0.3	0	0	0.4	0.298	4.033	0.748	0	0	0.9	0.35	1.127
43142	0.1	0	0	0.2	0	0	0.563	0.437	1.01	0.8	0.087	3.339	0.9	0	0
43143	0.11/L	0/h	0	0.4	0.543	4.789	0.4	0	0	0.6	0	0	0.8	0.206	2.157
43144	0.16	0.359	1.616	0.4	0	0	0.6	0.176	3.621	0.6	0	0	0.9	0	0
43145	0.1	0	0	0.2	0	0	0.6	0.5	1.3	0.644	0.565	3.206	0.8	0.029	0.543
43146	0.077	0	0	0.341	0.043	1.464	0.507	0.099	4.494	0.615	0.574	4.407	0.899	0	0
43147	0.1	0	0	0.3	0.26	3.476	0.6	0.256	4.201	0.734	0.284	0.199	0.8	0	0
43148	0.1	0	0	0.2	0.507	0.106	0.4	0.363	0.253	0.6	0.429	0.382	0.9	0	0
43149	0.2	0	0	0.2	0	0	0.5	0.467	4.144	0.7	0.626	2.912	0.918	0.304	1.41
43150	0.1	0	0	0.2	0.09	3.608	0.5	0.046	4.223	0.739	0.249	0.187	0.9	0	0
43151	0.1	0.072	1.923	0.222	0	0	0.5	0.353	4.422	0.7	0.16	1.975	0.8	0	0
43152	0.1	0.196	0.562	0.4	0	0	0.574	0.398	4.491	0.7	0.602	3.304	0.9	0	0
43153	0.1	0	0	0.3	0	0	0.5	0.078	4.449	0.773	0.132	3.974	0.9	0.299	0.655
43154	0.1	0	0	0.2	0.349	4.955	0.55	0	0	0.6	0.354	3.214	0.9	0.166	3.94
43155	0.1	0	0	0.3	0.173	2.096	0.409	0	0	0.7	0.102	2.114	0.9	0.301	2.286
43156	0.1	0	0	0.243	0.543	0.147	0.6	0	0	0.6	0.358	2.238	0.9	0.182	4.034
43157	0.1	0.14	2.639	0.353	0	0	0.4	0	0	0.6	0.397	1.616	0.8	0.568	3.039
43158	0.1	0	0	0.2	0.168	2.895	0.5	0.121	3.223	0.7	0.4	3.661	0.912	0	0
43159	0.133	0.404	1.267	0.2	0	0	0.5	0	0	0.8	0.104	3.352	0.9	0.148	1.383
43160	0.1	0.44	1.92	0.3	0.427	1.035	0.5	0.093	2.133	0.65	0.014	3.794	0.8	0	0
43161	0.2	0	0	0.3	0.192	3.219	0.6	0.062	3.754	0.8	0.084	0.079	0.893	0.28	3.562
43162	0.2	0.56	1.337	0.3	0.42	3.354	0.549	0	0	0.6	0.627	3.643	0.8	0.241	4.823
43163	0.081	0.387	4.748	0.2	0.384	1.322	0.6	0	0	0.8	0.165	2.571	0.8	0.567	3.291
43164	0.134	0.196	4.038	0.3	0.535	4.232	0.6	0	0	0.7	0.232	4.02	0.8	0.615	1.682
43165	0.2	0.419	2.71	0.2	0.417	0.067	0.4	0	0	0.8	0.464	2.486	0.845	0.498	1.818
43166	0.1	0.2	2.613	0.262	0	0	0.4	0.469	3.404	0.7	0.621	0.59	0.9	0.007	0.212
43167	0.2	0.185	1.684	0.2	0.633	4.81	0.5	0.46	0.303	0.6	0.405	2.299	0.885	0	0
43168	0.1	0.537	0.346	0.3	0.484	0.907	0.4	0	0	0.7	0.121	3.051	0.857	0.182	1.889
43169	0.186	0.203	1.965	0.3	0.615	3.013	0.4	0.461	2.84	0.6	0.09	1.272	0.8	0	0
43170	0.199	0	0	0.2	0.627	2.406	0.4	0.41	2.566	0.7	0.165	3.625	0.8	0.012	4.788
43171	0.1	0.131	3.223	0.4	0.391	3.207	0.5	0	0	0.8	0.535	2.785	0.88	0.108	0.163

ID	b_{cr1}/L	d_{cr1}/h	w_{cr1} (mm)	b_{cr2}/L	$d_{cr2}h$	w_{cr2} (mm)	b_{cr3}/L	d_{cr3}/h	w_{cr3} (mm)	b_{cr4}/L	d_{cr4}/h	w_{cr4} (mm)	b_{cr5}/L	d_{cr5}/h	w_{cr5} (mm)
43172	0.2	0.364	4.816	0.3	0.635	0.247	0.5	0.345	2.985	0.6	0	0	0.912	0.139	0.469
43173	0.1	0.106	0.354	0.3	0	0	0.5	0.335	1.614	0.751	0.129	2.937	0.8	0.207	1.847
43174	0.1	0.033	1.333	0.4	0	0	0.5	0.136	4.734	0.638	0.175	0.795	0.8	0.575	3.258
43175	0.2	0.18	4.674	0.2	0.055	4.924	0.5	0.003	4.063	0.7	0.111	3.152	0.873	0.204	4.204
43176	0.2	0.031	4.148	0.323	0.351	2.364	0.5	0.105	1.623	0.7	0.21	2.003	0.9	0.076	0.049
43177	0.2	0.387	3.781	0.3	0.197	2.52	0.6	0.397	1.225	0.6	0.375	3.021	0.918	0.494	1.905
43178	0.2	0.618	4.526	0.3	0.571	1.657	0.4	0.407	4.9	0.7	0.019	0.806	0.869	0.511	4.52
43179	0.1	0.454	2.664	0.2	0.501	0.623	0.523	0.239	3.826	0.8	0.331	2.958	0.8	0.37	0.243
43180	0.1	0.349	1.64	0.2	0.217	2.548	0.5	0.027	0.343	0.601	0.565	0.053	0.8	0.048	1.516
43181	0.1	0.231	1.545	0.277	0.359	3.194	0.6	0.377	4.983	0.7	0.187	2.534	0.8	0.536	1.461
43182	0.1	0.199	4.177	0.252	0.05	4.026	0.5	0.174	0.057	0.7	0.467	1.444	0.9	0.336	4.502
43183	0.081	0.47	0.463	0.286	0.406	4.072	0.444	0.249	4.086	0.762	0.272	0.578	0.885	0.471	2.723
43184	0.1	0.184	4.241	0.2	0.427	4.619	0.593	0.35	0.347	0.7	0.155	3.092	0.9	0.203	3.066
43185	0.085	0.272	2.656	0.4	0.026	0.967	0.5	0.175	2.974	0.7	0.294	2.573	0.9	0.073	0.601
43186	0.1	0.529	2.543	0.4	0.561	3.98	0.5	0.245	0.33	0.6	0.351	2.381	0.8	0.451	3.863
43187	0.149	0.596	2.277	0.3	0.397	3.82	0.5	0.162	2.08	0.7	0.449	1.95	0.9	0.397	3.961
43188	0.2	0.087	3.645	0.305	0.107	4.223	0.4	0.272	2.035	0.6	0.098	3.531	0.9	0.403	0.777
43189	0.1	0.077	2.878	0.3	0.213	0.052	0.594	0.388	0.712	0.8	0.567	1.066	0.9	0.36	1.366